Nucleic Acid Amplification Testing for Point-of-Care Diagnostics of Bloodborne Viruses

Kelli N. Shimazu

A dissertation

submitted in partial fulfillment of the

requirements for the degree of

Doctor of Philosophy

University of Washington

2026

Reading Committee:

Jonathan D. Posner, Chair

Paul K. Drain

Jaehyun Chung

Barry R. Lutz

Program Authorized to Offer Degree:

Mechanical Engineering

University of Washington

Abstract

Nucleic Acid Amplification Testing for Point-of-Care Diagnostics of Bloodborne Viruses

Kelli N. Shimazu

Chair of Supervisory Committee:

Jonathan D. Posner

Department of Mechanical Engineering

Access to effective diagnostics remains a critical barrier to healthcare equity in low-resource settings, where bloodborne diseases like HIV, hepatitis C, and Zika continue to significantly contribute to global morbidity and mortality rates. Early diagnosis is essential for timely treatment initiation, disease monitoring, and transmission prevention, yet access to centralized laboratory testing remains limited in many regions due to infrastructure, equipment, and personnel requirements. Point-of-care (POC) molecular diagnostics have the potential to overcome these barriers by providing access to rapid, sensitive, and low-cost testing at the point of patient care. The widespread implementation of point-of-care nucleic acid amplification tests (POC NAATs) remains constrained due to the complexity of sample preparation, amplification, detection, and overall user requirements.

This dissertation addresses several key challenges in the development of simplified POC NAATs by improving paper-based isothermal NAAT reactions, simplifying sample preparation for blood, testing with clinical samples, and reducing user steps through workflow integration. To enhance amplification performance in paper-based recombinase polymerase amplification (RPA) reactions,

I developed a vibration-based platform to improve reagent redistribution and reaction kinetics within porous membranes. This approach significantly enhanced reaction performance, resulting in improved overall amplification, lower limits of detection, and reduced time-to-threshold when compared to typical unmixed paper-based reactions.

To address challenges associated with sample preparation from blood-derived samples, I developed and integrated an extraction-free workflow that enables the direct addition of thermally incubated samples into scalable RT-RPA reactions. In parallel, I formulated a concentrated custom RPA rehydration buffer that improved assay repeatability, robustness, and increased allowable sample volume. The extraction-free amplification workflow was evaluated using both cultured HIV in plasma and HCV clinical samples. Using a scalable reaction format, the assay achieved a sensitivity of 800 copies/mL for HIV plasma. Successful amplification from HCV clinical samples further demonstrated the feasibility of the approach and provided early validation that this workflow could successfully process and detect viral RNA from clinical serum specimens.

Finally, I developed a sample-to-answer cartridge and reader NAAT platform designed to further reduce user steps, minimize instrumentation requirements, and maintain an overall assay time under 30 minutes. By integrating sample preparation and amplification components into a more streamlined format, this platform moves toward a practical implementation of molecular testing in decentralized settings.

Overall, this work advances the development of simplified, low-cost, and portable molecular diagnostic workflows that are better suited for POC use in resource-limited environments. Through improvements in amplification performance, sample preparation simplification, and device integration, these contributions help address critical barriers to the broader development of POC molecular diagnostics.

Acknowledgements

I would like to acknowledge and give my warmest thanks to my committee members for their time, thoughtful guidance, and invaluable feedback throughout this process. Their insights have strengthened this work and shaped my development as a researcher.

I am grateful to my advisor for their mentorship, support, and encouragement over the course of my graduate studies. Your guidance has challenged me to think critically, approach problems with rigor, and grow both technically and professionally. I deeply appreciate the learning opportunities you have provided.

To my lab members, thank you for creating such a collaborative environment. I am grateful for the discussions, troubleshooting sessions, and shared experiences that made even the difficult moments manageable. Your willingness to help and provide feedback made a lasting impact on my journey. I would also like to thank the broader community of collaborators, colleagues, and mentors that I have met along the way. This experience has been enhanced by the people who made it meaningful and I look forward to continuing to learn and grow from these connections. Finally, I am incredibly thankful to my family and friends for their support and encouragement. To Jason, thank you for always being there for me, I could not have done this without you. I am especially grateful for your patience, your understanding, and for the countless pickup and drop-offs at the lab. Thank you for being someone I can always count on, your support means more to me than I can express.

Table of Contents

List of Figures and Tables

List of Abbreviations

AIDS	Acquired Immunodeficiency Syndrome
ART	Antiretroviral Therapy
BBP	Bloodborne Pathogens
DAAs	Direct-acting Antivirals
DNA	Deoxyribonucleic Acid
dsDNA	Double Stranded Deoxyribonucleic Acid
DTT	Dithiothreitol
HCV	Hepatitis C Virus
HIV	Human Immunodeficiency Virus
LAMP	Loop mediated isothermal amplification
LOD	Limit of Detection
NA	Nucleic Acid(s)
NAAT	Nucleic Acid Amplification Test
NTC	Non-template Control
µPADs	Microfluidic paper-based analytical devices
PCR	Polymerase Chain Reaction
PEG	Polyethylene Glycol
POC	Point-of-Care
PTC	Positive Temperature Coefficient Heater
RNA	Ribonucleic Acid
RNases	Ribonucleases
RPA	Recombinase Polymerase Amplification
RT-RPA	Reverse Transcription Recombinase Polymerase Amplification
SPE	Solid Phase Extraction
SSB	Single Stranded Binding Protein
TPP	Target Product Profile
WHO	World Health Organization

Chapter 1 Introduction

1.1 Point-of-Care (POC) Diagnostics

Inequities in access to healthcare remain a major concern in low and middle income countries (LMIC) and low-resource clinics, where limited medical infrastructure contributes to high infection and mortality rates from bloodborne diseases such as HIV, hepatitis C, and zika.[1] Many of these countries operate in resource-limited settings that lack essential laboratory requirements such as reliable electricity, cold chain storage, and access to high-cost instrumentation. Point-of-care (POC) diagnostics aim to provide low-cost, rapid results at the place of patient care to alleviate these obstacles for widespread access and dissemination.[2,3] To guide the development of POC technologies, the WHO established the ASSURED criteria (Affordable, Specific, Sensitive, User-friendly, Rapid and robust, Equipment-free, and Delivered) to describe the ideal point-of-care diagnostic.[4] More recently, the REASSURED criteria has been proposed, adding "Real-time connectivity" and "Ease of specimen collection" to the original framework.[5] In response, ongoing research focuses on integrating gold standard diagnostic capabilities into a POC, user-friendly format to reduce the need for centralized laboratories.

1.2 Nucleic Acid Amplification Tests (NAATs)

Nucleic acid amplification tests (NAATs) are crucial tools for diagnostics and disease monitoring due to their high clinical sensitivity and specificity. They are typically conducted in centralized laboratories using expensive automated platforms capable of high-throughput testing. This

centralized approach is driven by the requirement of thermocycling, high cost instrumentation, cold chain logistics for reagents, trained staff, and infrastructure to store required equipment.[2]

The NAAT workflow is separated into three main steps: sample preparation, amplification, and detection. Sample preparation typically requires pathogen lysis and the purification of target DNA or RNA from sample inhibitors, usually through nucleic acid extraction or purification.[6,7] Lysis is the disruption of the viral envelope or cell wall, which releases nucleic acids into the solution. It can be accomplished through various methods such as chemical, mechanical, thermal, or enzymatic based approaches.[7,8] Traditional sample preparation for whole blood and blood-based samples use solid phase extraction (SPE), where target is bound and released from silica columns or similar media, or through liquid phase extraction, such as phenol-chloroform extraction.[7] These methods use high-molarity chaotropic salts like guanidine thiocyanate or guanidine hydrochloride, which facilitate lysis, denature ribonucleases (RNases) and other enzymes, and help nucleic acid adsorption onto the silica material.[9] Despite providing highly purified nucleic acid targets for amplification, these protocols can be difficult to implement in a point-of-care (POC) environment due to the multiple pipetting and centrifuging steps, requirement of concentrated toxic chaotropic salts that can inhibit nucleic acid amplification, and long timespan of 30 minutes to an hour to extract DNA and RNA targets.[6] Figure 1 illustrates a typical solid-phase extraction protocol for RNA extraction from plasma samples.

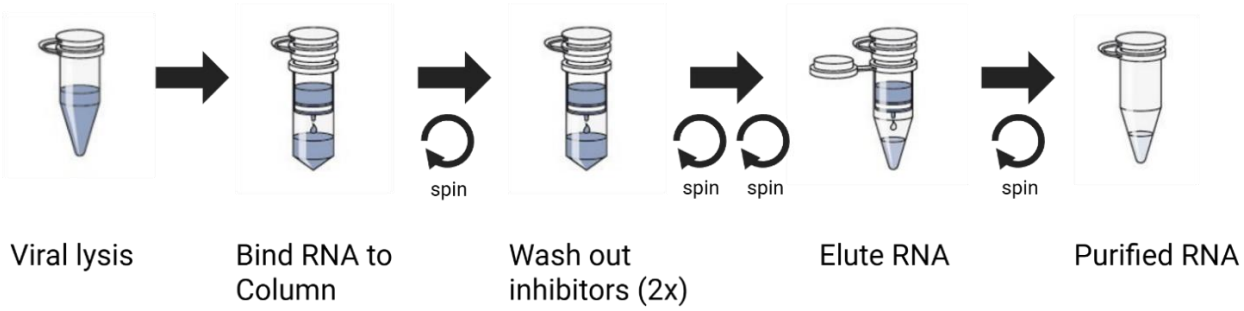

Figure 1. Qiagen Viral RNA mini kit solid-phase extraction procedure for a plasma sample. Each spin symbol represents a centrifuge step. In total, there are approximately eight fluid manipulation and four centrifugation steps.

Following sample preparation, the purified nucleic acid is then added to an amplification assay, which duplicate nucleic acids to detectable levels. The gold standard NAAT is polymerase chain reaction (PCR), which relies on precise thermocycling to denature, anneal, and extend targets, as seen in Figure 2.[10,11] During each PCR cycle, the temperature is first raised to 94 - 97 °C to denature double-stranded DNA. The temperature is then lowered to 50 - 65 °C to anneal the sequence specific primers and raised to 72 °C for the DNA polymerase to bind to the attached primers. DNA polymerase extends from the primer in the 5' to 3' direction, synthesizing a complementary strand thereby doubling the amount of DNA with each cycle. The cycle is repeated up to 45+ cycles.[10–12] Due to these steps, PCR has a slow amplification process of 45 - 90 minutes.[10]

Detection of amplified nucleic acids is typically done using fluorescence, either using intercalating dyes or sequence-specific probes. Alternative detection mechanisms such as electrochemical and colorimetric have also been explored.[13–16]

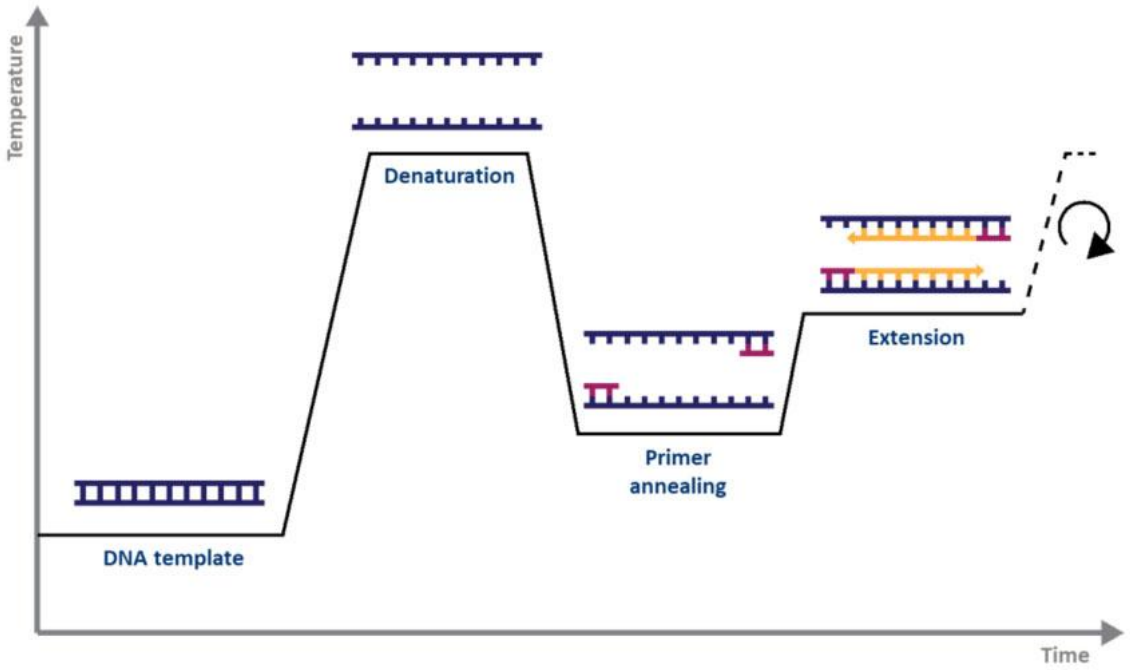

Figure 2. PCR Amplification mechanism.[17]

While this process can be done manually, requiring multiple user steps and apparatuses, it is more commonly carried out using large high-throughput platforms. Machines such as the Roche *cobas* systems integrate sample preparation, amplification, and detection, processing up to 864 samples every 14 hours using complex robotics and electronics to replace manual user steps. However, these and similar platforms cost as much as $140,000 and require significant infrastructure to meet its power, temperature control, and cold storage requirements. The complexity of the process from sample preparation to detection and cost associated with the required rapid temperature control makes PCR and its high-throughput machines difficult to apply for low-cost NAATs. PCR is typically performed in centralized laboratories, which often results in delayed diagnoses that hinder immediate follow up treatment.[18] As a result, there is a critical need for affordable POC

NAATs that are suitable for outpatient, resource-limited clinics, particularly in low- and middle-income countries where disease burden is high.[2]

1.3 Isothermal Amplification Methods

To overcome the limitation of PCR in resource-limited settings, isothermal nucleic acid amplification methods have emerged as promising alternatives for POC diagnostics. Isothermal NAATs can match the sensitivity and specificity of PCR, while operating at a single incubation temperature, alleviating the need for rapid and precise temperature control hardware.

1.3.1 LAMP

Loop-mediated isothermal amplification (LAMP) is an increasingly popular nucleic acid amplification technique that is well-suited for POC applications due to its constant operation temperature of 60 - 65 °C and compatibility with various detection methods, including colorimetric, turbidity, lateral flow, and real-time fluorescent readouts. LAMP relies on four to six primers (B3, BIP, F3, FIP, and loop primers LF and LB) that recognize specific regions of the target DNA, forming loop structures that enhance amplification speed and efficiency.[19] While software tools like NEB LAMP Primer Design or Eiken Chemical PrimerExplorer V5 assist in primer design, the assay remains complex due to the number of primers involved and the potential for nonspecific amplification. Amplification times typically range from 30 to 60 minutes. Although LAMP has demonstrated utility in detecting pathogens such as HIV-1, HPV-16, SARS-CoV-2, and hepatitis B and C, challenges remain with assay multiplexing and minimizing false positives that occur from contamination and primer-dimer formation.[20–23]

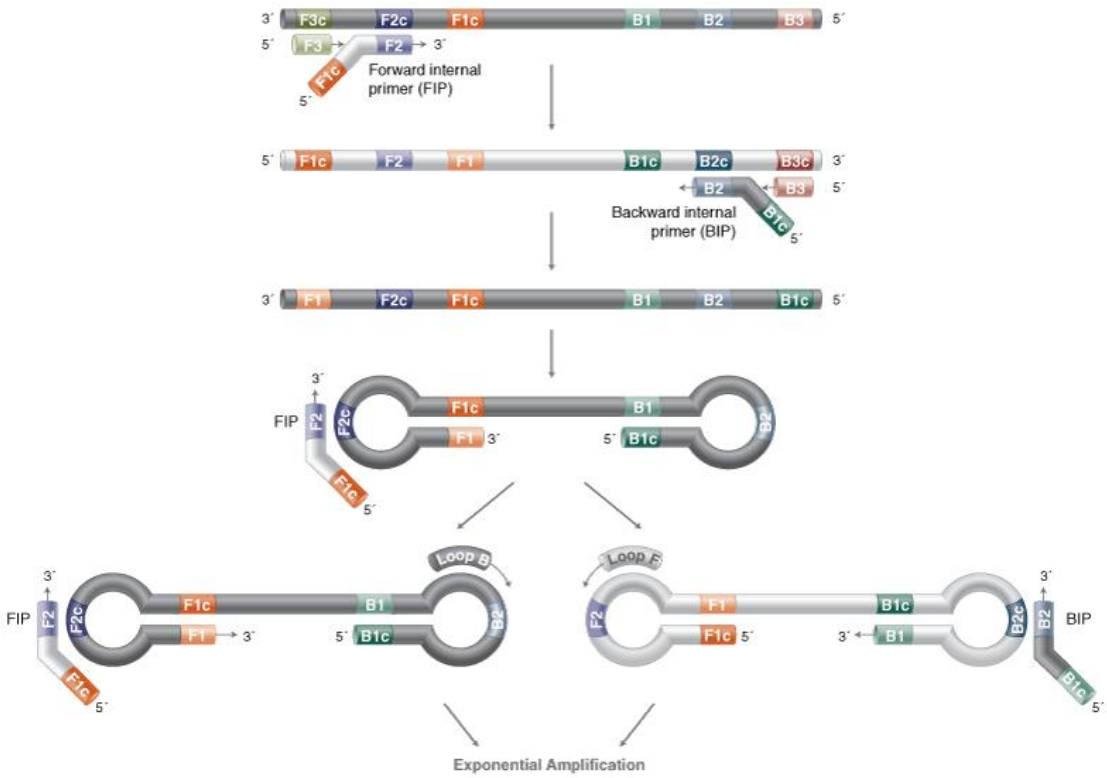

Figure 3. Schematic of LAMP mechanism.[24]

1.3.2 RPA

Recombinase polymerase amplification (RPA) is a highly attractive isothermal amplification method for POC NAATs due to its rapid assay time of 15 - 20 minutes, low incubation temperature of 37 - 42 °C, high specificity, and exceptional sensitivity, capable of detecting fewer than 10 copies per reaction. RPA requires only two primers and a sequence-specific probe, thus enhancing its specificity while simplifying assay design.[25,26] RPA tolerates many inhibitors and is stable at room temperature when lyophilized.[8] In the amplification process, shown in Figure 3, recombinase proteins from a recombinase-primer complex that facilitates strand invasion and attaches primers to the DNA target, forming D-loops. Single-stranded DNA-binding proteins (SSBs) stabilize the

D-loops, and a strand-displacing polymerase initiates DNA synthesis using dNTPs. Real-time fluorescence detection is done using a cleavable, internally quenched probe. When the probe is bound to DNA target, exonuclease III cleaves the THF residue on the probe, separating the black hole quencher from the fluorophore.[27] Other detection mechanisms such as lateral flow assays or gel electrophoresis are also common. In 2024, the patents for RPA expired and since then, many companies have developed their own RPA formulations and comparable products.

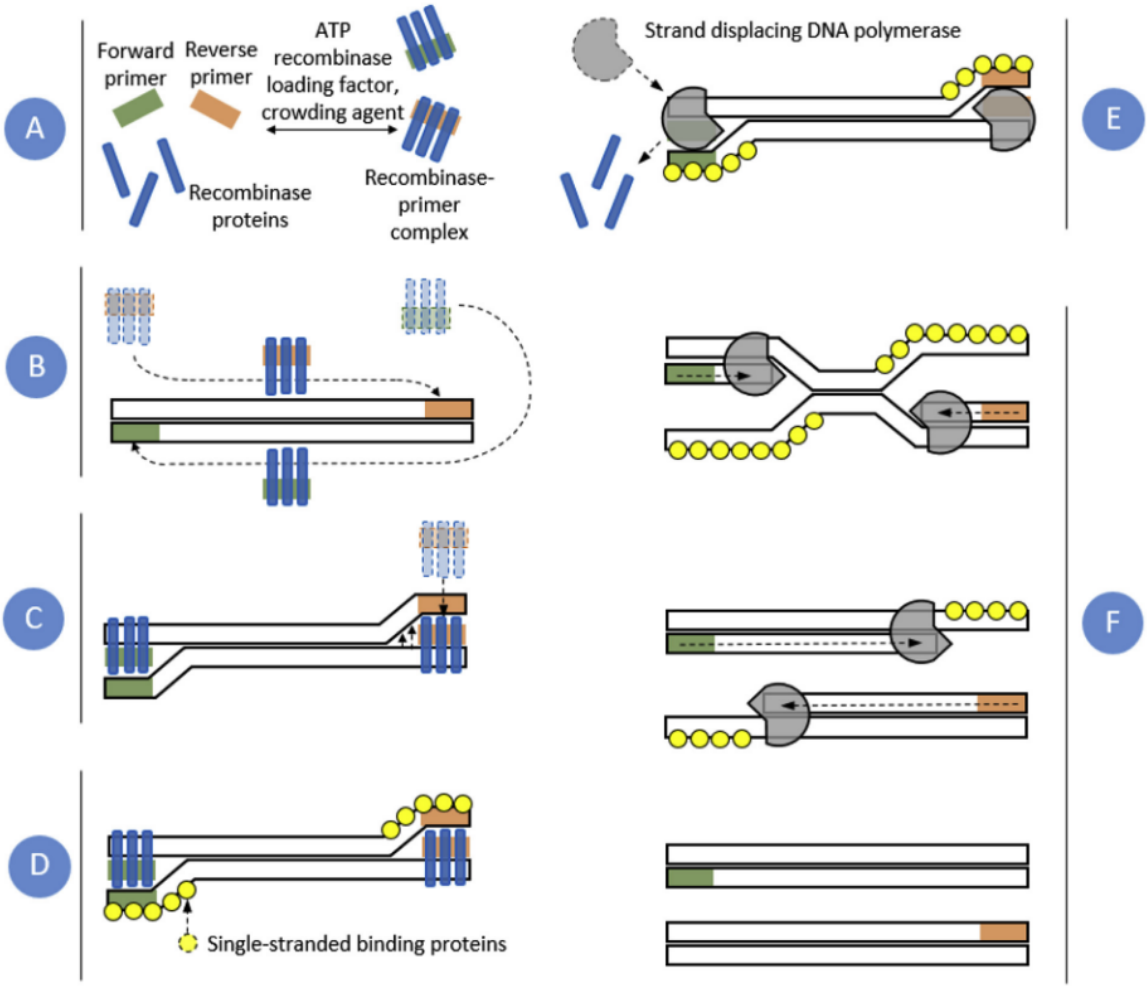

Figure 4. Schematic of RPA mechanism.[27]

1.4 POC NAAT Platforms

In response to the need to meet the REASSURED criteria, several POC NAAT platforms have been commercialized, including the Abbott *m-PIMA*, Diagnostics for the Real World *SAMBA II*, and the *Enigma ML*. These platforms are designed to simplify user steps and minimize the need for specialized training, with many receiving CLIA-waived status.[28] Despite their accuracy and relative ease of use for decentralized testing, their long runtimes and high upfront costs, ranging from $10,000 - 25,000, remains a significant barrier to their adoption at primary and community healthcare levels.[29,30] Similar to high-throughput platforms, these POC systems often rely on complex mechanical and hydraulic designs to automate user steps, which contributes to their elevated cost.

Figure 5. Commercialized point-of-care NAATs. From left to right: Abbott *m-PIMA*, DRW *SAMBA II*, and *Enigma ML*.

More recently, home-based NAAT testing has expanded with companies like Cue Health, Lucira, and Detect commercializing POC diagnostic tests using isothermal NAATs for SARS-CoV-2 and Flu. While these home-use devices are less expensive than the POC platforms, they are still costly at $65 - 90 per test cartridge.[31–33] One of the key factors enabling their viability is that they use

saliva or nasal swab samples for respiratory infections which are easier to collect, use simplified sample preparation, and contain high target concentrations. Blood and plasma samples, are particularly challenging to use with isothermal NAATs as they contain clotting factors and human albumin that can easily coagulate due to changes in temperature or pH.[34] Additionally, blood-based samples contain significant NAAT inhibitors and have a high concentration of ribonucleases that degrade exogeneous RNA.[35,36] As a result, blood-based testing remains a significant challenge in the development of low-cost POC NAATs, with sample preparation continuing to be a critical bottleneck.[37,38]

Figure 6. Commercialized home-based NAATs for SARS-CoV-2 and Flu. From left to right: Cue Health, Lucira, Detect.

1.5 Trends in Research

Most currently available CLIA-waived molecular diagnostics systems and home-based NAATs target respiratory infections.[39] This focus has been driven in part by market demand for respiratory pathogen testing, as well as the relative ease of sample collection and processing.[40] Respiratory specimens are typically collected using non-invasive nasal swabs and generally contain fewer

interfering substances than blood.[39,41,42] As a result, these samples are less likely to introduce matrix-related inhibition of downstream processes such as nucleic acid amplification, making them straightforward to incorporate into a point-of-care nucleic acid amplification test.

In contrast, blood remains a critically important sample type for diagnostics because it can contain a wide range of pathogens circulating freely in plasma or residing within host cells. Many of the world's most significant infectious diseases including HIV, hepatitis C (HCV), hepatitis B, Ebola, and Zika, can be detected through blood testing. Together, these pathogens are responsible for millions of infections and deaths worldwide each year, with the greatest burden often occurring in low-resource settings where access to laboratory infrastructure is limited.[43,44] Among these diseases, HIV and HCV represent two of the most important global health challenges due to their high prevalence, long-term health consequences, and reliance on molecular testing for diagnosis and treatment monitoring.[29,43–45] The following sections provide an overview of HIV and HCV, their global impact, and the diagnostic challenges associated with their detection.

1.5.1 HIV Pandemic

HIV was first reported in 1981 and has since become a major global health challenge, with 39.9 million people living with the virus, 1.3 million new infections, and 630,000 HIV-related deaths reported at the end of 2023.[44] HIV is a bloodborne, enveloped virus with a single-stranded RNA genome of 9,749 bases that encodes for nine distinct viral proteins. The virus primarily targets CD4+ T-cells, depleting the patient's white blood cell count and progressively weakening the immune system. Upon infecting a host cell, HIV uses its viral reverse transcriptase to convert its RNA genome into proviral DNA, which is then integrated into the host genome. This proviral DNA directs the synthesis of viral components, producing new virions until the host cell undergoes

cellular death.[46] HIV infection often progresses silently for years without noticeable symptoms, and due to the error-prone nature of reverse transcription, the virus exhibits high genetic diversity, with multiple subtypes. In North America and Europe, subtype B is the most common.[46,47]

Antiretroviral therapy (ART) has transformed HIV into a manageable chronic illness and, when taken prophylactically by high-risk individuals as pre-exposure prophylaxis (PrEP), it can effectively prevent infection. Nonetheless, challenges such as poor adherence to ART regimens and the emergence of drug-resistant strains continue to hinder progress, particularly in low-and middle-income countries (LMICs) where the burden of disease remains disproportionately high.[48]

To address the HIV pandemic, UNAIDS established the 95-90-86 cascade targets, aiming that by 2030, 95% of all people living with HIV will know their status, 90% will receive sustained ART, and 86% will achieve viral suppression. By the end of 2023, global progress had reached 86%, 77%, and 72%, respectively, showing notable advancements but also highlighting the need for continued improvement in diagnosis, treatment access, and monitoring.[44]

Achieving these goals requires an enormous global testing infrastructure. It is estimated that more than 30 million HIV viral load tests are needed annually to support treatment monitoring and guide clinical decision-making worldwide.[49] However, access to molecular testing remains limited in many regions due to the reliance on centralized laboratories, expensive instrumentation, and complex cold chain logistics. These barriers are particularly pronounced in rural communities, decentralized healthcare facilities, and LMICs, where patients may face long travel distances, delayed result reporting, and interruptions in care. As a result, expanding access to decentralized and point-of-care viral load testing has become a major priority for global HIV programs.

One of the most powerful tools for monitoring HIV infection is viral load testing, which measures the concentration of HIV RNA in plasma. Viral load serves as a direct indicator of disease progression and ART effectiveness. According to the World Health Organization (WHO), individuals with fewer than 1,000 copies/mL are considered virally suppressed, whereas those exceeding this threshold may require adherence counseling, additional monitoring, or transition to second-line therapy.[50,51] Routine viral load testing, typically conducted every 3 to 12 months, is therefore essential for assessing treatment efficacy, identifying treatment failure, and guiding clinical management. Consequently, the development of affordable, decentralized molecular diagnostic technologies capable of performing HIV viral load testing at the point-of-care remains an important unmet need.

1.5.2 HCV Pandemic

Hepatitis C virus (HCV) is a bloodborne pathogen that affects an estimated 110 million people worldwide, including around 80 million with chronic infection.[52] HCV consists of 7 major genotypes with genotype 1 being the most dominant in North America.[53] The virus is a single-stranded 9.5 kb RNA genome enveloped in a lipid bilayer that translates into a 3000 amino acid long polyprotein.[54,55] HCV infects hepatocytes as well as dendritic cells, B cells, and peripheral blood mononuclear cells.[54] Following viral entry and uncoating, the viral RNA genome is released into the cytoplasm. The HCV genome serves as mRNA and is translated into a single polyprotein, which is cleaved by host and viral proteases into structural and nonstructural proteins. The viral RNA-dependent RNA polymerase (NS5B) synthesizes a negative-strand RNA intermediate, which serves as a template to produce new positive-sense genomic RNA. These newly synthesized genomes are assembled, packaged, and secreted through the host secretory pathway.[55]

Infection is often asymptomatic, with up to 80% of those infected unaware of their condition.[56] However, chronic HCV can lead to severe complications including cirrhosis, liver failure, and hepatocellular carcinoma, contributing to over 400,000 deaths globally each year.[57] While no vaccine or effective pre-exposure prophylaxis currently exists, the development of direct-acting antivirals (DAAs) has revolutionized HCV treatment. Modern DAA regimens achieve cure rates of 90 - 95% across all genotypes with only 8 - 12 weeks of oral treatment, making HCV one of the few chronic viral infections that can be reliably cured.[43]

In response, the WHO has established goals to expand diagnosis and provide DAA treatment to 80% of individuals living with chronic HCV infection.[52] Despite the availability of highly effective therapies, progress toward elimination has been hindered by limitation in current diagnostic workflows. Unlike HIV, where antibody positivity generally indicates a persistent lifelong infection, HCV antibody tests cannot distinguish between active infection and prior resolved infection because anti-HCV antibodies may remain detectable long after viral clearance. Therefore, HCV diagnosis typically follows a two-step testing strategy in which individuals are first screened using a serological antibody test and then referred for confirmatory HCV viral RNA testing to identify active infection and determine treatment eligibility.[43,58]

This two-step diagnostic cascade introduces substantial barriers to care. Patients who test positive for HCV antibodies must often return for additional blood collection, laboratory analysis, and follow-up clinical visits before treatment can be initiated. Most HCV RNA tests rely on PCR-based laboratory platforms located in centralized facilities, resulting in increased costs, long turnaround times, and a high risk of patient loss to follow-up. These challenges are particularly pronounced in rural settings, decentralized healthcare clinics, and LMICs where access to molecular testing infrastructure may be limited.

As global screening efforts expand, the demand for accessible HCV RNA testing is expected to increase substantially. POC molecular diagnostics offer an opportunity to simplify the diagnostic pathway by moving virological testing close to the patient. Rather than requiring an initial antibody test followed by confirmatory testing from a centralized laboratory, POC nucleic acid amplification tests could enable a one-step diagnostic strategy in which active infection is identified and treatment decisions are made within a single clinical visit.[58] Such an approach has the potential to reduce loss to follow-up, shorten time to treatment initiation, improve linkage to care, and accelerate progress toward global HCV elimination goals. Consequently, the development of low-cost decentralized HCV RNA testing platforms remains a major priority for expanding access to curative DAA therapies worldwide.

1.5.3 Blood-based Sample Preparation for POC NAATs

Traditional sample preparation for whole blood and blood-based samples use solid phase extraction (SPE). Despite providing highly purified nucleic acid targets for amplification, SPE can be difficult to implement in a POC environment due to the multiple user steps, requirement of chaotropic salts that can inhibit nucleic acid amplification, and long timespans of 30 minutes to an hour.[6] Nonetheless, some research have implemented SPE into a user friendly format. A handheld device developed by Adedokun *et al.* utilized integrated buffer wells and a sliding mechanism that allows users to sequentially introduce SPE buffers, enabling concentration of HIV RNA onto a paper-based capture pad.[59] Others have developed slide mechanisms to manipulate magnetic beads through SPE buffers.[60,61] However, significant efforts are still needed to reduce device complexity and the associated high costs of POC NAATs, particularly for application involving blood-based targets.

Some POC approaches have addressed sample preparation using microfluidic channels, functionalized magnetic beads to manipulate the sample, or slide mechanisms to introduce buffers to a sample membrane.[59–61] While these devices can reduce some pipetting and centrifuging steps, they still require multiple user interventions to purify and elute the nucleic acids, remove inhibitory agents, and often involve long runtimes. Approaches to automating these steps typically incur high costs due to pumps, actuators, and other robotic components required for fluid manipulation.[59–68] Others have used isotachophoresis (ITP), which implements an electric field and a buffer system, to concentrate and extract nucleic acids.[69,70] These purification techniques require additional time, user steps, and complexity to the workflow, complicating their use in low-cost sample-to-answer POC diagnostics.

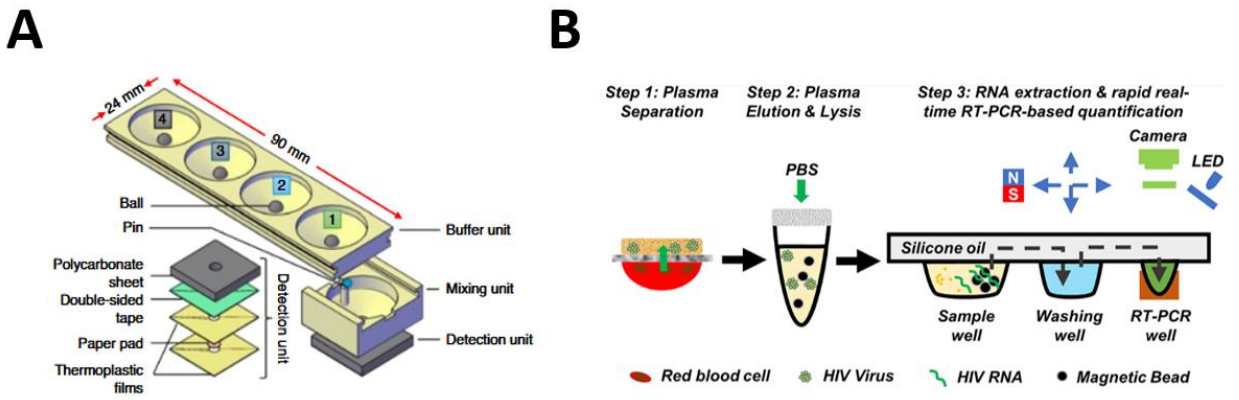

Figure 7. Examples of devices that address sample preparation for blood samples. (A) Handheld device for HIV RNA by Adedokun *et al.* (B) Sample preparation and RT-PCR method for HIV RNA by Ngo *et al.*

Extraction-free sample preparation is an emerging method that reduces workflow complexity and overall cost for POC NAATs. By using lysis and nuclease inactivation chemicals that are compatible with amplification techniques, users can directly add sample to the amplification assay

without the need for extensive preprocessing. Extraction-free protocols for DNA and RNA targets have been demonstrated on a variety of samples such as nasal swabs, saliva, urine, and blood.[8,23,71–74] Curtis *et al.* developed an extraction free protocol that adds minimally processed diluted whole blood directly into RT-LAMP.[71] More recently, Wang *et al.* developed an extraction-free method for serum and plasma samples by directly adding the sample into RT-LAMP and improving assay sensitivity by increasing reaction volume.[75] The direct sample addition approach by Wang *et al.* presents challenges for lower-temperature isothermal NAATs like RPA, as it does not provide sufficient heat required for complete pathogen lysis or ribonuclease (RNase) inhibition, which is problematic at low target concentrations. Additionally, the crude sample preparation approach is more effective for respiratory and saliva samples types, which contain fewer and less potent nucleic acid amplification inhibitors and coagulation factors, but remains challenging for viruses, like HIV, that have low limit of detection (<1000 copies/mL) requirements.[51,76] While some studies have demonstrated successful implementation of extraction-free sample preparation in blood products, their performance remains limited.[72,77] For example. Myhrvold *et al.* achieved detection of Zika RNA in blood and serum at an limit of detection of ~45,000 copies/mL.[72] These reports highlight that extraction-free approaches are feasible, but further improvements are required to improve the limit of detection (LOD), streamline user steps, and enhance the robustness of target RNA preparation from blood-based samples.

1.5.4 Microfluidic Paper-based Analytical Devices (μPADs)

Many POC NAATs use the term "paper-based" to refer to the use of cellulose, nitrocellulose, polyethersulfone, glass fiber, polycarbonate, and other types of fibers or membranes.[78–85] Paper is conducive to stack, store, transport, and incorporate into high volume manufacturing lines.

Chemical and biological reagents can be dried or lyophilized on membrane, similar to lateral flow rapid tests.[86–88] When dry, the wicking properties of paper facilitates the transport of solutions. Microfluidic paper-based analytical devices (μPADs) often leverage paper's wicking properties by layering or folding membranes over each other to increase contact area between liquids, transfer target between separate assay steps, or contain specific reaction volumes while removing excess buffer.[89,90] Many labs implemented POC μPADs for diagnostics using these sliding, layering, or folding techniques in their devices.[85,90–92] While paper POC devices are being used for complex assays, they often struggle with uneven analyte concentration profiles after reagent rehydration and assay integration steps.[89,93–95] Furthermore, the pore structure and surface properties of analytical membranes may inhibit nucleic acid amplification reactions through adsorption and/or limiting the diffusion of necessary biomolecular reagents, such as nucleic acids, oligonucleotides, and enzymes needed for amplification reactions. Several studies reported low assay efficiencies, poor detection output, and poorer limits of detection in porous membranes compared to traditional tube-based protocols.[79,85,96]

Previous work in the Posner lab implemented POC μPADs for RPA, with Sullivan *et al.* leveraging the high viscosity RPA buffer and diffusion limiting membrane for quantitative detection of RPA; however, the overall fluorescence product was low and the reported limit of detection (LOD) was higher than tube-based assays.[79] Other paper-based RPA assays showed that assays run in membranes have worse LODs and signal to noise ratios than tube-based ones.[78,85] Overall, the paper-based RPA studies in literature primarily address integration of reagents and target before amplification but have found poor to moderate LODs and low overall output signal.

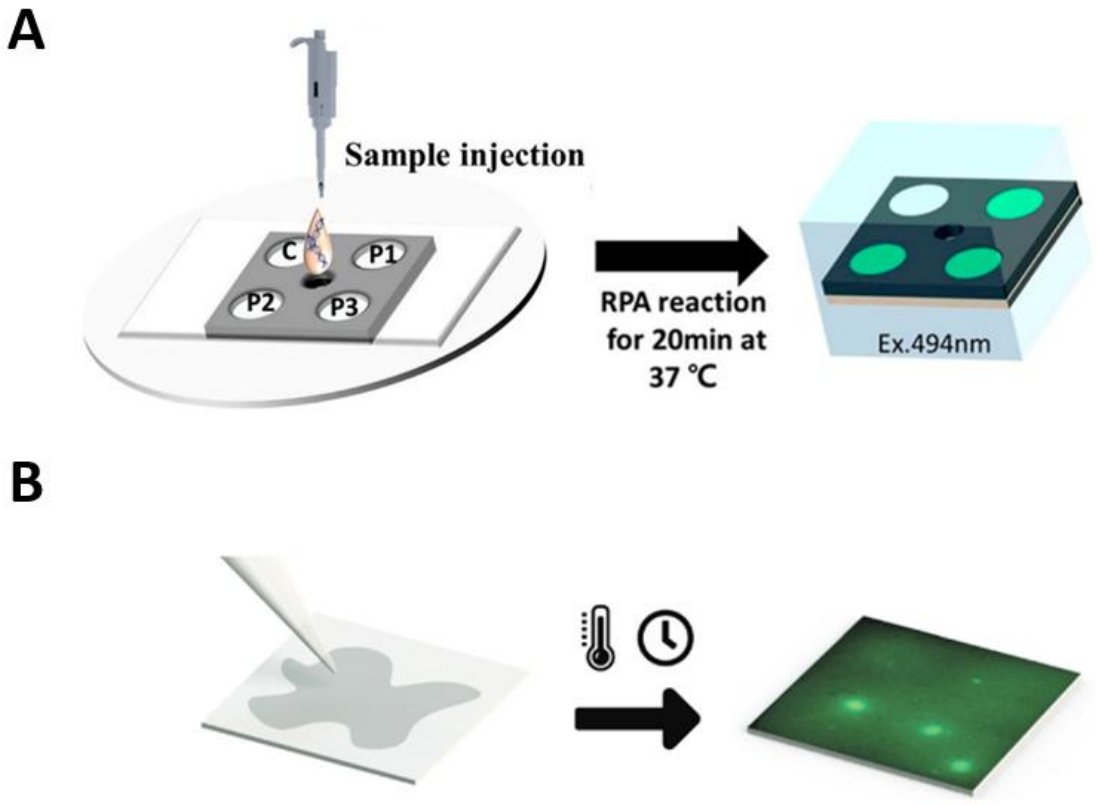

Figure 8. Examples of paper-based RPA. (A) Device by Ahn *et al.* (B) Method by Sullivan *et al.*

1.5.5 Microfluidic Mixing

Mixing, typically defined as bulk stirring with molecular diffusion,[97] is difficult to accomplish in membrane-based RPA reactions due to the high viscosity buffer, the porous structure of membranes, the low Reynolds number surface tension driven flow, and the requirement of vigorous mixing for high reaction efficiencies. Most examples of microfluidic mixing in porous substrates use passive mixing methods, which rely on diffusion by increasing contact area between separate solutions.[98,99] The stringent requirements for RPA makes it difficult to achieve efficient mixing using passive mixing methods. Active mixing methods addresses these problems as it uses external driving forces to produce efficient mixing and can be controlled with its power

input.[89,94,100–102] The limited examples of active membrane mixing include Y-shaped paper channels with surface acoustic waves or piezoelectric transducers.[103,104] Active mixing methods can be difficult to integrate into paper-based POC devices as complex lithographic fabrication is typically required and voltage requirements are considerably high (PZTs require 30 - 120 volts).[100,101,103,104] A simple active mixing strategy such as vibration based mixing was demonstrated to be effective in microfluidic devices and large liquid volumes.[105–108] They can use simple cost-effective solutions such as loudspeaker tweeters or eccentric rotating mass (ERM) motors. Motors such as coin cell ERM motors are typically found in cellphones or tablets and provide an attractive solution as they are robust, have a compact profile, are low cost, and require little voltage (0-5 volts). Microfluidic POC devices that have implemented these motors use them for lysis or sample prep applications in liquid volumes.[109–113]

1.5.6 Simple Diagnostic Devices for Sample-to-Answer Testing

Recent advances in POC diagnostics have focused on integrating full sample-to-answer workflows into a low-cost, portable microfluidic analytical device. Early work by Connelly *et al.* demonstrated mechanically actuated paper fluidic handling and reagent delivery in a disposable diagnostic platform for *E. coli* DNA detection.[90] This slide mechanism approach popularized foundational strategies for fluid control in paper-based diagnostics and inspired subsequent folding, laying, and sliding device configurations for assay integration. Work by Choi *et al.* further developed on paper based devices by implementing a sample-to-answer biosensor that stacks various membranes for the individual sample addition, washing, and amplification steps.[114] While these devices are very simple and easy to fabricate, they still require many user steps, multiple external equipment for incubation and analysis, and were used on easier DNA targets.

In the pursuit of reducing user steps, researchers have increasingly focused on more complex integrated devices that incorporate fluid metering, sample treatment, and thermal incubation into single platforms. A notable example is microRAAD, developed by Phillips *et al.*, a direct blood sample-to-answer device for HIV RNA detection. While this low-profile device significantly simplifies user steps, its reported analytical sensitivity was relatively limited (~2.3E7 copies/mL) with a total processing time of approximately 90 minutes.[115] More recently, Jiang *et al.* developed UbiNAAT, a disposable paper-based LAMP device for SARS-CoV-2 and Flu detection from nasal swabs.[116] UbiNAAT reduced operation to a simple nasal swab addition step and achieved a sensitivity of approximately 1E4 copies/mL, which is sufficient for respiratory viral testing. However, nasal swab specimens are substantially less challenging than blood-based samples, as blood contains abundant amplification inhibitors and RNases capable of degrading RNA.[35,36,117] Consequently, adapting these integrated platforms for bloodborne RNA viruses that require low limits of detection remains a significant challenge. These limitations continue to motivate the development of next-generation POC devices with improved materials, fluidic architectures, and amplification integration strategies capable of robust performance with complex clinical matrices such as whole blood or plasma.

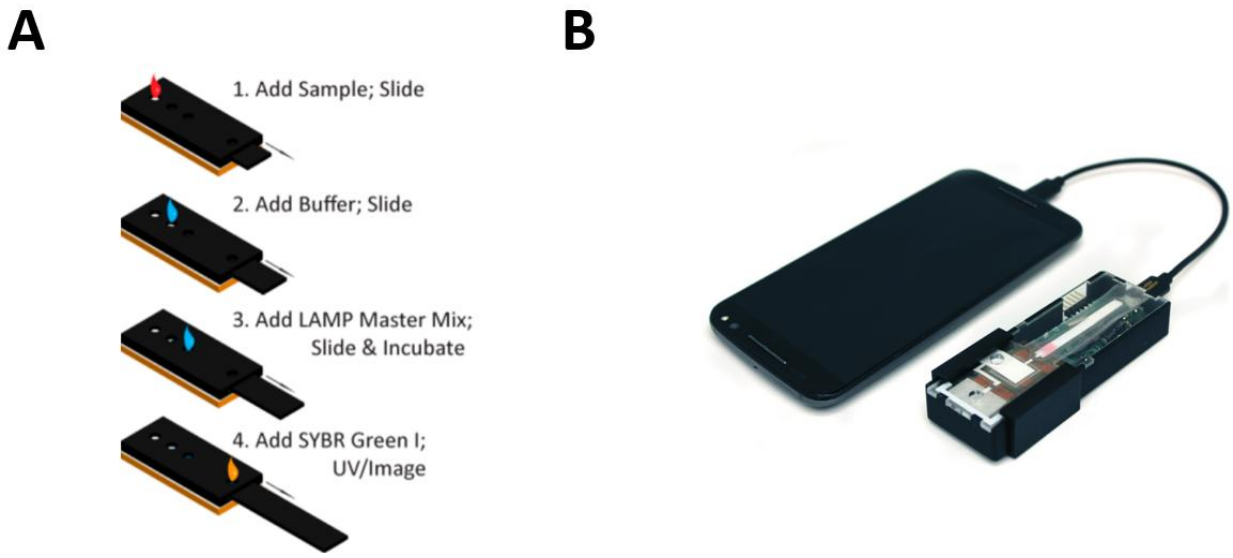

Figure 9. Examples of sample-to-answer devices. (A) Device by Connelly *et al.* (B) MicroRAAD by Phillips *et al.*

1.6 Research Goals and Rationale

In this work, I addressed key bottlenecks in the NAAT workflow, specifically in the areas of amplification and sample preparation, using HIV and HCV as model bloodborne viruses. To overcome the challenges of mixing in paper-based RPA reactions, I employed a novel vibration-based platform that enables simultaneous heating and mixing. This approach targets a critical limitation in paper-based RPA systems. Additionally, I implemented a simple extraction-free sample addition method for scalable reaction volumes that can detect viral loads at the WHO defined threshold for viral suppression of <1000 copies/mL. While effective, this method is limited due to the dilution factor required to prevent sample coagulation. I then optimized the assay to improve repeatability and robustness by developing a custom RPA buffer that allows for better pH control, buffering adjustments, ability to add and adjust additives like PEG or detergents, allow higher sample concentrations, and accommodate higher sample dilutions for difficult samples that

coagulate more easily. I then validated this optimized extraction-free method on hepatitis C clinical samples. Lastly, I integrated extraction-free sample preparation and paper-based RPA into a cohesive user-friendly test cartridge and heating platform, demonstrating considerable progress toward a low-cost and accessible POC diagnostic for bloodborne diseases.

1.6.1 Research Objectives

This work is split into the following objectives:

1. **Enhancing paper-based RPA reactions**

I employed a novel vibration-based platform to enable simultaneous heating and mixing of RPA reactions in paper membranes. Many paper-based isothermal methods do not incorporate active mixing. However, mixing is essential in RPA reactions due to the high viscosity buffer and limited diffusion of reactants.[26,118] This approach targets a critical limitation in paper-based RPA systems. Using a low-cost vibration-based method, I can enhance paper-based RPA reactions by improving the limit of detection, reducing time-to-threshold, and increasing overall fluorescence signal.

2. **Reducing complexity of sample preparation for blood-based samples**

I implemented an extraction-free method for blood plasma samples to reduce the difficulties in sample preparation. Traditional sample preparation requires multiple handling and user steps. With this approach, I reduced user steps and overall sample preparation time. By scaling the reaction volume, I achieved a limit of detection of <1000 copies/mL for HIV plasma. I then improved and optimized the extraction-free method by implementing a custom concentrated rehydration buffer and applying the improved method to hepatitis C Virus. I validated the improved method with HCV clinical samples.

3. Developing a user-friendly POC test format

I developed an integrated sample treatment to nucleic acid amplification device to reduce instrument requirements and simplify user steps toward a POC friendly format. The system enables a direct plasma-to-answer workflow in which minimal user intervention is required: the user powers on the device, introduces a plasma sample, and waits for approximately 5 minutes to allow sample treatment. A subsequent mechanical slide mechanism is then actuated to combine pre-stored reagents and initiate the RT-RPA reaction. This design eliminates the need for intermediate handling steps or external heating and mixing instrumentation. The device was validated using plasma samples spiked with HCV synthetic DNA as well as an HCV RNA-positive clinical specimen, demonstrating a successful proof-of-concept of the integrated workflow.

Chapter 2 Vibration-based mixing for enhanced recombinase polymerase amplification

2.1 Motivation

Nucleic acid amplification tests (NAATs) are used to detect infectious diseases due to their high clinical sensitivity and specificity. However, the application of PCR for low-cost NAATs is challenging due to the complexity and cost associated with the precise and rapid temperature control required for thermal cycling. Isothermal amplification methods are a solution to the limitations of PCR for POC diagnostic devices as they can match the sensitivity and specificity of PCR, while operating at a single incubation temperature, alleviating the need for rapid and precise temperature control hardware. Isothermal methods, such recombinase polymerase amplification (RPA) is an attractive isothermal amplification method as it produces results in less than 15 minutes, features a low incubation temperature (37 - 40 °C), and has high specificity due to its two primers and sequence-specific probe for fluorescence or lateral flow readout.[25,119]

Microfluidic paper-based analytical devices (μPADs) are gaining popularity due to their low cost and useful characteristics for the application of POC NAATs. Limited diffusion in paper-based RPA assays are specifically challenging because of the polymer crowding agent that is critical to stabilize enzymes and improve reaction efficiency.[26,120] The addition of crowding agents (typically polyethylene glycol) significantly increases viscosity and reduces diffusion of reactants in the system. For tube-based assays, the high viscosity of RPA buffers requires an intermediate mixing step at 4 - 5 minutes into the incubation to redistribute RPA reactants and improve amplification output signal.[26] Improved RPA reaction efficiency has also been observed under continuously stirred conditions.[118] Mixing is difficult to achieve in paper-based RPA, and may have hampered

its development. Improving mixing of paper-based RPA reactions may overcome issues with low diffusion and associated inhibition of RPA, enabling the use of low cost optical or electronic detection strategies and improving LOD.

In this chapter, I show that vibrational mixing from an ERM coin cell motor applied to paper-based fluidic systems improves mixing, RPA reaction efficiency, overall product output, and reduces time to detection. I use HIV-1 as the diagnostic target in this work since there is a prevailing need for highly-sensitive POC NAATs for HIV viral load monitoring (target LOD <1,000 cp/mL).[51,121,122] I show that vibrational mixing of paper-based RPA enables the detection of 12 copies of HIV proviral DNA per reaction and 50 copies of HIV RNA per reaction. Mixing in paper-based reactions improves the LOD by a factor of 6.4, reduces detection time from an average of 9.93 minutes to 5.17 minutes, and produces an overall fluorescence signal up to 15.8 times brighter compared to reactions without mixing. The mixing device achieves the optimal 38°C incubation temperature of RPA using a self-regulating positive temperature coefficient (PTC) heater. I demonstrate the heat generation from the coin vibration motor may be used on its own without a PTC for heating. I demonstrate that nonuniform initial distributions of reactants drastically inhibit unmixed paper-based RPA and that vibrational mixing readily overcomes these concentration gradients, enabling robust detection at low copy numbers. This platform addresses challenges facing membrane-based POC diagnostic devices such as uneven distribution of reagents, integration of separated components or reagents, and mixing of low volume and viscous samples. The mixing strategy for improved paper-based diagnostics is inexpensive, simple to implement, and has low power consumption. This mixing platform can also be applied to other membrane-based assays or processes that require high reaction efficiency, rehydration of reagents, high signal output, and device integration with multiple separated steps. Similar isothermal amplification

methods such as membrane LAMP assays, sample preparation, or enzymatic reactions may also benefit from efficient membrane-based mixing.

2.2 Experimental Section

2.2.1 Device Fabrication

The vibrational mixing device consists of a 3D printed assembly that integrates the motor and PTC heater with a glass slide that supports the amplification membrane, as shown in Figure 10. The 3D printed part consistently positions the RPA membrane on the glass slide relative to the motor for each experiment, ensuring repeatable results. The motor assembly consists of a vibration coin cell motor (VC1234B016F, Vybronics, CN), a PTC heater (PTC Heating Element, DFRobot, CN), an isolation material, and a 3D printed plate (S Series Tough PLA, Ultimaker, USA). I use epoxy adhesive (BONDiT B-45, Reltek, USA) and thin double-sided adhesive (CBGNHW011091, Scotch, USA) to attach the foam and coin cell motor to the 3D printed base plate. Both motor and glass slide holder components attach to a base acrylic plate (8505K748, McMaster-Carr, USA) cut on a CO_2 laser (PLS6.150D, Universal Laser Systems, USA). I use commercially available isolation materials in varying thicknesses ranging from 4.75 - 8 mm (DualPlex 6 mm Neoprene, Honwally 6 mm Silicone Gel, Thermwell 6 mm Polyfoam, Thermwell 4.75 mm PVC based foam, and Thermwell 8 mm rubber foam) between the base plate and PTC heater to assess the effect of isolation materials on mixing and resultant RPA performance. Low-cost, off-the-shelf materials that were close in thickness were used to provide a sufficient variety in material type. Here I focus on screening off-the-shelf materials for the best mixing performance rather than a systematic and rigorous evaluation of material composition, thickness, and its impact on mixing. To account for height differences, the 3D printed platform is adjusted for each isolation material to maintain the

same distance between the motor and glass fiber reaction membrane. Glass fiber membranes (GF/DVA, Whatman, UK) are cut on a flatbed cutter (FCX4000-50ES, Graphtec America, Inc., USA) into uniform squares with a 7.2 mm side length and 785 µm thickness to fit a 50 µL reaction for RPA and RT-RPA assays. I place glass fiber amplification membranes onto a 2" X 3" glass slide (CA6101, Premiere, CN). After adding 50 µL to the membrane, the reaction is fully sealed with PCR film (TempPlate RT Select Optical Film, USA Scientific, USA) and slotted into the device with the film in contact with the motor. The coin vibration motor uses a 2 volt input, unless otherwise specified.

2.2.2 Visualization of Bulk Stirring

To visualize and validate bulk stirring due to the vibrational motor, I track fluorescently labeled DNA over 20 minutes of mixing in a liquid saturated membrane. To maintain the viscous and proteinaceous reaction conditions of RPA, I rehydrate a lyophilized RPA TwistAmp exo pellet with 29.5 µL of the TwistAmp reaction buffer and 16 µL of water. I pipet 4.5 µL of 70 base pair DNA tagged with Alexa Fluor 488, taken from the pol region of the HIV-1 genome, onto the center of the membrane. For a *homogenized* control experiment, fluorophore-tagged DNA is initially and uniformly distributed within the RPA reaction mixture (via vortexing) before pipetted evenly over the membrane.

2.2.3 RPA and RT-RPA Reactions

For RPA experiments, I target synthetic DNA (gBlocks Gene Fragments, Integrated DNA Technologies, USA) that contain 1000 base pairs of the HIV-1 genome (group M, subtype A). RT-RPA amplifies purified HIV RNA using HIV-1 supernatant, as described in Lillis *et al.*[119] HIV-1

supernatant (group M, subtype A, NCBI accession number: JX140650) provided by the External Quality Assurance Program Oversight Laboratory at Duke University, and is extracted using QIAamp Viral RNA Mini Kits (Qiagen, DEU).[123] The viral RNA concentration is verified with quantitative real-time PCR. Both targets are diluted in DEPC-treated water and are used in establishing the quantifiable ranges for RPA amplification. The primers and probe used in both RPA and RT-RPA are developed by Lillis *et al.* for cross-subtype HIV-1 detection.[119] The RPA mastermix consists of a TwistAmp exo kit lyophilized pellet (TwistDx, UK), 29.5 μL rehydration buffer, 14 mM magnesium acetate, 540 nM forward and reverse primer (Integrated DNA Technologies, USA), and 120 nM exo-probe (LGC Biosearch Technologies, GBR). For RT-RPA experiments, 0.5 U/μL of reverse transcriptase (Agilent AffinityScript, USA) is added to the mastermix. The mastermix consisting of rehydration buffer, primers, probe, and reverse transcriptase (for RT-RPA experiments) is added to a lyophilized exo-kit RPA pellet.

2.2.4 Paper-based RPA Reactions

I conduct *homogenized* paper-based RPA experiments with mastermix, magnesium, and target uniformly distributed onto a reaction membrane. For this set of *homogenized* experiments, target (DNA or RNA) and MgOAc are added to the cap of the RPA tube. I close the tube and shake it manually for 20-30 seconds to ensure homogeneous distribution of reactants. Then, I evenly pipet 50 μL of the RPA reaction (mastermix, magnesium and target) onto the membrane before sealing the amplification membrane with PCR film and slotting it into the assembly. I set the voltage on the PTC heater voltage to result in 37 - 39 °C output on the face of the motor to provide heat to the RPA reaction. Lower PTC voltage is required at higher motor voltages due to the internal heat generation of the motor.

To demonstrate integration of separated RPA components, I conduct paper-based *isolated* RPA experiments with mastermix distributed onto the reaction membrane with magnesium and target added separately. To consistently pipet magnesium and target in discrete and locations on the membrane, I place a clear acrylic (4615T94, McMaster-Carr, USA) laser cut template with two 0.9 mm circular cutouts spaced 4.5 mm apart (center to center). For these experiments, I pipet 45.5 µL of RPA reaction (mastermix) onto the membrane before aligning the template over the membrane and pipetting 2.5 µL of magnesium acetate and 2 µL of target onto the membrane. Lastly, I remove the laser cut template and place PCR film over the glass slide to seal the membrane.

2.2.5 Data Collection and Analysis

I use an epifluorescence fluorescence microscope (AZ100, Nikon, JPN) and illumination system (X-Cite exacte, Excelitas Technologies, USA) to image the RPA membrane amplification with a 1X objective and field of view diameter of 35 mm. The epifluorescence filter cube set (XF100-2, Omega Optical, LLC., USA) and CMOS camera (Prime BSI Express, Teledyne, Photometrics, USA) captures grayscale images every 5 seconds up to 20 minutes.

I use an image analysis algorithm (MATLAB, MathWorks, USA) to calculate the fluorescence intensity increase over the full 20-minute image-stack. Background subtraction eliminates artifacts caused by auto-fluorescence due to the membrane, PCR film, glass slide, and initial nonspecific interactions in the assay. The intensity over the entire membrane is averaged and plotted against time. The positive threshold of an RPA reaction is the area averaged intensity of no template control (NTC) HIV DNA experiments plus three standard deviations. All reactions are analyzed for limit of detection at the 15-minute mark.

To examine bulk stirring, I use the standard deviation of the averaged fluorescence intensity as a function of time, also known as the macro-mixing index. This is given as $\sigma = \langle (I - \langle I \rangle)^2 \rangle^{1/2}$, where intensity I is scaled from 0 to 1 with $\langle \quad \rangle$ indicating the area average intensity in the region of interest. The region of interest for all experiments is 7.2 mm by 7.2 mm. In this scaling, 0 represents a fully mixed membrane experiment and 1 represents an unmixed experiment. This is the same metric used by Stroock *et al.* to represent channel mixing for chaotic microchannel mixers.[124] The macro-mixing index is initially set to 1 by dividing the standard deviation over time, σ, when the motor is running by the standard deviation of the first frame, before the mixing motor is turned on, code available in SI.

I determine the z-axis, perpendicular to the motor face, amplitudes produced by the motor using a single-point laser doppler vibrometer (Polytec, DE) to measure the outer edge of the motor face, for each isolation material assessed. Velocity data is recorded using a vibrometer controller (OFV 2600, Polytec, DE) and integrated with respect to time to calculate amplitude data.

To determine the temperature of the RPA reactions, I attach a thermocouple (80BK-A, Fluke Networks, USA) to the motor face and record the data using a digital multimeter (Fluke Networks, USA) every minute. The temperature is monitored without the glass slide, glass fiber membrane, and PCR film due to limited spacing for the thermocouple. When the RPA reaction plate is added to the system, the warmup time to reach incubation temperature will be impacted due to its larger thermal mass; however, I expect this difference to be small as the thermal mass of the glass slide and membrane is relatively low compared to the amount of heat generated from the PTC heater and motor platform. For the motor only case, I remove the PTC heater and place styrofoam under the vibration motor as well as on top of the platform with a central opening to visualize the membrane reaction. Insulation material such as styrofoam and rubber isolation material help retain

heat produced from the motor and provide more consistent temperature profiles for the 20-minute duration.

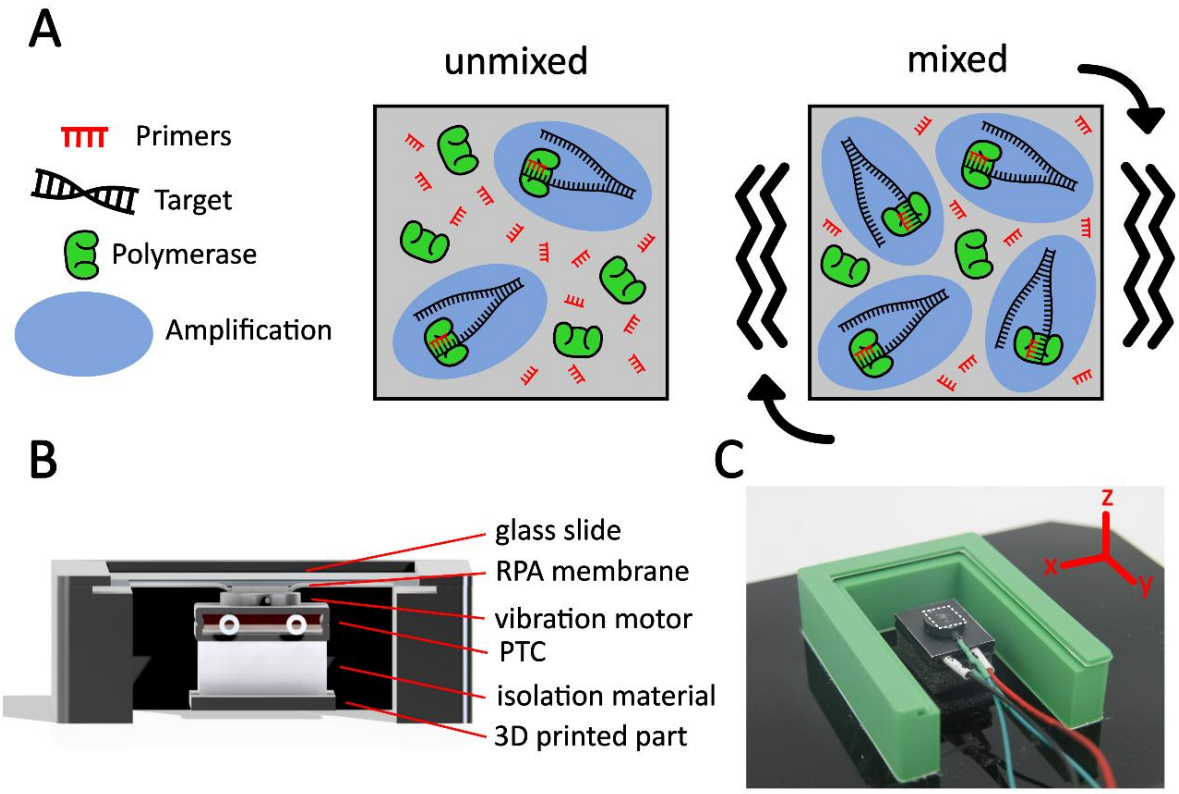

Figure 10. (A) A simplified representation of *homogenized* membrane-based RPA reactions for unmixed and mixed scenarios. When continuously mixed, reaction products and RPA reagents are redistributed, resulting in increased amplification regions and an overall improvement in reaction efficiency. (B) Image of platform cross section with RPA reaction plate, which consists of: a glass slide, RPA membrane, and PCR film. (C) Photo of platform. The white, dashed-line box represents the location of the RPA membrane in the experiment. The x and y axis are in plane to the motor and the z-axis is perpendicular to the motor face.

2.3 Results and Discussion

I demonstrate that continuous membrane mixing of RPA reactions redistributes reactants and increases amplification regions, thus increasing reaction efficiency and total fluorescence products. To determine the effectiveness of the vibration platform for RPA, I observed and quantified the overall bulk stirring in the system and evaluated various materials and input voltages for the motor to find the most favorable conditions for RPA amplification. I then performed RPA and RT-RPA experiments on glass fiber membranes for 10 - 1,000 cps rxn^{-1} and 50 - 1,000 cps rxn^{-1} respectively, to measure the impact on RPA detection limit, time-to-threshold, and total fluorescence. I additionally compared 30,000 cps rxn^{-1} DNA unmixed experiments to 200 cps rxn^{-1} DNA mixed experiments to observe unmix and mixed scenarios with similar fluorescence curves. I examine conditions with initially *homogenized* RPA experiments (with and without a PTC heater) as well as *isolated* RPA experiments.

2.3.1 Visualization of Bulk Stirring Efficiency

I first studied bulk stirring efficiency in a glass fiber membrane using fluorescently labeled DNA. I pipetted viscous RPA reaction buffer evenly to the membrane and then pipetted a small volume of labeled DNA in the center of the membrane. Using this experimental setup, I can track the efficiency of bulk stirring in the membrane.

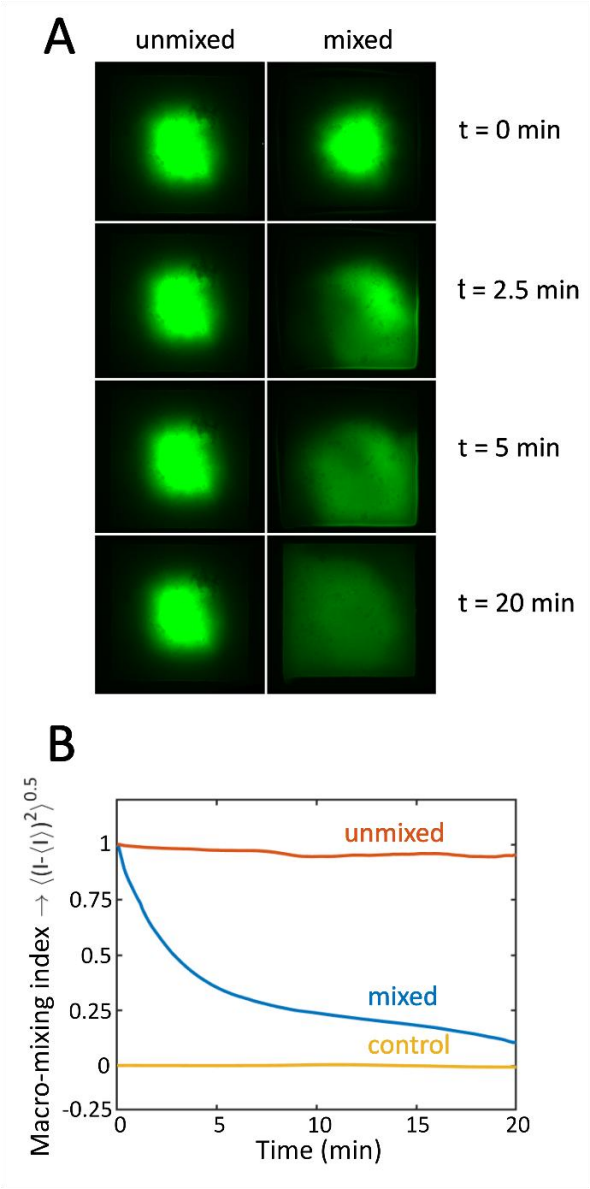

Figure 11. (A) Fluorescence images of fluorescently labeled DNA within glass fiber membranes that were either unmixed or continuously mixed with a coin motor over a 20-minute period. (B) Macro-mixing index, indicating the stirring efficiency of the platform, as a function of time for a control, mixed, and unmixed conditions. The unmixed state will have a value of 1, and if the system is fully mixed, it will have a value of 0. The red line is an unmixed experiment where minimal mixing due to diffusion occurs over the span of 20 minutes. The mixed experiment in blue indicates a well-mixed experiment by the end of 20 minutes. A 2V input was applied to the motor.

Figure 11A depicts images of fluorescently labeled DNA that was pipetted onto a membrane that is saturated with viscous RPA mastermix. Qualitatively, I find that the labeled DNA in the unmixed case does not noticeably diffuse during the 20-minute timespan. In the mixed scenario, I observe rapid mixing with a clockwise bulk flow over the 20-minute timespan. I hypothesize that the clockwise motion is due to the rotation of the ERM motor. Figure 11B presents a plot of macro-mixing index versus time for a mixed, unmixed, and *homogenized* control case. The *homogenized* case represents a fully pre-stirred control where the concentration is uniform across the entire membrane. In this experiment the labeled DNA is uniformly distributed in the mastermix, via vortexing, before applying the solution to the membrane. I observe bulk stirring efficiency by analyzing the standard deviation of the fluorescence intensity, labeled as macro-mixing index. At a value of 1, the macro-mixing index represents an unmixed experiment and 0 represents a fully mixed experiment. The *homogenized* sample has a value of nearly zero for the 20-minute timespan. In the unmixed case, the index begins at a value of 1 and marginally decreases as the fluorescent dye diffuses over time. In the mixed case, the area averaged standard deviation originates at an unmixed value of 1 and declines rapidly over the first five minutes to a value of 0.35. After 20 minutes, the index reached 0.1. These results demonstrate effective stirring using vibration-based mixing. The macro-mixing index is indicative of fluid stirring at a length scale finer than the spatial resolution of the imaging system.

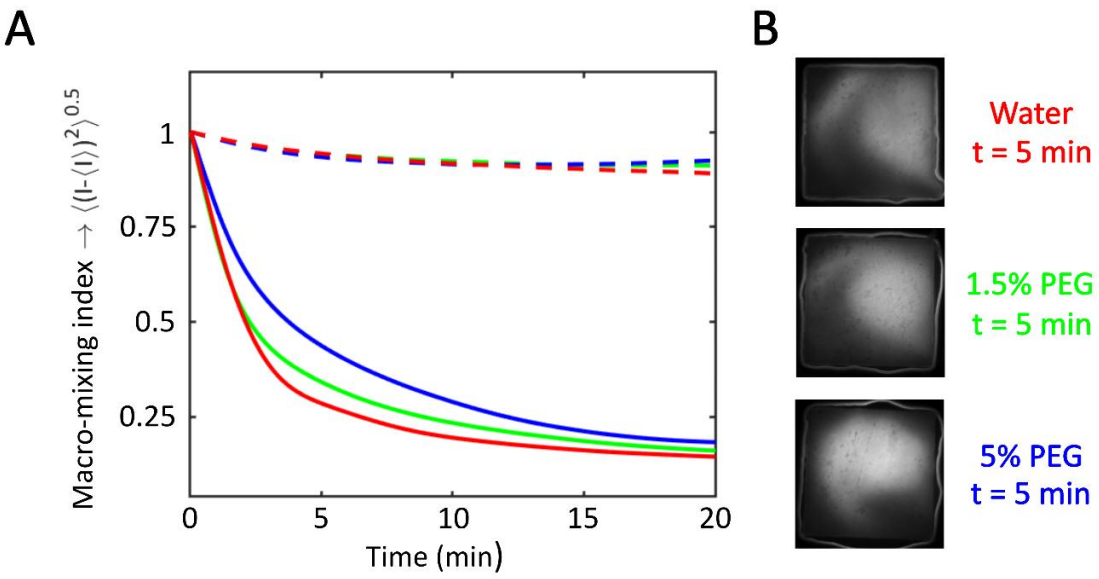

Figure 12. (A) Macro-mixing index vs time for varying PEG concentrations. Dotted lines represent unmixed and solid lines represent mixed experiments. Red line represents water only in solution, green line represents 1.5% PEG solution, and blue line represents 5% PEG solution. Lines are averaged plots from n = 3 experiments. (B) Images of mixed experiments at the 5-minute mark.

Figure 12 shows bulk stirring with varying percentages of PEG in the solution. To perform these experiments, I added 45.5 µL of solution (nuclease-free water with varying PEG percentages) to the GF/DVA membrane. I then pipetted 4.5 µL of fluorescently labeled DNA to the center of the membrane before sealing it with PCR film and inserting it into the platform. I found that for varying percentages of PEG, the platform can effectively stir the labeled DNA. At five minutes, the water only solution reached a macro-mixing index of .28, where 1 represents a fully unmixed experiment. For 1.5% PEG, the macro-mixing index reached 0.34 at the 5 minute mark. In comparison, the RPA stirring experiments done, in Figure 11, reached a similar mixing index of 0.35. Lastly for 5% PEG, the experiment dropped from an index of 1 to .44 at the end of 5 minutes. Overall, PEG (a highly viscous crowding agent) slightly affects the mixing performance of the

platform. Nevertheless, the platform is still able to sufficiently stir high viscosity solutions with all mixed experiments reaching a mixing index below 0.2 by the end of 20 minutes. These experiments do not demonstrate mixing, which requires both stirring and molecular diffusion. I use RPA reactions to provide a clear indication of mixing. RPA requires reagents, magnesium, and target to be mixed at a molecular scale to provide the amplification reaction and resulting fluorescence product. Many mixing demonstrations use colorimetric or fluorescent dyes to represent mixing.[98,99,103,124] These often provide ambiguous metrics that do not necessarily indicate interaction and molecular diffusion between dyes. When using reaction-based assays, such as RPA, I am able to demonstrate clear and unambiguous mixing measurements in the form of a distinct colorimetric or fluorescent reaction product.[125–128]

2.3.2 Evaluation of Vibration Mixing Platform Parameters

To optimize the mixing platform for enhancing RPA reactions, I examined a range of mixing conditions, including various soft isolation materials. The isolation material can be selected to significantly increase the induced vibration amplitude of the analytical membrane by the ERM motor, causing an increase in reaction efficiency and overall fluorescence output as well as decreasing the time-to-threshold.

Figure 13A shows the bulk fluorescence as a function of time for RPA experiments with no mixing, mixing with no isolation material, and mixing with an added rubber foam isolation material. When no mixing is used, the fluorescence intensity at 15 minutes reaches around 1.5 units (a.u.). When I apply 2V to the coin cell motor to generate vibration, mixing increases and results in a fluorescence intensity of 7.2 a.u. at 15 minutes, as shown in blue in Figure 13A. Compared to an unmixed reaction, the mixed experiment with isolation foam increases overall fluorescence output

by 14.4 times and reduces time-to-threshold by 5.7 minutes. This data shows that mixing enhances RPA reactions and using isolation materials results in greater mixing compared to a rigid attachment to the plate.

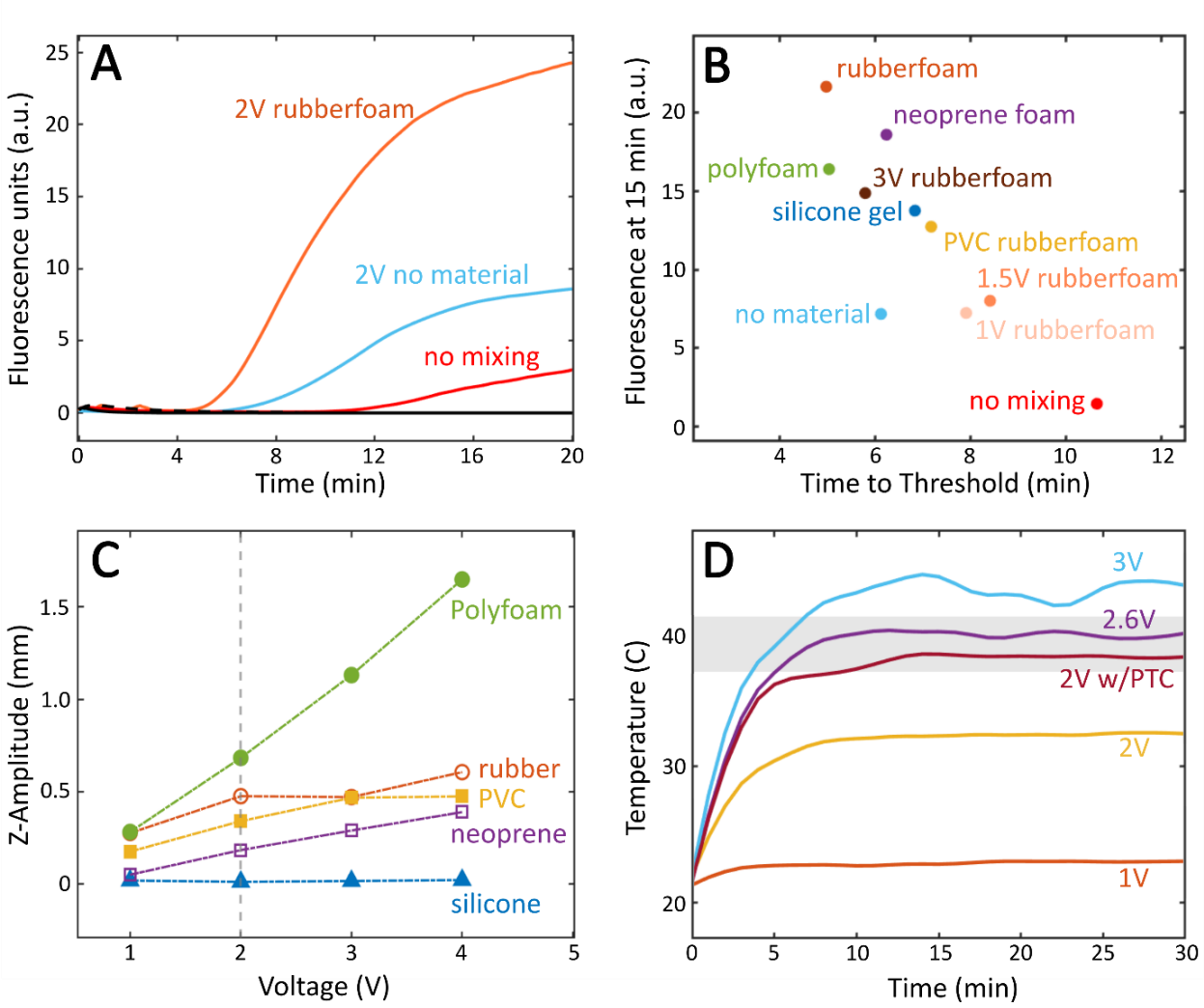

Figure 13. (A) RPA (200 copies HIV DNA per reaction) results for no mixing (red), mixing with no isolation material (blue), and mixing with rubber foam isolation material (orange). (B) RPA (200 copies HIV DNA) results for various isolation materials. Materials without a voltage label use a 2 volt motor input. (C) Vibrometer results for z-amplitude at edge of motor for various isolation materials. The z-amplitude motion is a metric used to analyze optimal isolation material. Grey dashed line at 2 volts represents motor input voltage used for majority of the screened

isolation materials in Figure 11B. (D) Temperature profiles for the platform at motor inputs from 1 - 3 V. With a PTC added to the system, the 2V motor input increases the temperature profile by 2 ºC from 10 - 12 minutes and the PTC maintains a steady temperature profile within RPA conditions (grey shading).

Figure 13B depicts the RPA time-to-threshold versus the area average fluorescence at 15 minutes for varying motor inputs and isolation materials. Ideally, RPA reactions will exceed the threshold rapidly (short times) and yield high fluorescence (upper left-hand corner). I screened five off the shelf isolation materials that are used to reduce vibrations to determine which material provided the best RPA results in terms of time-to-threshold and overall fluorescence product. Compared to the unmixed and no material mixed reaction, the isolation materials significantly improved overall fluorescence and moderately improved time-to-threshold results. I observed that the silicone gel and PVC based rubber foam materials performed similarly in terms of time-to-threshold (around 7 minutes) and endpoint fluorescence at 15 minutes (around 13 a.u.). I observed a moderate improvement in time-to-threshold and endpoint fluorescence for the polyfoam and neoprene material as well. Depending on the assay used, how the platform is configured or integrated into a larger device, or what materials are used for the device, these results will likely change. For this assay, I chose the rubber foam material as it provided the most consistent results while reducing the time-to-threshold and significantly improving the overall fluorescence.

Figure 13C shows the maximum z-amplitude of the coin motor as a function of the motor driving voltage for five materials. These results indicate that the amplitude increases with increasing driving voltage and that foam materials produce higher z-amplitudes for a given driving voltage. I hypothesize that a low stiffness insulation material acts as a loose spring in a mass-spring system and produces a pronounced rocking motion in the z-axis, perpendicular to the face of the motor,

when the ERM motor spins in-plane. As a result of the rocking motion, I expect the outer edge of the motor to have the largest amplitude delta. Out of the materials tested, the rubber foam had a high z-amplitude and provided the best RPA performance in terms of time-to-threshold and fluorescence signal output.

RPA reactions require a temperature of 37 - 42 ºC for optimal reaction kinetics.[26,129] I achieve this in the system using a PTC heater in combination with heat released from the coin cell motor. The PTC element is a self-regulating heater that can maintain a constant temperature. I observed that with the PTC added into the system, I can achieve consistent RPA results. Figure 13D shows the temperature of the motor surface as a function of time. The data demonstrates that when 4V is applied to the PTC heater and 2V is applied to the coin cell motor, 38 ºC is achieved with little temperature variation when the system reaches its steady state. To ensure all experiments are within the RPA temperature window, I monitor the temperature using a thermocouple before and after each experiment.

I additionally ran mixing conditions with the rubber isolation foam for a motor input range of 1 - 3 Volts, see Figure 13B. For each motor input, I adjusted the PTC input voltage to reach a temperature of 38 ºC at the start of each experiment. With higher motor input, I expected to achieve more mixing and as a result, an improved fluorescent output. However, I found that with 3 Volts applied to the motor with the PTC, it had a much lower endpoint fluorescence than the 2V motor input. The 2 Volt motor input with the rubber foam insulation material again had the fastest time-to-threshold and highest fluorescence intensity. I hypothesize the lower RPA reaction for the 3V motor is due to the difficulties in maintaining ideal RPA temperature at higher motor inputs and possible reduced contact to the RPA membrane due to increased vibration. The tests indicate that the highest amplification results came from a 2 Volt motor input, 0.08 Watts, and using rubber

foam insulation material, which was used as the condition for all the other experiments shown in this work. For the 20-minute duration of the experiment, the motor usage is 0.027 Watt-hours or equivalent to ~1.1% of the capacity of two AA batteries connected in series.

2.3.3 Limit of Detection for Homogenized RPA

Here I study the impact of mixing on the limit of detection of RPA reactions in membranes. In this case, the DNA target, RPA reagents, and magnesium are stirred in a tube, *homogenized*, and then pipetted onto a membrane. I performed membrane experiments for mixed and unmixed reactions for 10 - 200 copies and 10 - 30,000 copies per reaction, respectively. Figure 14A illustrates the initial distribution of reagents within the membrane and fluorescence images of mixed and unmixed reactions after 20 minutes of incubation at 38 ºC. Figure 14B depicts the area averaged fluorescence for RPA reactions as a function of time for a range of DNA target concentrations in mixed and unmixed states. The results show that RPA fluorescence begins to increase above the baseline level after 5 - 8 minutes. The reaction proceeds until 14 or more minutes before the fluorescence output asymptotes. This data shows that mixing results in reactions occur sooner and to a greater extent due to significant improvement in reaction efficiency.

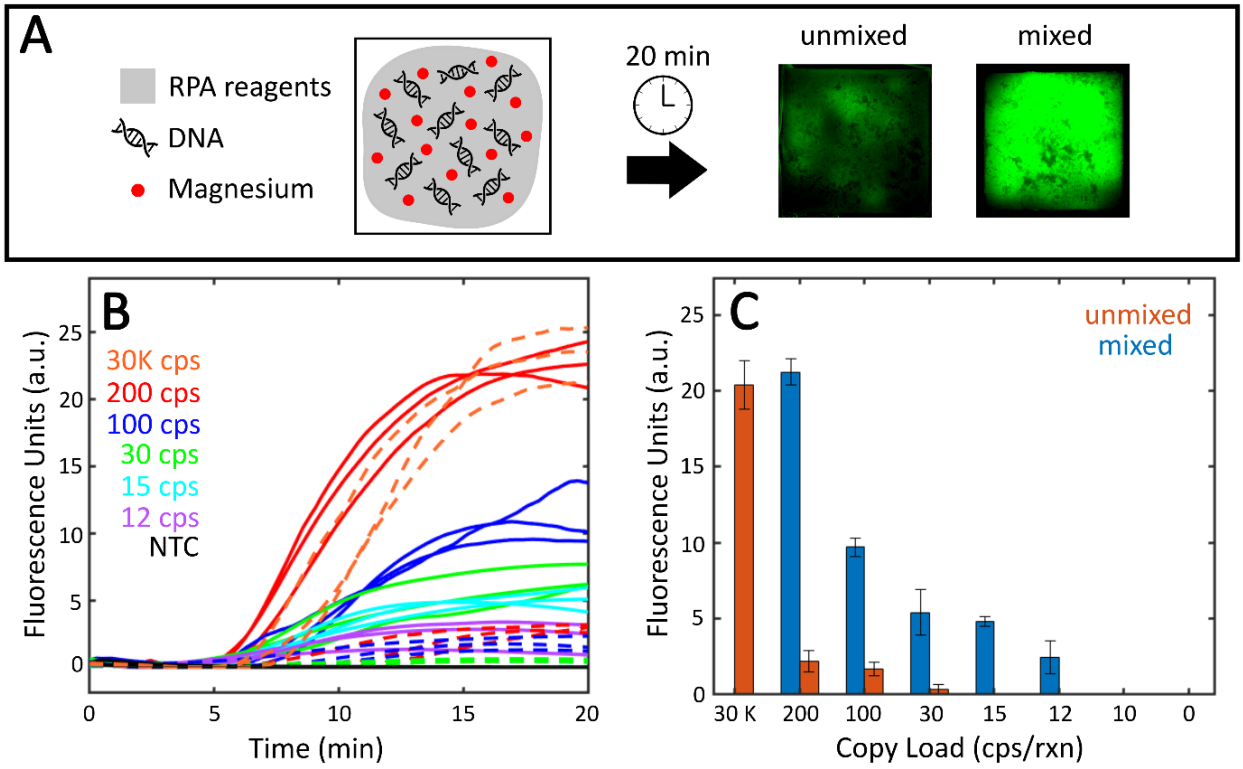

Figure 14. (A) Schematic of distribution of RPA reagents, target, and magnesium at the start of the experiment. Fluorescence images for unmixed and mixed results after 20 minutes for 200 copies HIV DNA. (B) Bulk fluorescence as a function of time for unmixed (dashed lines) and mixed (solid lines) reactions. Color indicates specific copy number. Black lines represent no template controls (NTC) for both mixed and unmixed configurations. For unmixed experiments, 30 - 30,000 copies per reaction can be seen from (dashed green to dashed orange respectively). For mixed reactions, 12 - 200 copies per reaction is seen from (solid purple line to solid red line respectively). (C) The area averaged fluorescence after 15 minutes for mixed and unmixed reactions for n = 3. Red represents unmixed reactions while blue bars represent mixed reactions. 10 and 0 copies per reactions did not amplify for both mixed and unmixed experiments and therefore did not have any noticeable bar.

Figure 14C shows the area averaged fluorescence after 15 minutes for mixed and unmixed reactions with varying input copy numbers. This data shows that fluorescence is greater for higher

input copies and when mixing is employed. The mixed reactions exhibit 5 to 16 times greater fluorescence output than the unmixed cases, depending on respective input copy number. The time-to-threshold for positive mixed reactions is on average 4.7 minutes less than in the unmixed case. The limit of detection for mixed experiments is 12 copies per reaction with all 3 experiments amplifying. In comparison, the limit of detection for unmixed experiments is 77 copies per reaction, determined using probit analysis (see Figure 15). To emphasize the degree to which mixing improves paper-based RPA, I included unmixed reactions with high input copy numbers, and I find that mixed reactions at only 200 copies yield comparable output fluorescence and faster times to threshold than unmixed reactions at 30,000 input copies. In summary, mixing improves the fluorescence output, the time-to-threshold, and the limit of detection of RPA reactions in porous substrates.

A

outcome	copies
0	0
0	0
0	0
0	15
0	15
0	15
0	30
1	30
1	30
0	60
1	60
1	60
1	100
1	100
1	100
1	200
1	200
1	200

B

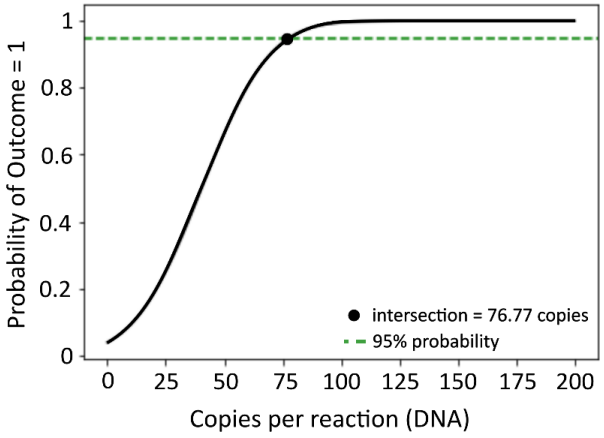

Figure 15. Table A: Binary outcomes for tested copy numbers on unmixed RPA reactions with DNA and MgOAc integrated into RPA reagent and buffer (Fig 13b). The value of 1 represents a

positive result and 0 represents a negative result. B: Probit model results. At a 95% probability of success, the LOD is approximately 77 copies per reaction of DNA for unmixed reactions in Figure 13B.

To determine the limit of detection for the unmixed reaction in Figure 14, I used a probit analysis to find the approximate copy number that corresponds to a 95% outcome probability. For both 30 and 60 copy reactions, only two of the three experiments were positive reactions. All positive and negative reactions are based on the overall bulk fluorescence with the threshold set as the average of the NTCs plus 3 standard deviations. Based on the probit model, the LOD for unmixed reactions is around 77 copies per reaction for HIV DNA.

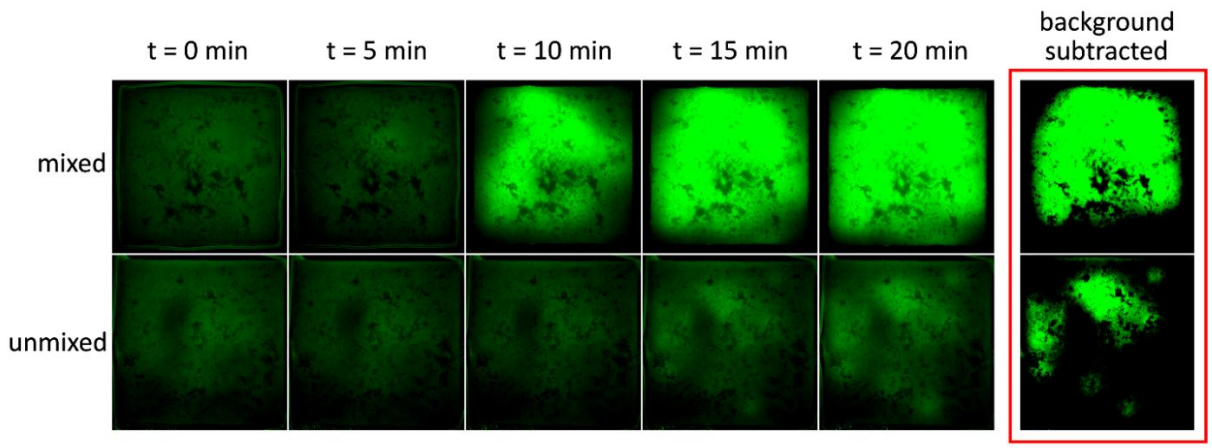

Figure 16. Top row: Images of progression of mixed, homogenized, RPA from 0 - 20 minutes. Bottom row: Image of progression of unmixed, homogenized, RPA from 0 - 20 minutes.

Figure 16 displays the image progression of mixed and unmixed *homogenized* RPA experiments. The images for t = 20 minutes are also seen in Figure 14A. Boxed in red, are the background subtracted images for t = 20 minutes. Here I find that the mixed reactions can be easily seen with and without background subtraction. However, for the unmixed reactions, amplification is much

more difficult to see unless the background is subtracted, or the image contrast is significantly increased.

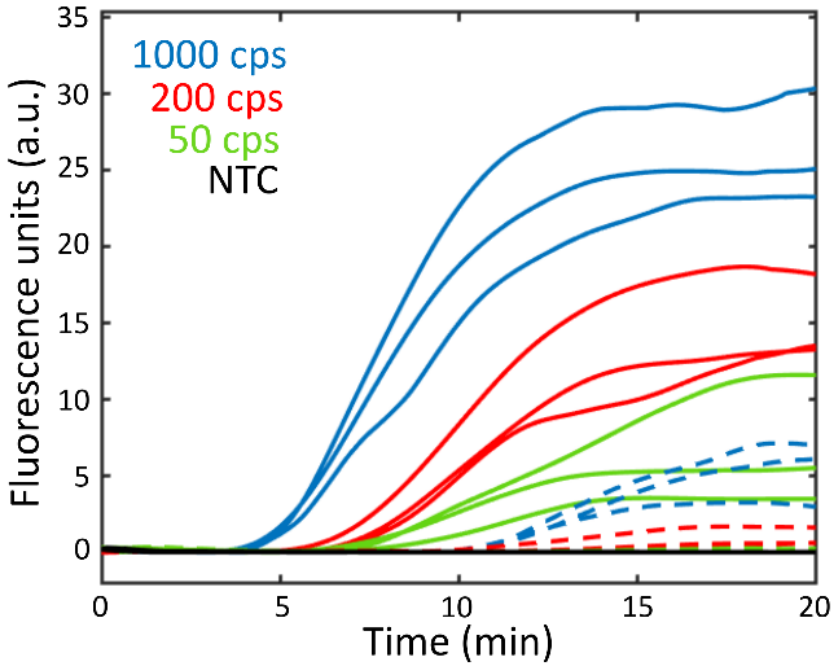

Figure 17. HIV RNA results for 1000, 200, and 50 copies per reaction. Solid lines represent mixed reactions, and dashed lines represent unmixed reactions. Black lines represent no template controls (NTCs).

Many viruses, such as HIV, have RNA genomes which are difficult to amplify because RNA is fragile and requires an additional reverse transcription step. To observe if the platform improves single-step reverse transcription RPA, I conducted experiments with and without mixing at 50, 200, and 1,000 HIV RNA copies per reaction. Figure 17 shows RT-RPA fluorescence as a function of time. For 1,000 copies of RNA per reaction, the mixing increased the fluorescence output more than 6 times higher than the unmixed experiments. The time-to-threshold also decreased by 5 minutes. For 200 copies, the endpoint fluorescence output for mixed experiments is more than 20

times higher than unmixed experiments. At a low copy reaction of 50 copies of RNA, all mixed experiments amplified whereas for the unmixed experiment, only two out of three experiments amplified. These experiments correlate well with the DNA experiments and demonstrate improved LOD, overall fluorescence output, and time-to-threshold values with continuous mixing.

2.3.4 Mixing Results of Isolated RPA: Spatially Separated Magnesium and Target

In many POC devices, sample preparation requires integration of purified target into an amplification or detection reaction. As a result, target and other additional components, like magnesium cofactor that is typically added last, may not be well mixed with the rest of the reactants in the assay. RPA reactions in membranes are especially challenging because of the high viscosity and porous membranes. The high viscosity RPA mastermix results in lower diffusion rates when compared to reactions of other NAAT chemistries, such as LAMP. Membranes such as glass fiber, further reduce effective diffusion due to various factors, including its pore structure (porosity and high tortuosity).[130–132] To examine this scenario of spatially separated reactants, I performed *isolated* RPA experiments with target and magnesium separately applied to RPA reagents, as shown in Figure 18A.

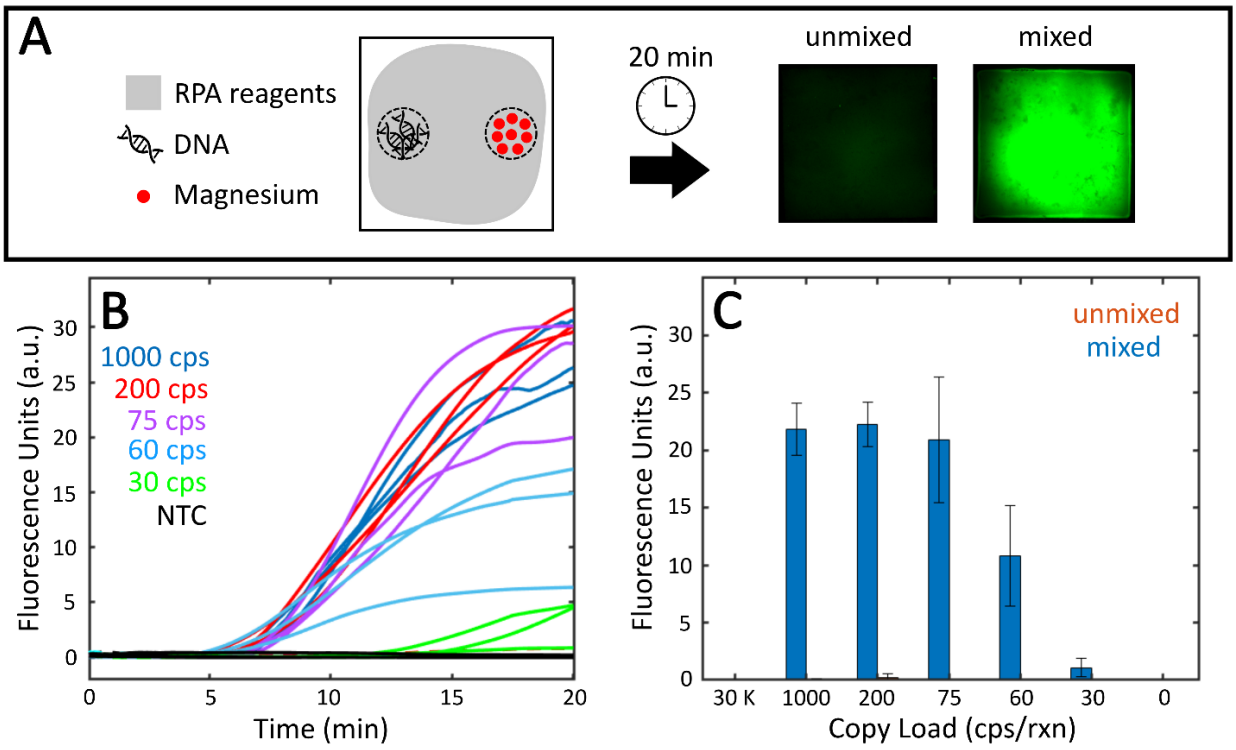

Figure 18. (A) Depiction of distribution of RPA reagents, target, and magnesium at start of experiment. Fluorescence images for unmixed and mixed results at 20 minutes for 200 copies HIV DNA. (B) Bulk fluorescence results for unmixed reactions (dashed lines) and mixed reactions (solid lines). Color indicates specific copy number. Black lines represent the no template controls (NTC) for mixed and unmixed reactions. (C) Area averaged fluorescence (n = 3) at 15 minutes for mixed and unmixed reactions.

Images of membrane *isolated* RPA reactions for the mixed and unmixed conditions for 200 copies of HIV DNA after 20 minutes of heating at 37 ºC, are shown in Figure 18A. The mixed reactions resulted in high fluorescence output while the unmixed reactions did not produce any. This indicates the importance of mixing in reactions that have spatially separated reaction components. Figure 18B presents the bulk fluorescence as a function of time for the mixed and unmixed conditions at various input copy numbers of DNA. The data shows that the average fluorescence

for unmixed reactions does not exceed the background level except for one weak reaction at 200 copies per reaction. The background fluorescence for these experiments was less than that of assays that were *homogenized* with target and cofactor before being deposited on the membrane (see Figures 14 and 17). The low initial background is the reason the overall bulk fluorescence is sometimes higher for these experiments than in the *homogenized* reactions. When mixing is used, RPA amplifies in 6 minutes and increases exponentially, similar to typical in-tube RPA experiments.

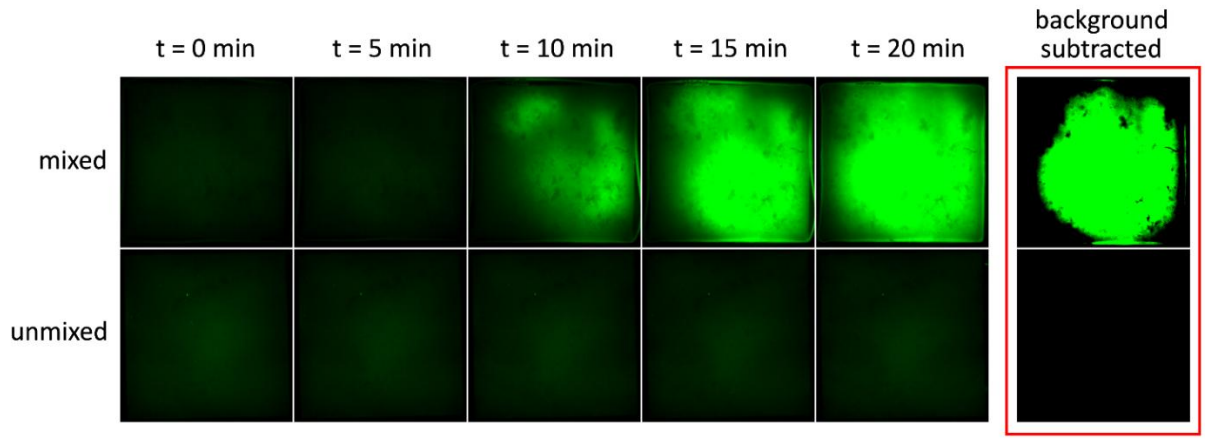

Figure 19. Top row: Images of progression of mixed, isolated, target and magnesium RPA from 0 - 20 minutes. Bottom row: Image of progression of unmixed, isolated, target and magnesium RPA from 0 - 20 minutes.

Figure 19 displays the image progression of mixed and unmixed separated target and magnesium RPA experiments. The images for t = 20 minutes are also seen in Figure 18A. Figure 18C depicts the area averaged fluorescence after 15 minutes with n = 3. The unmixed case shows almost no fluorescence while the mixed case indicates strong fluorescence that increases with number of copies of target DNA. I tested 30,000 copies for the unmixed scenario to see if increasing copy

numbers would result in amplification; in this experiment, all three experiments did not amplify. This underscores that in *isolated* RPA reactions without mixing, limited diffusive mixing occurs between target, magnesium, and RPA reagents during the 20-minute incubation. This suggests that for similar scenarios where uneven integration of target and cofactor are introduced, continuous mixing can effectively distribute separate components and significantly improve membrane amplification results.

2.3.5 Vibration Based Mixing with No Additional Heating

I show that the coin motor can generate sufficient heat to bring the *homogenized* RPA reactions to the optimal temperature range (37 - 42 ºC). Removing the PTC heater may reduce the cost, complexity, and power requirements for the system. Instead of a heater, amplification reactions could use a mixing module that can both mix and incubate a reaction. In Figure 13D, I show that the temperature profile can reach 37 - 42 ºC in the absence of the PTC heater with a driving motor voltage of 2.4 - 2.6 volts, 0.1 - 0.12 Watts. When compared to the system with the PTC, this configuration requires more time to heat to RPA temperatures and has higher temperature profile instability as the motor input is increased.

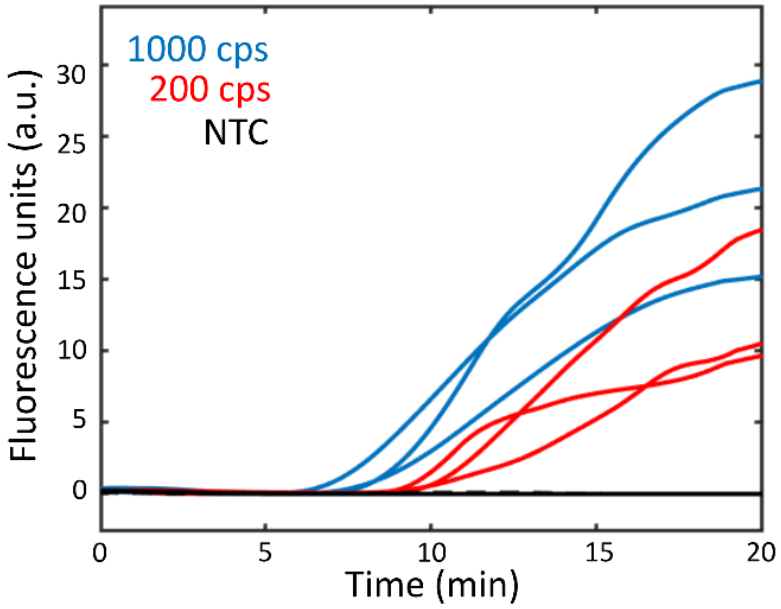

Figure 20. Bulk fluorescence plots for 1000 and 200 copies HIV DNA for vibration-based mixing with no PTC. Solid lines represent mixed experiments, dashed lines represent unmixed experiments, and black lines represent no template controls (NTC).

Figure 20 shows the area-averaged fluorescence as a function of time for 200 and 1,000 copies of HIV-1 DNA in RPA reactions conducted in membranes with mixing and heat generated by a coin motor. In this demonstration, *homogenized* RPA is deposited onto a GF/DVA membrane. In unmixed reactions where no heat is generated, there is no amplification seen over the 20-minute duration of the test. All six experiments conducted with the coin cell motor running resulted in positive amplification. These experiments with no PTC heater exhibit lower amplification fluorescence compared to a mixed scenario with a PTC (Figure 14) and have higher variability between tests. This is likely due to the significantly smaller heating area and non-regulating heating, typically provided by the PTC.

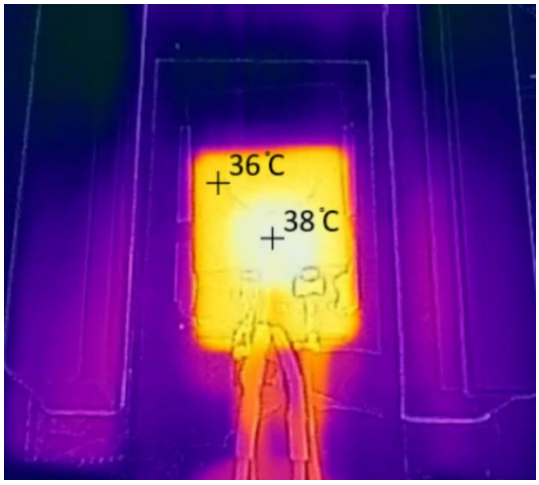

Figure 21. Forward-looking infrared (FLIR) thermal imaging of the motor and PTC on with a 2V and 4V input, respectively. With the motor on, the motor face increases to 38 ºC while the PTC remains at 36 ºC.

Figure 21 shows thermal imaging reporting the temperature profile of the motor and PTC on. With a 2V input to the motor, the motor face increases from 36 ºC to 38 ºC. The surrounding area of the PTC remains at 36 ºC and provides additional surface area to maintain RPA temperature and improve temperature stability over time. Without the PTC, only the motor area is heated to 38 ºC. The motor-only assembly is more susceptible to temperature fluctuations and requires a slightly longer heat up time to reach RPA temperatures. These temperatures were confirmed using a thermocouple (80BK-A, Fluke Networks, USA) attached to the surface of the motor face and PTC.

With the PTC added in the system, the larger PTC area provides a lower surrounding temperature of 36 ºC with the motor head having a temperature of 38 ºC when turned on (see Figure 21). In comparison, heating solely provided by the motor provides a small surface area, approximately 4.4 times smaller than the area of the PTC and does not have any self-regulating heating ability. The PTC adds a larger overall area with sufficient heating and prevents significant temperature

fluctuations on the motor face due to its self-regulating behavior, providing more consistent results. Compared to unmixed reactions with PTC heating (dashed lines in Figure 14B), mixing with no PTC still provides significantly improved amplification results. These experiments demonstrate the feasibility of performing mixed RPA without any dedicated heat source.

2.4 Conclusions

I present a vibration-based platform to improve RPA reactions in porous membranes. When continuously mixed, I observe a significant improvement in limit of detection, time-to-threshold, and fluorescence signal output for HIV-1 DNA and RNA. For DNA targets, I report a limit of detection of 12 copies per reaction (6.4 times improvement in LOD), a reduction in time-to-threshold from an average of 9.93 minutes to 5.17 minutes, and an overall fluorescence output up to 16 times brighter when compared to unmixed experiments. I show that when the target and magnesium cofactor are initially spatially separated, RPA reactions do not occur unless active mixing is employed. These results also demonstrate amplification without any additional heating module. The mixing device significantly increases endpoint fluorescence in all conditions.

The high viscosity of RPA, due to its PEG crowding agent, and the porosity of the membrane both contribute to lower diffusion rates in paper-based RPA. The high viscosity reduces diffusion due to Stokes-Einstein diffusivity, and the glass fiber membranes reduce the effective diffusivity due to its porosity (ω) and tortuosity.[130,132] In the simplest scaling model for porous media, the effective diffusivity scales as, $D_{eff} = \omega^{3/2} D$.[131] With mixing, I am able to address the lowered effective diffusion and improve reaction efficiency of paper-based RPA. While RPA is the focus of this work, I hypothesize that continuous active mixing may enhance other paper-based isothermal

nucleic acid amplification assays, such as LAMP or strand displacement amplification (SDA). I observed that diffusive mixing in glass fiber membranes is limited even in the absence of the PEG crowding agent (see Figure 12); therefore, this mixing platform may improve the efficiency of paper-based NAATs that do not feature highly viscous buffer conditions.

This chapter shows that mixing modules for membrane-based NAATs can be leveraged for low-cost, point-of-care nucleic acid amplification to provide robust tests with high reaction efficiency and fluorescence output. Effective mixing can improve clarity of results, consistency at lower copy numbers, and further reduce costs in detection equipment by increasing reaction output (i.e., fluorescence). None of the experiments required intermediate user steps after depositing the reaction on the membrane as mixing and heating was triggered remotely and remained on for the entire duration of the experiments. This work shows that reagents that are initially spatially separated (e.g., target and cofactors) can be mixed effectively, which may be a helpful tool when integrating on-chip sample preparation steps with nucleic acid amplification and detection. Future work is needed to compare with other mixing methods, compare vibration devices such as tweeters or PZT transducers, observe output with low-cost sensors and filters, explore mixing for enhanced paper-based LAMP, and integrate sample preparation with the platform.

Chapter 3 Bloodborne Virus Detection from Human Plasma using Minimal Sample Preparation and Scalable In-tube and Membrane Recombinase Polymerase Amplification

3.1 Motivation

Sample preparation typically requires pathogen lysis, denaturation of DNases and RNases, and the purification of target DNA or RNA from sample inhibitors.[6,7] Despite providing highly purified nucleic acid targets for amplification, solid phase extraction and similar protocols can be difficult to implement in a POC environment due to the need for multiple buffer exchanges, requirement of concentrated toxic chaotropic salts that can inhibit amplification, and long runtimes of 30 - 60 minutes.[6]

Blood is an essential sample type for molecular testing, as many pathogens can be found suspended in plasma or residing in host cells, and is a relatively consistent sample.[39] However, blood samples pose major challenges to POC NAATs because they require stringent and complex sample preparation, can contain lower target concentrations, and include numerous inhibitors to nucleic acid amplification assays and nucleases that can degrade target strands.[133]

Blood and blood-based samples are challenging to use as they have a high concentration of ribonucleases that degrade exogeneous RNA and contain significant NAAT inhibitors like immunoglobulins, lactoferrins, and hemoglobin.[35] Blood-based testing remains a significant challenge for POC NAAT development.[37,38] Significant efforts in reducing device complexity and the associated high costs for POC NAATs are still needed for blood-based targets.

Isothermal NAATs are well-suited for POC settings as they have similar limits of detection as PCR while operating at a single temperature, thus reducing the requirement of hardware with precise temperature control. Crude, extraction-free sample preparation is an emerging strategy that reduces workflow complexity and cost for POC NAATs. While PCR is highly sensitive to sample inhibitors, isothermal amplification assay such as RPA tolerates many inhibitors and is stable at room temperature when lyophilized.[8] By using lysis and nuclease inactivation reagents that are compatible with NA amplification, users can directly amplify targets without the need for cumbersome nucleic acid extraction methods.[8] While extraction-free approaches are feasible, improvements are required to make extraction-free sample preparation compatible with RPA for BBP detection.

In this chapter, I present an extraction-free sample preparation method for in-tube and paper-based reverse transcription recombinase polymerase amplification (RT-RPA) for the detection of HIV in blood plasma samples. I use a rapid thermal incubation and dithiothreitol treatment protocol that inhibits RNases and lyses virions to enable effective RNA preservation and direct amplification without the need for complex purification steps. I then directly add the incubated sample into RT-RPA for paper-based or in-tube reactions. I demonstrate sample treatment in 5 minutes and amplification within 20 minutes. I perform RPA reactions in reaction volumes ranging from 50 to 300 µL and show that large volume reactions achieve a limit of detection (LOD) of 800 copies/mL (16 copies/reaction) for HIV-positive plasma in both paper and tube formats. I then improved the extraction-free method by increasing assay repeatability and demonstrated the improved method's broader applicability to bloodborne targets, HIV and hepatitis C. While the same protocol can be used for both assays, I found that adjusting PEG, plasma, and additive concentrations improves individual assay performance. Using the optimized extraction-free method for hepatitis C, I was

able to validate the assay with clinical samples and observe its performance with a variety of serum and plasma matrices. I ran 15 positive clinical samples ranging from genotypes 1-3, 5 as well as 5 negative patient samples and found a 100% sensitivity and 100% specificity for this preliminary evaluation. These extraction-free results highlight the potential for scalable, user-friendly, and sensitive molecular diagnostics for blood-borne diseases in resource-limited settings.

3.2 Experimental Section

3.2.1 Biological Samples

I use pooled human plasma (BioIVT, Westbury, NY, USA) and cultured HIV-1 subtype B (8E5) linearity panel stored in plasma (SeraCare, Milford, MA, USA). The 8E5 HIV virus contains a single base pair addition in the pol gene of the genome, resulting in reverse transcription-defective virus.

For HCV validation, I use synthetic DNA (gBlocks Gene Fragments, Integrated DNA Technologies, USA) that contain 978 base pairs from the 5' UTR region of the HCV genome (genotype 1). HCV RNA clinical samples were obtained by Gastrointestinal Center for Analytical Research and Exploratory Science (GiCasRes) at the University of Washington. Patient samples were originally collected from the Hepatitis & Liver Clinic at Harborview Medical Center (Seattle, USA) under ethical approval by the UW review board. All samples were obtained with written consent. Additional patient samples were purchased from SeraCare (Massachusetts, USA). All specimens were confirmed HCV-positive using the Abbott *Realtime* HCV Genotype Assay (Abbott Laboratories, Abbott Park, USA) and selected samples were quantified by UW Medicine Laboratories services (Seattle, USA), which use the Hologic Aptima HCV Quant Dx assay

(Hologic, Massachusetts, USA). For HCV validation with RNA, the samples were extracted using QIAamp Viral RNA mini kits (Qiagen, DEU). Using the manufacturer's protocol, 140 µL of serum or plasma was added to obtain 80 µL of purified RNA per sample. The eluted RNA was aliquoted and stored at -80 °C. For the extraction-free protocol, HCV samples in plasma or serum were aliquoted and stored at -80 °C. HCV-negative serum samples were obtained from individual donors from BioIVT (Hicksville, NY).

3.2.2 Sample Preparation Protocol and RNase Activity Measurements

To enable extraction-free detection of HIV positive plasma samples, I use dithiothreitol (DTT) and thermal treatment to inactivate ribonucleases. The structure of RNases is stabilized by disulfide bonds.[134] Reducing agents such as DTT break disulfide bonds, effectively destabilizing RNases and inhibiting their activity.[135] The addition of heat further relaxes the RNase structure, allowing DTT to more effectively break down disulfide bonds while concurrently lysing HIV virons.[8] Pooled human plasma is diluted 1:3 - 1:3.33 in nuclease-free water containing 7.5 - 7.7 mM dithiothreitol (DTT, Sigma-Aldrich, MA, USA). The diluted sample is incubated at 70 °C for 5 minutes, achieving viral lysis and inactivation of plasma-derived RNases.

To evaluate the sample preparation protocol, I used an RNaseAlert Substrate Detection system (Integrated DNA Technology, Coralville, IA, USA) and varied DTT concentration as well as incubation temperature. The assay employs a short RNA oligonucleotide with fluorescein and a quencher on either end. Upon cleavage, the fluorophore is separated from the quencher, resulting in a measurable green fluorescence signal. The experiments were conducted in a black 96 well plate (M9685, Corning Inc., Corning, NY, USA) and sealed with PCR film before testing. Each well contained 1x RNase Alert buffer, 10 µL RNaseAlert substrate, 26 µL sample, and water to

reach a final volume of 100 µL. Negative sample controls consisted of water only, while positive controls contain 5 µg RNase A (ThermoScientific, MA, USA). The plates are heated to 37 ºC and fluorescence was monitored to determine residual RNase activity under various treatment conditions using a plate reader (SpectraMax iD3, Molecular Devices, San Jose, CA). An initial 10 second orbital mix step is performed before running the test for 30 minutes. The excitation and emission wavelengths are set at 485 and 535 nm respectively with the photomultiplier tube gain set at a 140-millisecond exposure.

3.2.3 Tube-Based RT-RPA Reactions

For sample preparation of 50 µL reactions, 3 µL of HIV positive plasma is added to 7.7 mM DTT and nuclease-free water at a 1:3.33 ratio of plasma to diluent. The sample is incubated at 70 ºC for 5 minutes on a heat block (10153-318, VWR, US). All 13 µL of the diluted sample is then added to the RT-RPA mastermix to reach a final 50 µL volume, as shown in Figure 22. I incubated the RT-RPA reactions at 39 ºC for 20 minutes in an isothermal fluorescence reader (T16-ISO VIC, Axxin, AU) to capture real-time RT-RPA fluorescence reactions. I perform a vigorous manual shaking step after 5 minutes of incubation before placing tubes back in the reader for the rest of the 15 minutes, as per TwistDx instructions.[136] In 50 µL reactions, the RT-RPA mastermix consists of a TwistAmp exo kit lyophilized pellet (TwistDx, UK), 29.5 µL rehydration buffer, 14 mM magnesium acetate, 540 nM forward and reverse primer (Integrated DNA Technologies, USA), 120 nM exo-probe (LGC Biosearch Technologies, GBR), and 0.5 U/µL of reverse transcriptase (Agilent AffinityScript, USA). I use HIV-1 primers and probe for RT-RPA reactions developed by Lillis *et al*.[137] I included 1% w/v Triton-X and 0.04% w/v BSA additives to the RT-RPA mastermix to help stabilize enzymes from amplification inhibitors present in plasma samples.[138,139]

I also perform experiments in larger, 300 µL, reactions to achieve lower limits of detection.[75,140] For sample preparation of 300 µL reactions, 20 µL of HIV-positive plasma is added to 7.5 mM DTT and nuclease-free water at a 1:3 ratio of plasma to diluent. The sample is incubated at 70 ºC for 5 minutes and added to the RT-RPA mastermix. All 80 µL of incubated sample is added to the mastermix to reach a 300 µL reaction volume. This plasma concentration is slightly higher than that used in 50 µL reactions to simplify dilution calculations across steps. This modest increase from 6 to 6.7% did not affect the extraction-free results. In 300 µL reactions, the RT-RPA mastermix consists of 6 TwistAmp exo pellets, 177 µL rehydration buffer, 14 mM magnesium acetate, 540 nM forward and reverse primer, 120 nM exo-probe, 1% w/v Triton-X, 0.04% w/v BSA, and 0.5 U/µL of reverse transcriptase. These in-tube reactions are performed at 39 ºC in the plate reader. The 300 µL RT-RPA experiment is evenly split into two wells of a black 96-well plate. A 2 mm steel ball (TwistDx, UK) is added to each reaction well and sealed with PCR film. A 40-second orbital mix step at the highest setting is done before running the test and after 5 minutes of incubation. To generate results, I take the average of the two wells and plot the bulk fluorescence against time.

3.2.4 Paper-Based RT-RPA Reactions

In 50 µL paper-based RT-RPA experiments, I add incubated HIV sample, magnesium, and RT-RPA mastermix (prepared as described above) onto a circular 9.21 mm diameter GF/DVA pad (1835-6621, Whatman, UK) that is supported by a 2” X 3” glass slide (CA6101, Premiere, CN). I manually shake the reaction in the tube for 20 - 30 seconds to ensure homogeneous distribution of reactants before evenly pipetting the reaction onto the circular pad and sealing it with PCR film (TempPlate RT Select Optical Film, USA Scientific, USA). The glass slide is slotted into the

mixing device with PCR film in contact with the motor. The vibration motor uses a 2 Volt input, and the PTC uses a 2 - 3 Volt input.

For 300 µL paper-based reactions, I add incubated HIV sample, magnesium, and mastermix onto a 20.55 mm diameter GF/DVA circular pad that is again supported by a 2" X 3" glass slide. I manually shake the reaction in the tube before evenly pipetting it onto the circular pad and sealing it with PCR film. The glass slide is slotted into the mixing platform with the PCR film in contact with the titanium foil circle. The motor uses a 2.4 Volt input, and the PTC is set at a 3 - 4 Volt input.

For paper-based reactions, I use a vibrational mixing device, that I reported on in previous work, to provide continuous mixing of the RT-RPA reaction and enhance the amplification.[141] Using the vibration platform I see a significant improvement in paper-based reactions for this extraction-free method, Figure 24. In brief, the mixing device consists of a 3D printed assembly with an eccentric rotating mass vibrational motor (VC1234B016F, Vybronics, CN), PTC heater (PTC Heating Element, DFRobot, CN), and a rubber isolation foam (Thermwell, USA). The vibration assembly positions the RPA reaction pad, which is supported by a glass slide and PCR film, in contact with the motor and PTC to provide sufficient mixing and heating for RPA reactions, as seen in Figure 10. This device is used for both 50 and 300 µL paper-based reactions. For 50 µL reactions, the RPA pad and PCR film are in direct contact with the vibrational motor. For 300 µL reactions, I cut a 0.12 mm thick titanium foil (LiteOutdoors, CAN) into a 25 mm diameter circle and adhered it to the top of the vibration motor using epoxy adhesive (Loctite, USA). The titanium foil supports the larger 300 µL reactions, providing even heating during RT-RPA, and distributing vibrational mixing to the entire circular pad. Without the foil, mixing and heating would be localized to the 12 mm diameter of the motor.

3.2.5 Custom Buffer Tube-based RT-RPA Reactions

To enable extraction-free detection of positive plasma samples with the custom buffer formulation, I use dithiothreitol (DTT), RNase inhibitor, and thermal treatment to inactivate ribonucleases. Samples are diluted 1:3 in nuclease-free water containing 10 mM dithiothreitol (DTT, Sigma-Aldrich, MA, USA) and 1U/µL RNasin Plus Ribonuclease Inhibitor (N2611, Promega, Wisconsin, USA). The diluted sample is incubated at 70 °C for 5 minutes on a heat block (10153-318, VWR, USA), achieving viral lysis and inactivation of plasma-derived RNases. RNase inhibitor is stable against oxidation and heat, with activity up to 15 minutes at 70 °C.

For HIV detection, 16 µL of diluted incubated sample is added to RT-RPA mastermix to reach a final 50 µL volume. The RT-RPA mastermix for the final 50 µL volume consists of a TwistAmp exo kit lyophilized pellet (TwistDx, UK), 12.5 µL of the HIV custom concentrated buffer, 14 mM magnesium acetate, 540 nM forward and reverse primer (Integrated DNA Technologies, USA), 120 nM exo-probe (LGC Biosearch Technologies, GBR), 1% w/v Triton X-100, and 0.5 U/µL of reverse transcriptase (Agilent AffinityScript, USA). I use HIV-1 primers and probe for RT-RPA reactions developed by Lillis *et al*.[137] The HIV custom concentrated buffer is a 4X solution consisting of 140 mM Tris Acetate pH 8, 400 mM Potassium Acetate, and 16% w/v 35,000 MW PEG. When added into RPA, the final concentration for the 50 µL reaction volume is 35 mM Tris Acetate, 100 mM Potassium Acetate, and 4% w/v 35,000 MW PEG.

For HCV detection, 16 µL of diluted incubated sample is added to RT-RPA mastermix to reach a final 50 µL volume. The RT-RPA mastermix for a final 50 µL volume reaction consists of a TwistAmp exo kit lyophilized pellet, 12.5 µL of the HCV custom concentrated buffer, 14 mM magnesium acetate, 420 nM forward and reverse primers, 120 nM exo-probe, 125 ng/µL T4 gene

32 protein (NEB, Massachusetts, USA), 0.5 U/µL RNasin Plus, and 2 U/µL of SuperScript IV reverse transcriptase (Thermo Fisher Scientific, USA). The custom concentrated buffer for HCV is a 4X solution consisting of 140 mM Tris Acetate pH 8, 400 mM Potassium Acetate, and 12% w/v 35,000 MW PEG. When added into RPA, the final concentration for the 50 µL reaction volume is 35 mM Tris Acetate, 100 mM Potassium Acetate, and 3% w/v 35,000 MW PEG.

For assay optimization, 12 - 28 µL of diluted incubated sample is added with RT-RPA mastermix to reach a final 50 µL reaction volume. The mastermix for the 50 µL reactions consists of a TwistAmp exo kit lyophilized pellet, 12.5 µL of the custom concentrated buffer, 14 mM magnesium acetate, 420 - 540 nM forward and reverse primers, 120 nM exo-probe, 0 - 1% w/v detergent, 0 - 125 ng/µL T4 gene 32 protein, 0 - 0.5 U/µL RNase inhibitor, and reverse transcriptase.

To run the reactions, I incubated the RT-RPA reactions at 39 ºC for 20 minutes in an isothermal fluorescence reader (T16-ISO VIC, Axxin, AU) to capture real-time RT-RPA fluorescence reactions. I perform a vigorous manual shaking step after 5 minutes of incubation before placing tubes back in the reader for the rest of the 15 minutes, as per TwistDx instructions.[136]

3.2.6 Imaging and Data Analysis

I image paper-based reactions using an epifluorescence microscope (AZ100, Nikon, JPN) and illumination system (X-Cite exacte, Excelitas Technologies, USA) with a 1X objective and 35 mm field of view. I use an epifluorescence filter cube set (XF100-2, Omega Optical, LLC., USA) and CMOS camera (Prime BSI Express, Teledyne, Photometric, USA) to capture grayscale images every 5 seconds for 20 minutes. I use an image analysis algorithm (MATLAB, MathWorks, USA) to calculate the fluorescence intensity over the full 20 minutes. For analysis of membrane

reactions, I imaged the entire pad area. I set a region of interest as the active membrane. For 50 µL reactions the ROI was a 9.2 mm diameter circle and for 300 µL reactions it was 20.6 mm. I perform a background subtraction to eliminate auto-fluorescence from the reaction pad, PCR film, glass slide, and initial nonspecific assay interactions. For each specific timepoint, I calculated the total fluorescence by summing the intensities over the ROI. The intensity over the entire circular pad is averaged and plotted against time. To determine the threshold between positive and negative reactions for all experiments, I set it as the averaged intensity of the no template control (NTC) experiments plus three standard deviations. I use this threshold for all amplification figures.

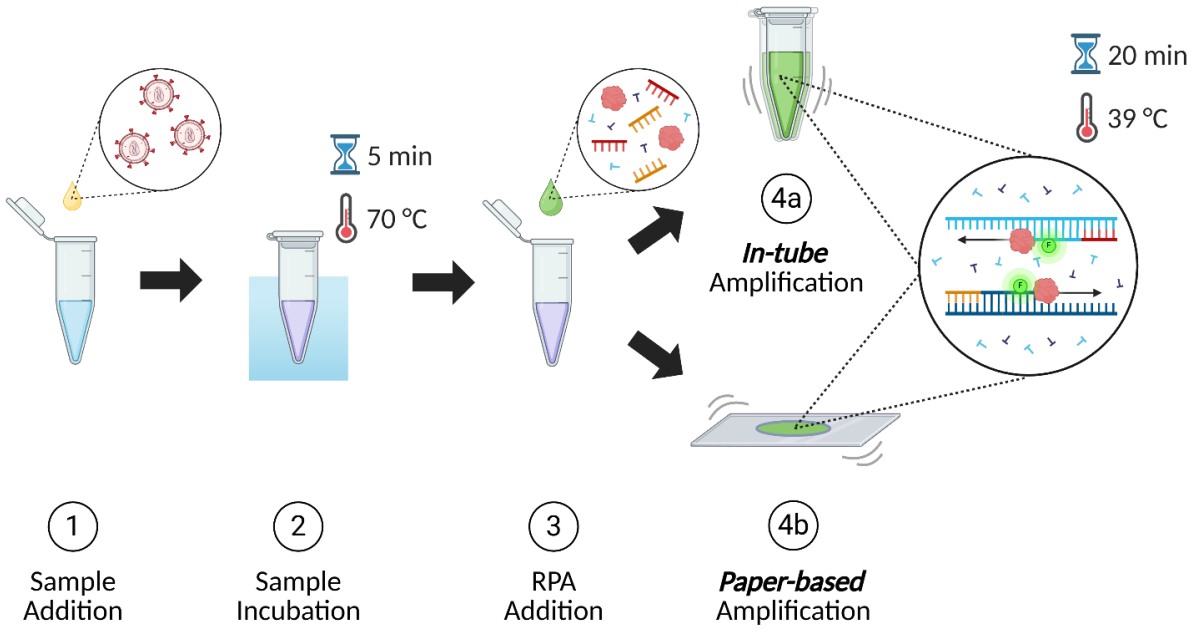

Figure 2. Overview of the extraction-free sample preparation for HIV in plasma. First, plasma is added to the diluted DTT solution. The sample is incubated for 5 minutes at 70 ºC and added to the RT-RPA reaction solution. The reaction is incubated at 39 °C for 20 minutes on a benchtop fluorometer or in a paper membrane set on a custom vibration mixing and heating platform (see Figure 9) and imaged with a fluorescence microscope. Tube-based reactions include a vigorous mix step after 5 minutes of incubation as recommended.[136] For paper-based reactions, continuous

vibration-based mixing is done on a mixing and heating platform to continuously redistribute RPA reagents and improve paper-based reaction efficiency.[141]

3.3 Results and Discussion

I demonstrate a simple, rapid, and extraction-free sample preparation strategy for tube and paper-based RT-RPA. For this extraction-free approach, diluted pooled blood plasma or serum is incubated with DTT and optionally RNase inhibitor. The thermal and chemical process inhibits ribonucleases (RNases) as well as lyses HIV virions. The resulting plasma lysate is then directly added to RT-RPA for tube or paper-based amplification. I validate the sample preparation method for inactivation of RNases using the RNase Alert assay. I show that HIV can be amplified in tube or paper-based formats, and I demonstrate that this approach exceeds the recommended LOD requirements for HIV-1 testing using rapid, extraction-free sample preparation. I additionally demonstrate a custom concentrated buffer that is compatible with RT-RPA for HIV and hepatitis C assays. Using the custom concentrated buffer, I validated the increased flexibility of the extraction-free method by enabling higher plasma percentages and optimized the extraction-free method for both HIV and hepatitis C by screening additives such as PEG, RNase inhibitor, and detergents. With the optimized extraction-free method for hepatitis C, I validated the assay on 20 clinical samples and found positive amplification for the lowest viral load clinical sample of 50,000 IU/mL.

3.3.1 Sample Preparation Validation

I first focus on demonstrating successful HIV viral lysis and inactivation of RNases in a short, thermal incubation step. To achieve this, I studied the RNase inactivation step, as there are high

concentrations of RNase enzymes in blood plasma that degrade RNA.[35] I studied various DTT concentrations and incubation temperatures to develop a sample preparation method that sufficiently inhibits RNase activity in plasma samples. I then paired this sample preparation method with 50 µL tube-based RT-RPA reactions to detect HIV from plasma.

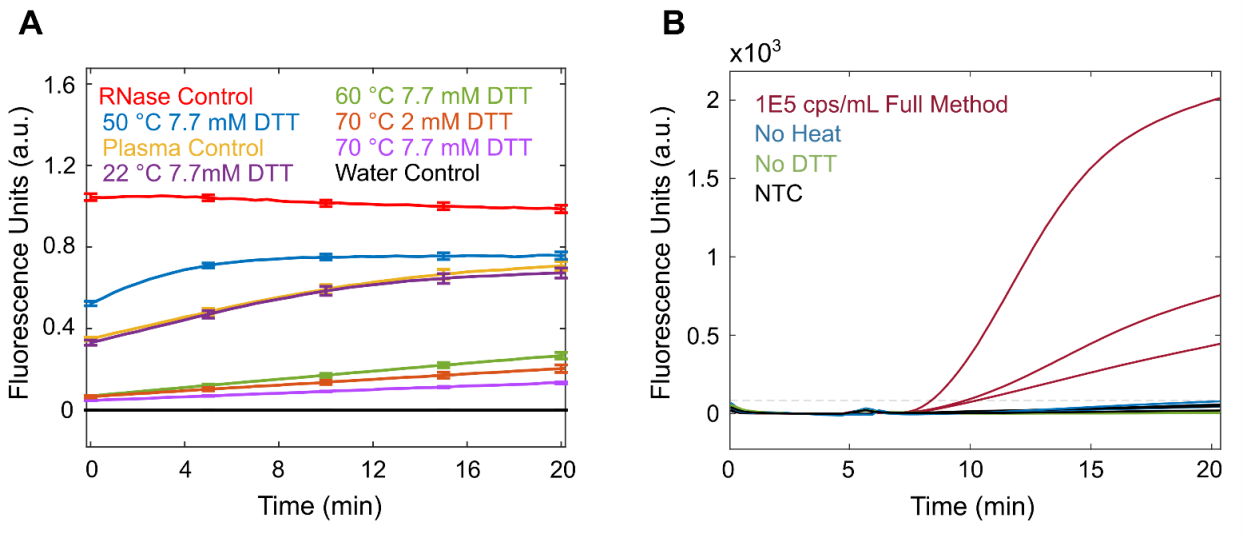

Figure 23. I monitored RNase activity of plasma samples after a 5-minute, heated incubation with DTT to determine the most effective DTT concentration and incubation temperature required to deactivate RNases in plasma. (A) Fluorescence of the RNase Alert assay is plotted as a function of time for various DTT concentrations and incubation temperatures. Sufficient RNase inhibition was observed with 7.7 mM DTT incubated at 70 ºC for 5 minutes. Without the incubation method, no heat, or no DTT, there is little to no RNase inhibition. For all experiments, n = 3 with error bars representing standard error. (B) I performed RT-RPA reactions of samples that underwent extraction-free sample preparation with both thermal and DTT treatment, without DTT treatment, or without thermal treatment. Using the full method, I show positive amplification for 1E5 copies/mL HIV plasma samples. Without the full initial incubation method (i.e., no heat, or no DTT), little to no amplification is observed due to the degradation of the target HIV-1 RNA by RNases. The dashed line represents the threshold.

Figure 23A shows the RNase Alert activity of plasma lysates under various DTT concentrations and incubation temperatures. When RNases are present, the RNA oligonucleotide is cleaved, and fluorescence intensity increases rapidly with time. The RNase control experiments represent the maximum fluorescence in the assay, or what would result in experiments with strongly active RNases. Note that significant increase in fluorescence occurs prior to time zero because there is finite time required to mix the components and begin the fluorescence read. I examined incubation temperatures ranging from 22 - 70 ºC and DTT concentrations between 2 - 7.7 mM (final concentration of 0.5 - 2 mM DTT). The results show that incubating at higher temperatures improves RNase deactivation, resulting in lower fluorescence slopes. At temperatures greater than 70 ºC I observed sample coagulation that inhibited pipetting and sample manipulation. Additionally, significant RNA degradation is known to occur at elevated incubation temperatures.[142] To mitigate sample coagulation while effectively inhibiting RNases, I set the plasma-to-buffer ratio to roughly 1:3 and identified 70 ºC as the minimum temperature required for a 5-minute incubation period. For the buffer, I used nuclease-free water with 7.7 mM DTT to inhibit RNases. In these experiments, the 1:3 dilution ratio resulted in a total reaction concentration of 6% plasma. At this concentration, the assay provided consistent results and represents the maximum sample volume the assay can accept with the dilution step. I consistently observed high RNase activity for the 5-minute incubation setting at 50 °C. To mitigate this while maintaining a low incubation temperature, longer incubation times with higher reducing agent concentrations may be necessary.

I evaluated the extraction-free plasma sample preparation protocol in 50 µL, tube-based HIV-1 RT-RPA reactions to demonstrate its compatibility with RT-RPA, as shown in Figure 23B. Using a 5-minute incubation at 70 ºC with 7.7 mM DTT, I observe positive amplification for 1E5 copies/mL

of HIV-1 plasma. Without DTT or 70 ºC incubation, I observe little to no fluorescence for 1E5 copies/mL HIV plasma. These experiments demonstrate the compatibility of the sample preparation method with RT-RPA for HIV positive plasma as well as the need for both DTT and elevated incubation temperatures to adequately lyse virions and inactivate RNases. Some residual RNase activity remains after incubation; however, with subsequent dilution of the sample into the RT-RPA reaction, the low RNase activity does not prevent amplification. RNase inhibitor can be added to both sample treatment and the RPA mastermix to further reduce RNase activity, as seen in Figure 35. This residual activity along with plasma inhibitors and varying degrees of RNA degradation during the incubation period, may explain variations in the amplification curves for a given concentration. I do not address plasma separation in this work, but this step is necessary for processing whole blood samples. Plasma extraction is typically achieved through centrifugation; however, for point of care applications, low-cost plasma separation membranes and commercial membrane-based devices have become available.[143–146] In future work, I aim to integrate this step along with sample metering to develop a more comprehensive, extraction-free plasma sample preparation protocol.

3.3.2 Observation of Residual RNase Activity after Sample Treatment

After sample treatment, the sample is quickly added to RT-RPA. Since there is likely still some residual RNase activity that can slowly degrade the sample over time, I looked at various wait times between the sample treatment and the addition of the sample into RT-RPA to determine how long the RNA is stable in the incubated sample.

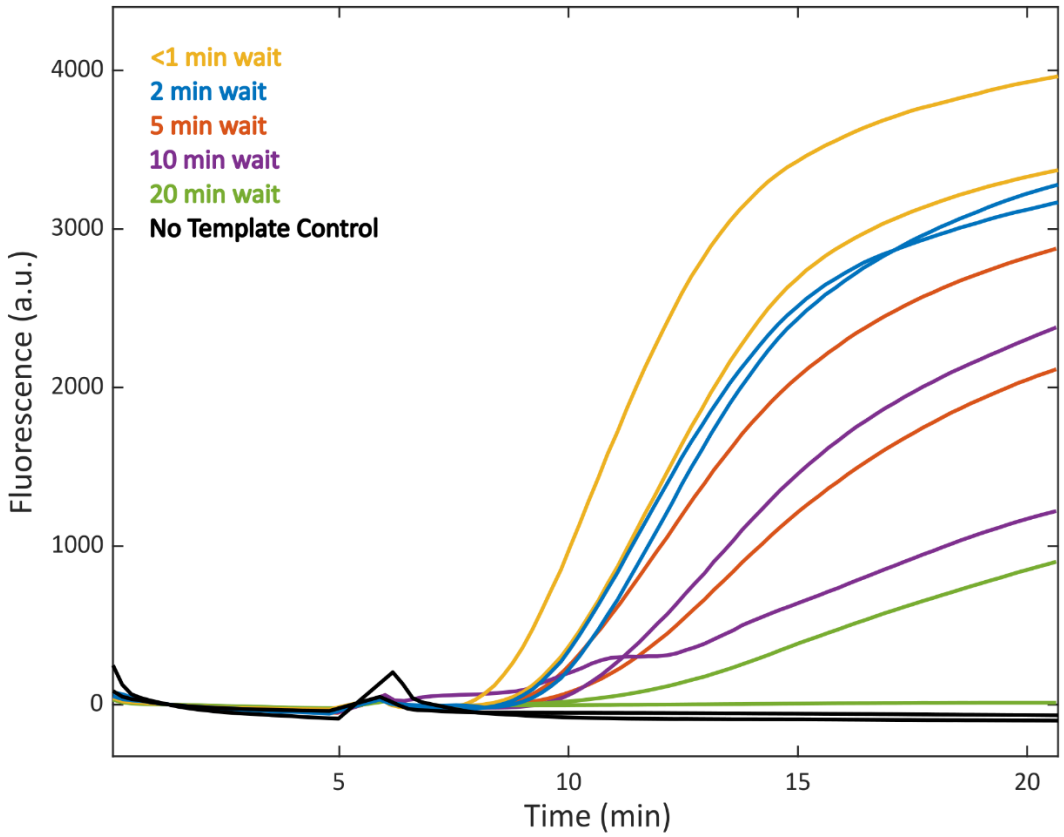

Figure 24. Extraction-free amplification of 1E6 copies/mL of HIV in plasma for various wait times between sample treatment and RT-RPA.

I experimented with waiting times ranging from <1 - 20 minutes between sample treatment and the addition of the sample to RT-RPA, Figure 24. Incubation times from <1 - 2 minutes represents the typical time it will take someone to add the incubated sample to RT-RPA and run the reaction. We find that while <1 - 5 minutes sufficiently amplified 1E6 copies/mL of HIV, wait times of 10 and 20 minutes had significantly worse amplification. This indicates that while a typical extraction-free protocol will amplify HIV well, residual RNase activity remains after sample treatment and will slowly degrade RNA over time. One way to further reduce RNase activity and improve this sample treatment would be to increase the concentration of RNase inhibitor before incubation or

add more RNase inhibitor to the sample right after thermal incubation. Other ways to improve the method and reduce RNases would be to assess higher temperatures, longer incubation times, increased DTT concentrations, add in a plasma separation or filtration step, and include additional additives.

3.3.3 50 μL Paper-Based RT-RPA Reactions

I evaluated the LOD for standard 50 μL RT-RPA reaction volumes with the extraction-free sample preparation protocol for HIV-1 in plasma in paper-based RT-RPA reactions performed on this custom vibration mixing and heating platform. I implemented the mixing and heating platform to improve the performance of paper-based reactions and maximize assay sensitivity. In the previous chapter, I showed that vibration mixing significantly improved paper-based RPA reactions by continuously redistributing reagents for the reaction, as seen in Figure 11. With this mixing mechanism, I found an overall fluorescence output increase up to 16-fold and up to a 50% reduction in time-to-threshold when compared to unmixed experiments for HIV DNA.[141] With the mixing platform, I see similar results to these with the extraction-free method, as seen in Figure 25.

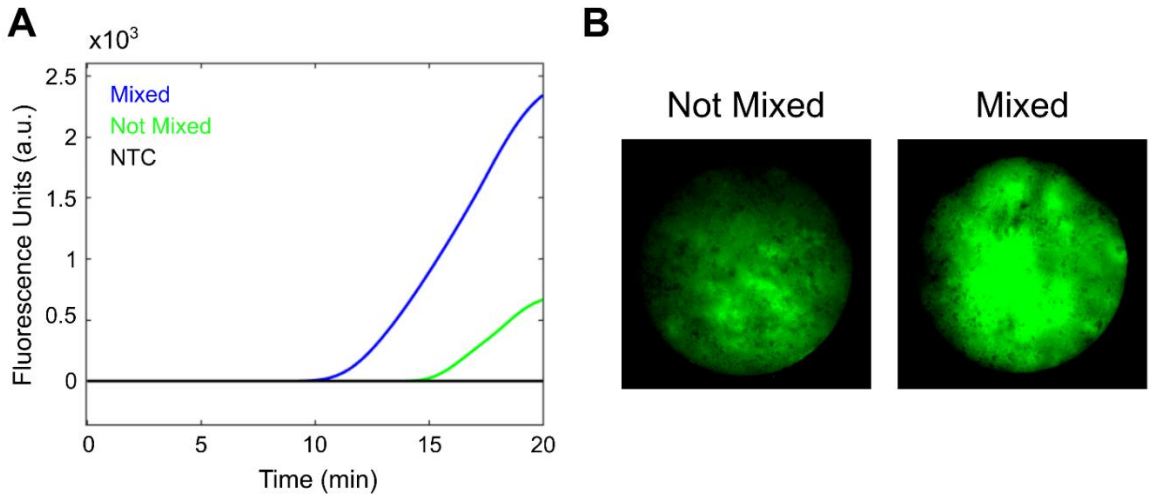

Figure 25. Comparison between paper-based 300 µL reactions with and without continuous mixing for 1E4 cps/mL HIV positive plasma. (A) Amplification curves for 300 µL paper-based reactions. I found a 4.5-minute improvement in time-to-threshold and 34 times improvement in overall amplification at t = 15 minutes using continuous mixing. The text color correlates to the same color on the plot. (B) Epifluorescence images of RT-RPA reactions in glass fiber pads at t = 20 minutes with and without continuous mixing.

Figure 25 compares paper-based 300 µL reactions with and without continuous mixing for 1E4 copies/mL of HIV positive plasma. Like the work in the previous chapter, these results also show significant improvement in amplification when continuous mixing is implemented. There is a 5 minute improvement in time-to-threshold for the mixed reaction when compared to the not mixed scenario. Additionally, overall amplification has significantly improved.

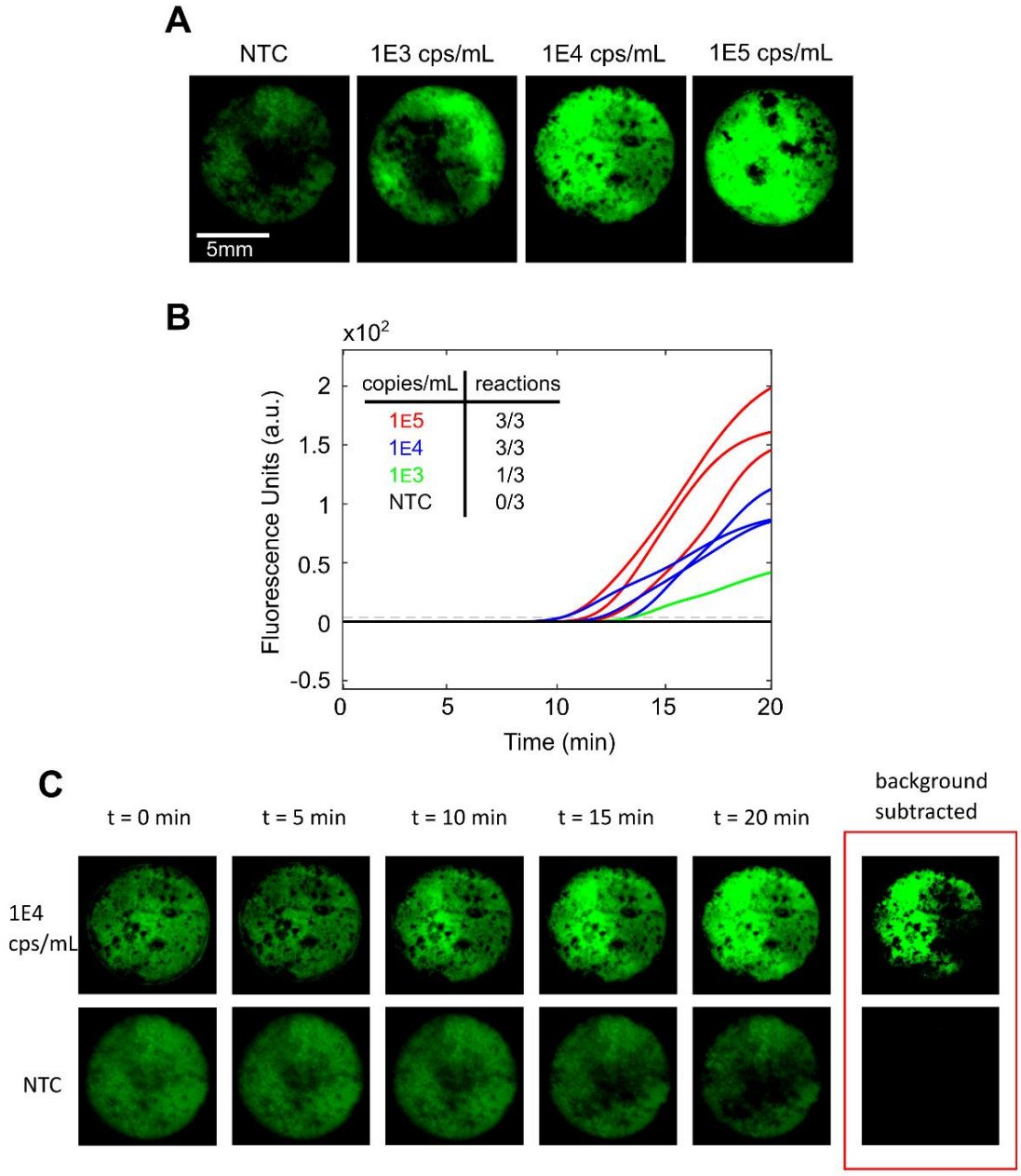

Figure 26. (A) Epifluorescence images of 50 µL, paper-based, RT-RPA reactions for no template control, 1E3, 1E4, and 1E5 copies/mL of HIV-1 positive plasma using the extraction-free sample preparation protocol at t = 20 minutes. These images have no background subtraction added and use the same brightness and image contrast settings. (B) Total fluorescence amplification curves for 50 µL paper-based reactions for n = 3. For these experiments, the LOD is 1E4 copies/mL or 30 copies/reaction with all three reactions showing positive amplification. At 1E3 copies/mL, only

one reaction was positive and for all NTCs, none of the reactions amplified. Data includes initial background subtraction to remove background autofluorescence. (C) Top row: Progression images of 1E4 copies/mL for 50 µL paper-based reactions from 0 - 20 minutes. Bottom row: Progression images of NTC 50 µL paper-based reactions from 0 - 20 minutes. First five columns are raw images without background subtraction. The sixth column boxed in red is the background subtracted image at t = 20 minutes. The background is calculated as the average of the first four minutes. The total fluorescence of the non-template control experiments tends to remain constant or decrease over the 20-minute incubation period, yielding background subtracted images with little fluorescence. In comparison, the total fluorescence of positive experiments amplifies and increases over time, resulting in background subtracted images with patches of positive amplification fluorescence at t = 20 minutes.

Figure 26A shows RT-RPA fluorescence images at t = 20 minutes for no template control, 1E3, 1E4, and 1E5 copies/mL plasma samples, with no background subtraction added. The results show that without HIV-1 target present, there is minimal fluorescence, mainly autofluorescence due to the reaction pad, PCR film, and initial nonspecific interactions in RT-RPA. The autofluorescence is initially observed at t = 0 minutes for both NTCs and positive samples and remains constant throughout the entire experiment for NTC trials. When HIV-1 is present in the sample, strong fluorescence intensity is observed, indicating positive amplification. With background subtraction, I find the membranes to be completely dark for NTCs and have fluorescence patches in positive experiments, as seen in Figure 26C.

Figure 26B depicts the total fluorescence for paper-based RT-RPA reactions as a function of time for HIV-positive plasma samples and NTCs. Fluorescence remains constant at the baseline level until 10 minutes when it rapidly increases, consistent with exponential amplification. The fluorescence intensity increase appears later and is inhibited relative to typical paper-based RT-RPA based experiments conducted in clean (no plasma) samples at similar HIV-1 concentrations.

Fluorescence intensity grows more rapidly with time as the number of target copies increases. The average endpoint fluorescence at t = 20 minutes also increases with higher concentrations. The threshold is determined as the average intensity of the no template control (NTC) experiments plus three standard deviations. I observed an LOD for 50 µL paper-based reactions of 1E4 copies/mL or 30 copies/reaction. The LOD of 1E4 copies/mL does not meet WHO HIV-1 testing recommendations of 1,000 copies/mL,[51] and so I explored larger volume RPA experiments with the goal of lowering the LOD to meet WHO recommendations.

3.3.4 Improving the Limit of Detection using Large Volume RT-RPA Reactions

To improve the LOD, I adapted the assay to accept larger volumes of plasma sample by increasing the RT-RPA reactions to a 300 µL reaction volume. Larger volume RPA reactions have been shown to improve assay analytical sensitivity by accommodating larger sample volumes and increasing dilution to mitigate challenges with coagulation and sample inhibitors.[140] Previous research by Wang *et al.* showed that 500 µL RT-LAMP reactions maintains the analytical sensitivity, in terms of copies per reaction, as the typical 20 µL RT-LAMP reactions, while accepting a larger volume (20 µL) of serum, effectively resulting in improvements in the LOD (copies/mL).[75] I use this large volume amplification approach to improve the LOD by accepting 20 µL plasma samples, within the range of a typical fingerstick sample.[147]

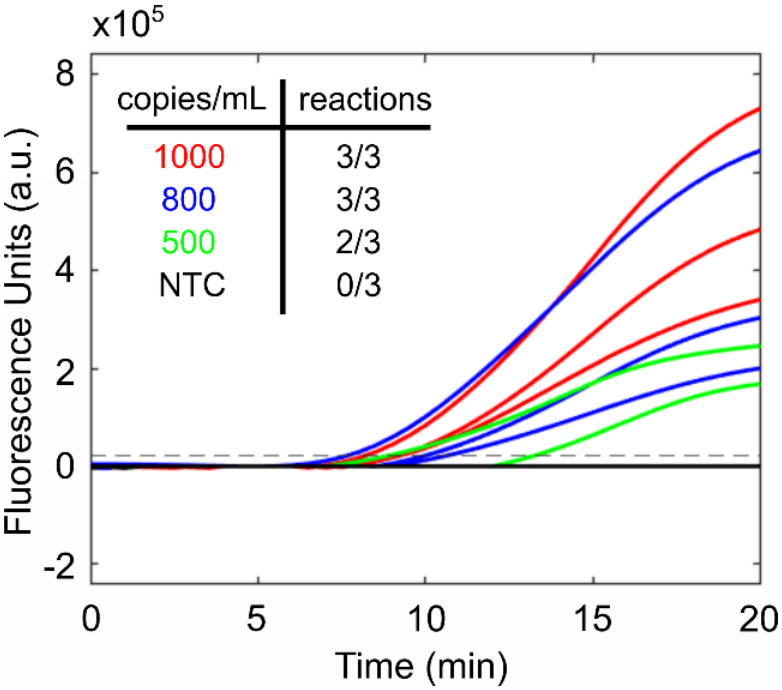

Figure 27. Bulk fluorescence curves from 0 to 1000 copies/mL of HIV-1 positive plasma for 300 µL in-tube RT-RPA reactions at the extraction-free sample preparation method (n = 3). The LOD for these reactions was 800 copies/mL or 16 copies/reaction. At 500 copies/mL, two of three replicates amplified within the 20-minute span of the assay.

I evaluated the extraction-free plasma sample preparation strategy for 300 µL tube-based RT-RPA reactions. Figure 27 shows the bulk, tube-based fluorescence curves for 300 µL RT-RPA reactions as a function of time for HIV-1 positive plasma samples. With increasing concentrations of HIV-positive plasma the maximum fluorescence at t = 20 minutes increases. At 1E5 cps/mL, the average endpoint fluorescence is ~4.9E5 a.u. and for 1E4 cps/mL, ~3.6E5 a.u. For 500 copies/mL, only two of three reactions amplified. As expected, the NTC or 0 copies/mL reactions did not amplify. For these large volume tube-based reactions, I achieved a limit of detection of 800 copies/mL or 16 copies/reaction, exceeding the WHO LOD recommendation of 1000 copies/mL.

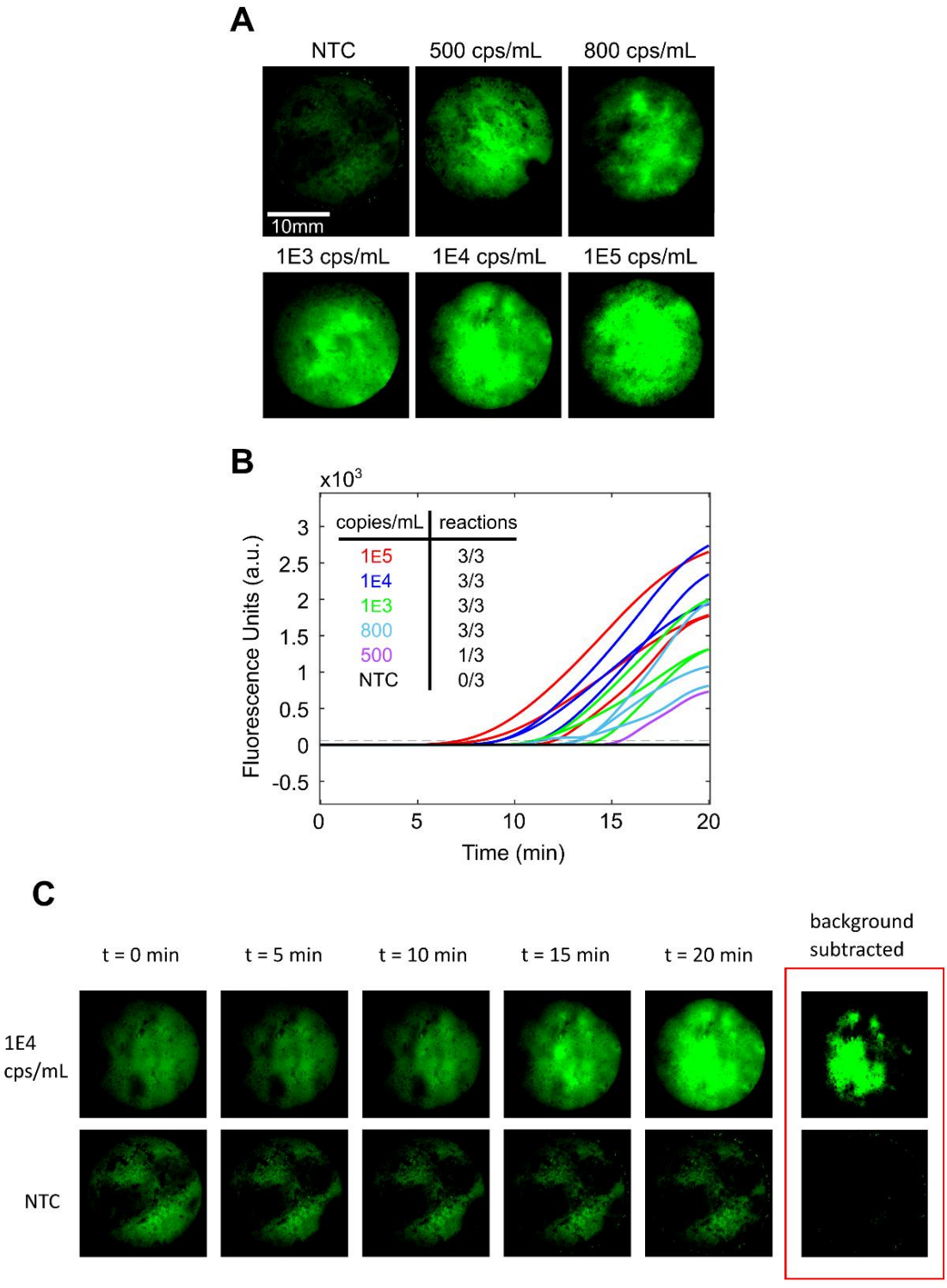

Figure 28. Epifluorescence images and total fluorescence curves for 300 µL paper-based RT-RPA reactions using extraction-free sample preparation from 0 - 1E5 copies/mL of HIV-1 positive

plasma. (A) Epifluorescence images of 300 µL volume RT-RPA reactions in glass fiber pads at t = 20 minutes for all tested concentrations of 0 - 1E5 copies/mL. These images have no background subtraction added and use the same brightness and image contrast settings. (B) Total fluorescence curves for 300 µL paper-based reactions, at n = 3. I evaluated concentrations from 0 - 1E5 copies/mL of HIV positive plasma and found the LOD to be 800 copies/mL or 16 copies/reaction. At 500 copies/mL, one of three reactions was positive. The text color for copies/mL correlates to the same color on the plot. Data includes initial background subtraction to remove background autofluorescence. (C) Top row: Progression images of 1E4 copies/mL for 300 µL paper-based reactions from 0 - 20 minutes. Bottom row: Progression images of NTC 300 µL paper-based reactions from 0 - 20 minutes. First five columns are raw images without background subtraction. The sixth column boxed in red is the background subtracted image at t = 20 minutes. The background is calculated as the average of the first four minutes. The total fluorescence of the non-template control experiments tends to remain constant or decrease over the 20-minute incubation period, yielding background subtracted images with little fluorescence. In comparison, the total fluorescence of positive experiments amplifies and increases over time, resulting in background subtracted images with patches of positive amplification fluorescence at t = 20 minutes.

Paper-based NAAT reactions typically perform worse than tube-based reactions resulting in reduced amplicon yield and poor limits of detection.[79,93,148,149] I perform 300 µL RT-RPA reactions in glass fiber membranes using the vibration platform to provide continuous mixing and a constant 39 ºC incubation temperature. Figure 28A shows the fluorescence images for 300 µL paper-based RT-RPA reactions at t = 20 minutes for all tested concentrations of 0 - 1E5 copies/mL. Like the 50 µL experiments, there is no background subtraction applied, so the NTC shows slight autofluorescence.

Figure 28B shows the area-averaged fluorescence curves for large volume paper-based RT-RPA reactions using HIV positive plasma. I assessed a range from 0 - 1E5 copies/mL of positive HIV

plasma. For 800 - 1E5 copies/mL, all reactions amplified. At 500 copies/mL, one reaction amplified after t = 14 minutes with two showing no amplification. In comparison, tube-based reactions showed slightly better performance with two positive reactions at 500 copies/mL and shorter times to threshold for 800 and 1000 copies/mL. The time-to-threshold of paper-based reactions were a minute and a half later compared to in-tube experiments. This demonstrates that extraction-free sample preparation of blood plasma is compatible with both paper and tube-based RT-RPA reaction approaches. Additionally, I further reduce user steps and device complexity that is associated with solid phase extraction methods and can achieve rapid HIV detection with a full workflow under 25 minutes.

3.3.5 Custom Concentrated Buffer

Although extraction-free amplification is compatible with plasma samples, the commercial rehydration buffer exhibited substantial variability in amplification performance and was additionally observed to vary between reagent batches. Compared to amplification reactions using solid-phase extracted samples or RNA transcripts in buffer, extraction-free plasma samples produced more inconsistent endpoint signal intensity (Figure 23B). These findings suggest that further optimization of both sample treatment and reaction mastermix composition is necessary in improving performance, repeatability, and robustness of the extraction-free workflow. Additionally, the commercial buffer and requiring sample dilution significantly restricts the assays' flexibility in adjusting additives, dilution ratio, and plasma concentration. The current commercial buffer occupies ~60% of the RPA reaction volume. This is typically not an issue, but when significant sample dilution is required, the lower available volume significantly limits the assay's flexibility. To inhibit ribonucleases, I use a combination of high heat (70 °C) and the reducing

agent, DTT, to inhibit RNases and thermal lyse the virus in a short 5-minute period. However, to prevent heat-induced coagulation at this temperature, a 1:3 plasma to dilutant is used. This dilution ratio has also been validated by other studies for serum and plasma stabilization under thermal conditions.[72] Consequently, after inclusion of dilution and all required RPA components, the maximum allowable sample input in a 50 µL RPA reaction is around 13 - 14 µL. This results in a maximum allowable plasma percentage of 6% for a 50 µL RPA reaction. Furthermore, plasma samples vary significantly in albumin content, coagulation factors, and inhibitory components, making it critical to accommodate for larger sample inputs, greater dilution flexibility, or additional additives to mitigate amplification inhibition when processing challenging specimens.[150] To address these limitations, I developed a 4X concentrated custom rehydration buffer that allows for higher sample input without compromising assay performance. Transitioning to a concentrated formulation will enable higher plasma input and provide greater flexibility in adapting the assay to a variety of RNA or DNA targets.

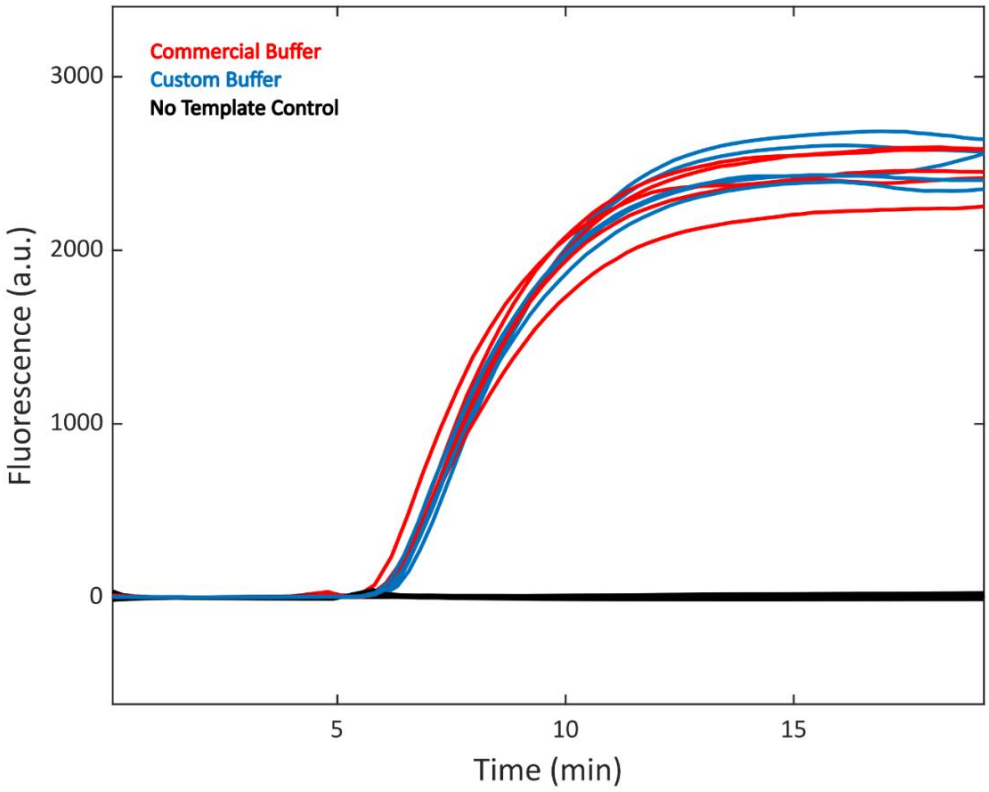

Figure 29. Results for a version of the custom concentrated buffer recipe. In red, is a 200 copy positive control using synthetic HIV DNA and commercial RPA buffer. The blue lines represent the concentrated custom buffer run at a 1X concentration for a 50 µL reaction and in black, is the no template control (NTC) for both buffers. In these experiments, n = 5. The custom buffer recipe increases sample volume from 13 µL to 28 µL, enough room for up to 14% of diluted plasma sample.

In Figure 29, I show that the custom buffer performs the same as the commercial buffer with synthetic HIV DNA. The no template controls (black lines) represent five reactions with the commercial buffer and the custom concentrated buffer. When compared to the RPA control reaction that uses 200 copies of synthetic HIV DNA with the commercial buffer (red line) the custom concentrated buffer (blue lines) matches the commercial buffer performance with a similar

time-to-threshold and overall fluorescence signal. For synthetic DNA in water, I found that the optimal 4X concentrated buffer recipe consists of 140 mM Tris Acetate pH 8, 400 mM Potassium Acetate, and 8% w/v 35,000 MW PEG. When diluted down to 1X for 50 µl reactions, this buffer becomes 35 mM Tris Acetate pH 8, 100 mM Potassium Acetate, and 2% w/v 35,000 MW PEG. While Tris Acetate and 35,000 MW PEG were used in the buffer recipe, alternative chemicals such as Tris-HCl or a higher concentration of lower MW PEG may also work. This buffer was applied to the extraction-free protocol to improve assay flexibility, enable higher plasma input, and increase space for more additives. and the protocol was then optimized for both HIV and hepatitis C assays.

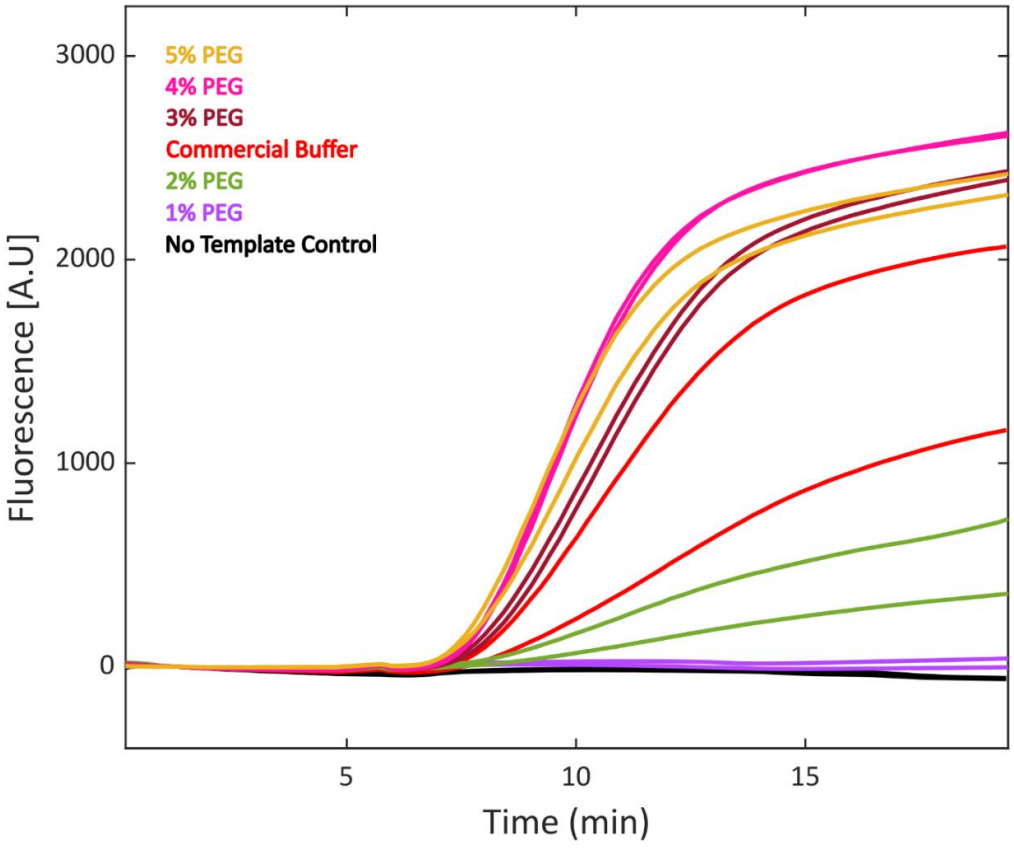

Figure 30. 1E6 cps/mL cultured HIV plasma used for the full extraction-free method using the custom concentrated buffer for RT-RPA. In this method, 6% plasma is used at a 1:3 dilution ratio

of plasma to dilutant. Varying PEG percentages in the custom buffer were tested against the commercial RPA buffer to determine the optimal concentration for the HIV assay (n = 3). The HIV assay performed the best when the concentrated buffer was at a final concentration of 4 - 5% PEG for a 50 µL volume. At $\leq$ 2% PEG (final concentration) the custom buffer performed worse than the commercial RPA buffer. All PEG concentrations in this figure represent final concentrations when custom buffer is run at a 1X concentration for a 50 µL reaction.

When applied to the extraction-free method for cultured HIV in plasma, increasing PEG percentage in the buffer was essential in improving overall amplification. In Figure 30, the full extraction-free method was applied for 1E6 cps/mL cultured HIV in plasma using the custom concentrated buffer in the RT-RPA mastermix. While 2% PEG (final concentration) amplified well for synthetic DNA in water, 4-5% PEG worked significantly better when applied with the extraction-free method with plasma samples for 50 µL reactions. Interestingly, the custom buffer with the final concentration of $\leq$ 2% PEG performed worse than the commercial buffer for the extraction-free method. Although the commercial buffer amplified, it had the largest variation in overall amplification between experiments. This is indicative that for the application of the extraction-free method, optimizing PEG concentration can significantly improve performance.

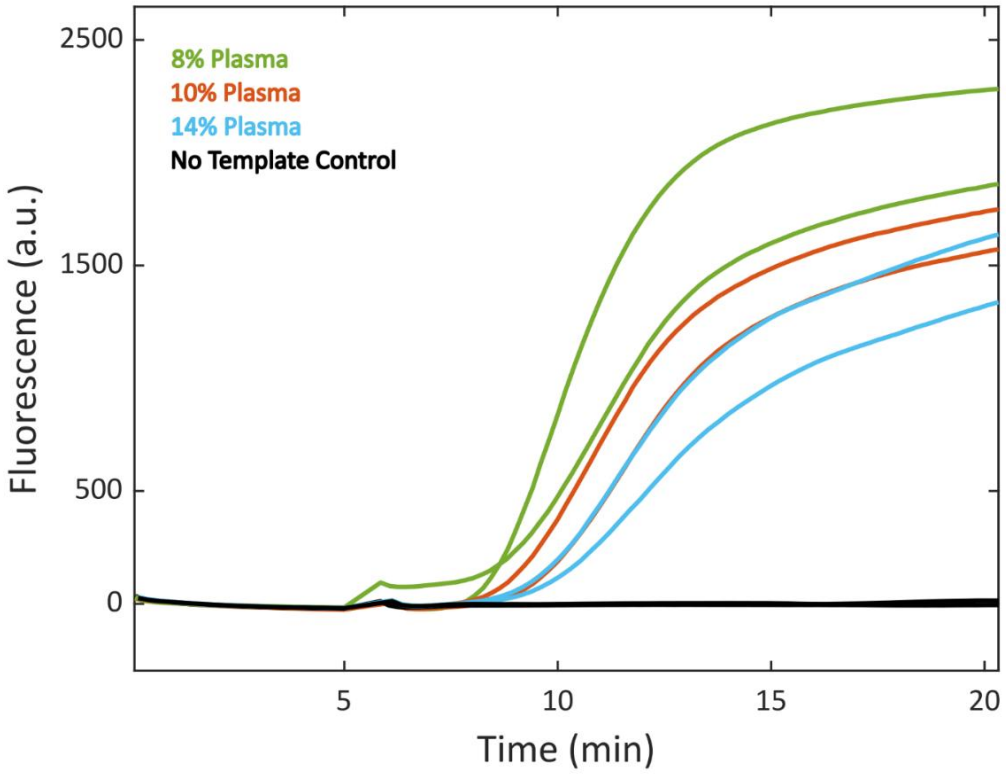

Figure 31. 1E5 cps/mL cultured HIV in plasma with custom buffer containing 4% PEG (final concentration). Plasma concentrations from 8-14% were evaluated to observe overall performance in the assay. After 10% plasma, there is a noticeable reduction in performance with longer time-to-thresholds and overall lower amplification.

By concentrating the custom buffer, I can increase sample percentage while maintaining the same dilution ratio. This can improve the assay performance by increasing amount of copies/reaction. I was able to increase the plasma concentration up to 2.3x from the original 6% plasma concentration. In Figure 31, I assessed concentrations from 8 - 14% for 1E5 copies/mL of HIV positive plasma using 4% PEG with the custom buffer (final concentration). After 10% plasma, the increase in plasma inhibitors started to affect the assay performance so for the HIV assay, I chose 10% as the maximum concentration of sample to add to the assay. In the case of hepatitis C,

the assay is more sensitive to plasma inhibitors so 8% plasma was used as the maximum sample concentration.

With the custom buffer I can improve overall amplification and consistency between replicates and increase final plasma concentration in the extraction-free method. Without the extraction-free method and using synthetic DNA, the concentrated buffer still matches and maintains a similar performance to the commercial buffer. While HIV and HCV plasma samples were limited to a final concentration between 8 - 10% due to inhibitory components, less inhibitor-rich sample types may tolerate higher concentrations. Overall, this work sought to increase target nucleic acid input during amplification to improve analytical sensitivity and repeatability.

3.3.6 Optimization for the Detection of HCV

In addition to transitioning to the custom buffer, several additives were examined for the HIV and hepatitis C assay. In the Posner group, we found that additional SSB protein was required to improve the HCV assay and reduce nonspecific activity in the no template controls. For the extraction-free method, I tested SSB proteins, various detergents, and high temperature resistant RNase inhibitor.

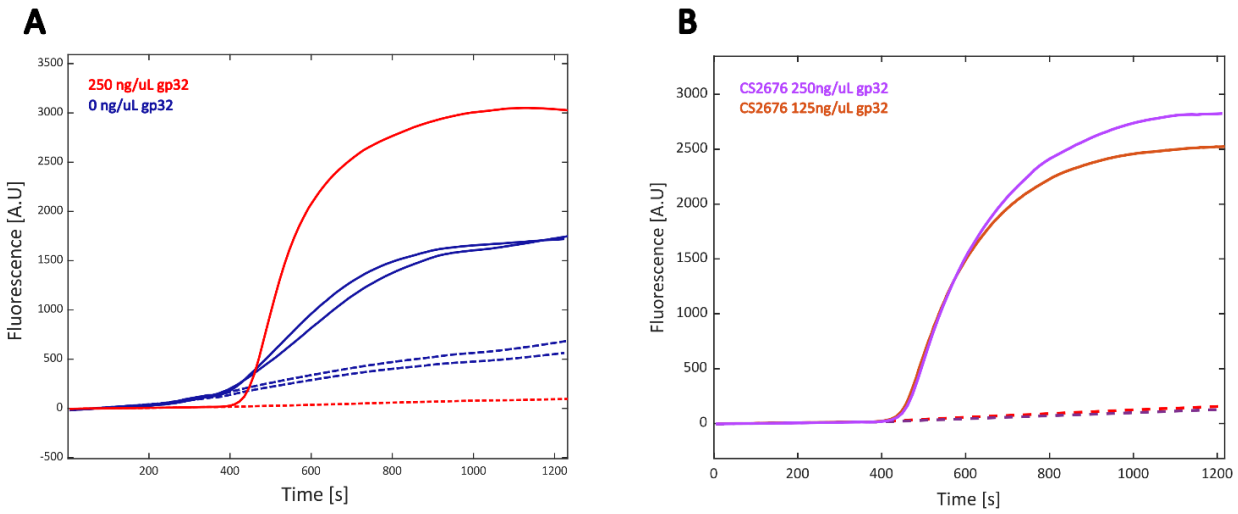

Figure 32. Comparison of the HCV assay with and without additional SSB protein. (A) Solid red line represents 200 copies of synthetic DNA added to the assay with 250 ng/µL of SSB gp32 protein. Solid blue line represents 200 copies of synthetic DNA added to assay with no additional gp32 added. Dotted lines represent the NTCs for the respective gp32 concentrations. (B) 125 and 250 ng/µL of gp32 protein tested against a solid phase extracted genotype 1a clinical sample. Lavender lines represent 250 ng/µL of gp32 added to the assay and orange lines represent 125 ng/µL of gp32 added.

SSB proteins bind to ssDNA to remove secondary structure, stabilize the D-loop during amplification in RPA, and protect DNA from nuclease digestion. They have also been shown to reduce background and nonspecific activity in isothermal amplifications.[120] For the hepatitis C assay, increasing SSB protein, T4 gene 32, significantly improved the overall amplification of positive tests while reducing nonspecific activity in the NTCs. In Figure 32, the addition of SSB gp32 protein is crucial in improving the assay performance. While the addition of 250 ng/µL SSB protein provides optimal performance, the associated reagent cost significantly increases the overall cost per test. Reducing the concentration to 125 ng/µL was found to be sufficient to maintain low NTC signals while still improving overall amplification, offering a more cost-

effective balance between performance and reagent use. While not directed evaluated in the HIV assay, the addition of SSB protein is expected to similarly enhance assay performance.

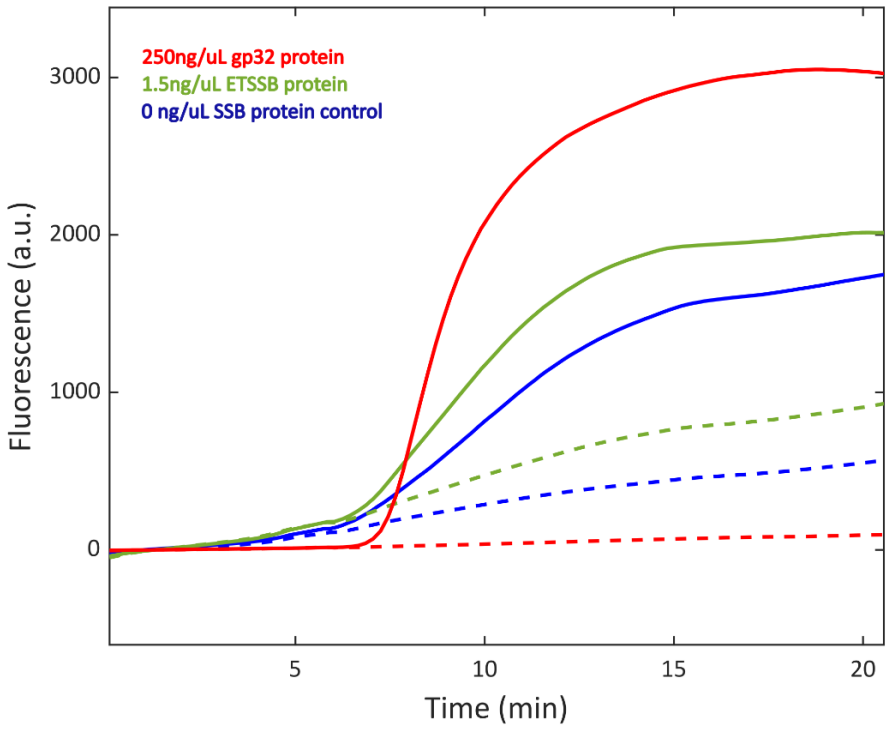

Figure 33. Comparison of the HCV assay with various SSB proteins. Solid red line represents 200 copies of synthetic DNA added to the assay with 250 ng/µL of gp32. Solid green line represents 200 copies of synthetic DNA with 1.5 ng/µL of ET SSB. Solid blue line represents 200 copies of DNA with no additional SSB protein. Dotted lines represent NTCs for respective SSB protein.

Extreme thermostable SSB protein (ET SSB) protein was evaluated but did not perform well with the RPA assay. Compared to the HCV assay with no SSB protein added, ET SSB protein had a slight increase in the delta between the positive and NTC test. However, the nonspecific activity in the NTC significantly increased with the ET SSB protein and did not match the performance of the T4 gp32 protein in both NTC and positive amplification, Figure 33. The direct comparison

between gp32 and ET SSB protein was difficult as the ET SSB protein stock concentration was too low so only 1.5 ng/µL could be used.

Another additive, Triton-X 100, was previously used in the extraction-free method to improve amplification in RT-RPA. Triton-X 100 is known to stabilize enzymes, maintain a soluble environment, and reduce impact from plasma inhibitors.[138,139] However, Triton-X 100 has been banned in the EU due to its toxicity to aquatic life.[151] As a result, I looked at eco-friendly detergents to replace Triton-X 100.

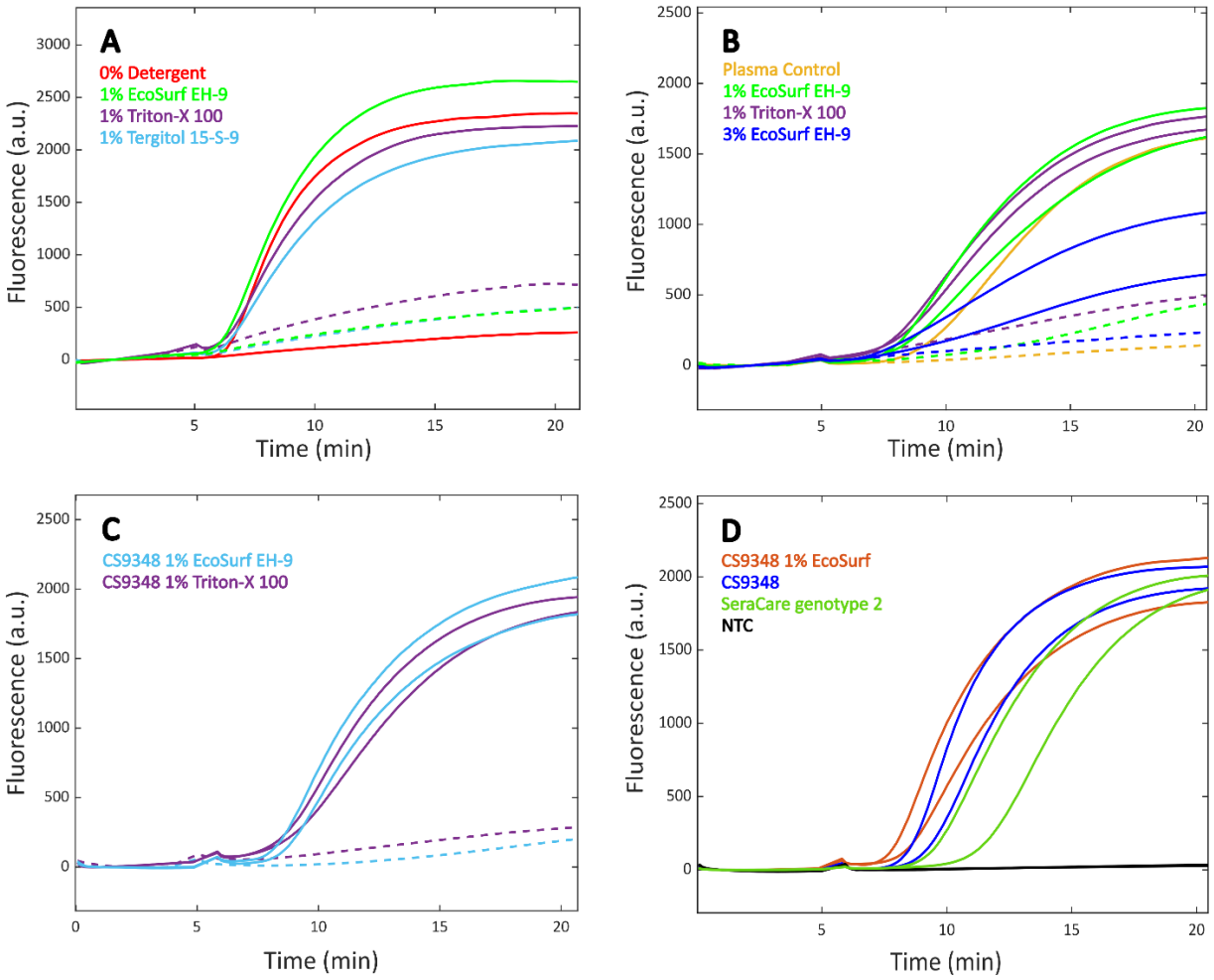

Figure 34. Comparison of the HCV assay with various detergents. (A) HCV ran with 2000 copies/reaction of synthetic DNA for various detergents at 1%w/v. Positive results are in solid

lines while NTCs are in dotted lines for the respective detergent color. No SSB protein is added to these tests. (B) 500 copies/reaction of HCV synthetic DNA spiked into plasma. Assay is run at a final plasma concentration of 8%. Solid lines represent positive tests while dotted lines represent NTCs. Plasma control (yellow lines) contains no detergent. 1% Triton X-100 and EcoSurf both amplify well. However, the NTCs increase as well. (C) 1% EcoSurf and Triton X-100 are tested on a solid phase extracted clinical sample 9348 (HCV RNA genotype 1). No SSB protein is added to the assay. (D) Full extraction-free RT-RPA tested on clinical sample 9348 in serum with and without 1% EcoSurf. SeraCare genotype 2 in plasma is tested without any detergent added. All experiments in this plot were tested with 125ng/μL of T4 gp32 protein added to the RT-RPA mastermix.

In Figure 34A, the hepatitis C assay was evaluated with 2000 copies/reaction of synthetic DNA in water to observe the assay performance with 1% detergent added. Here, the eco-friendly detergent EcoSurf EH-9 solution improved the endpoint fluorescence compared to the DNA positive control with no detergent. 1% Triton-X 100 and 1% Tergitol 15-S-9 solution were also compatible with RPA but had a slightly lower endpoint fluorescence compared to the DNA control and EcoSurf EH-9. I then spiked 500 copies/reaction of synthetic DNA into plasma and did the extraction-free method with a 8% final plasma concentration for 1 - 3% EcoSurf EH-9 detergent and 1% Triton-X 100 (Figure 34B). I found that when plasma is added into the assay, 1% Triton-X 100 and 1% EcoSurf EH-9 solution both improved the time-to-threshold and overall amplification for HCV RPA when compared to the plasma sample without any detergent added (yellow solid line). At 3% EcoSurf EH-9, there was a significant reduction in amplification (dark blue solid lines). Figure 34C shows amplification of a solid phase extracted clinical sample with 1% EcoSurf or Triton X-100 added with SSB protein. Again, I found similar performance for both, suggesting that EcoSurf EH-9 solution is a great eco-friendly substitution for Triton-X 100. However, even with SSB protein added to the mastermix to improve amplification and reduce non-template controls, the

addition of detergent still increased non-specific activity and increased the non-template controls. Lastly, in Figure 34D, I used the full extraction-free method into RT-RPA for a clinical serum sample (HCV genotype 1a) with and without EcoSurf EH-9 solution as well as a SeraCare genotype 2 plasma sample without any detergent added. While there is a slight decrease in time-to-threshold for the genotype 1 clinical sample with detergent added, the overall improvement with detergent is minimal. For the samples without any detergent added, the overall amplification is still high and maintains a similar endpoint fluorescence as the sample with detergent. Due to the detergent increasing non-specific activity in the NTC while only providing minimal improvement in the positives, I chose to remove detergents from the HCV assay.

Overall, the addition of detergent in the HIV assay did not affect the NTCs and significantly improved the positives. However, for HCV, 1% detergent did not significantly improve the positive experiments. More importantly, the HCV NTCs without any detergent added remained significantly lower (black solid lines in figure 34D) than the NTCs with detergent added (figure 34B and C dotted lines). Due to these results, I omitted the detergent for the HCV assay and kept 1% w/v Triton-X 100 or EcoSurf EH-9 solution for the HIV assay.

Lastly, high temperature stable RNase inhibitor among other additives were assessed to further reduce residual RNase activity. I used an enhanced heat and oxidation resistant ribonuclease inhibitor that can withstand up to 70 °C for 15 minutes. This allowed the addition of RNase inhibitor during the sample treatment process to protect RNA during thermal incubation. Additional RNase inhibitor can also be added to the RPA mastermix to further protect RNA during amplification.

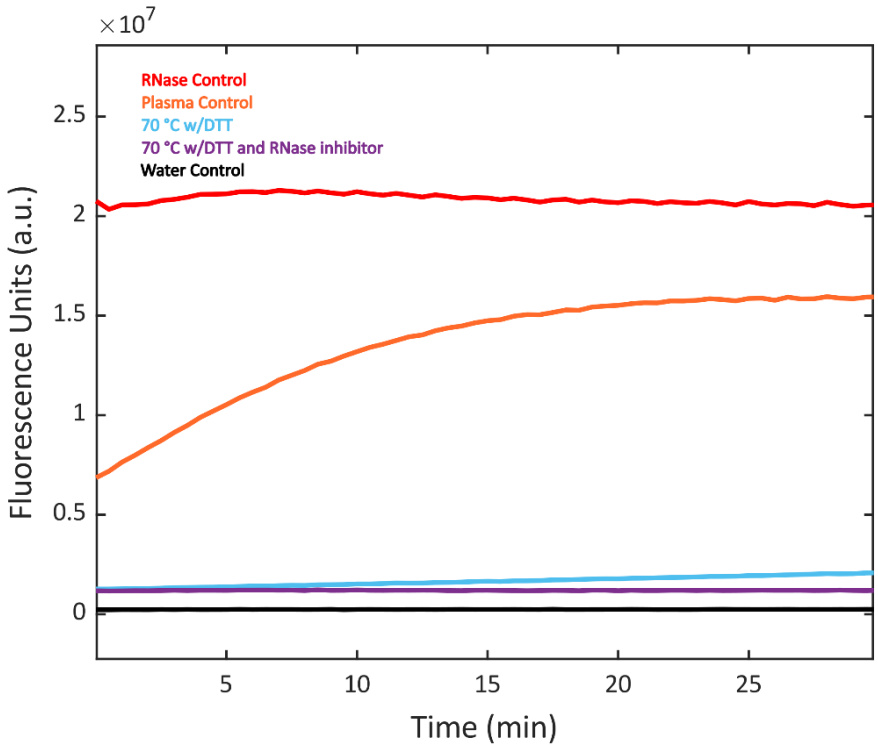

Figure 35. RNase alert assay to detect RNase activity with and without RNase inhibitor for DTT sample treatment. The red line represents the positive RNase control, the orange line represents the plasma control without any heat or DTT treatment, the blue line represents the original DTT treatment, the purple line represents the DTT treatment with 1 U/µL RNase inhibitor added to the incubated sample and 1 U/µL RNase inhibitor added to the RNase alert mastermix (final concentration of 1.26 U/µL RNase inhibitor in the final reaction), and the black lines represent the water control.

Figure 35 looks at the reduction in RNase activity with the addition of RNase inhibitor. Here, 1 U/µL of RNase inhibitor was added to the sample before thermal incubation at 70 °C for 5 minutes and 1 U/µL was added to the RNase alert assay master mix to bring the full assay to a final concentration of around 1.26 U/µL RNase inhibitor. I found that the addition of RNase inhibitor did help further reduce residual RNase activity in the assay. For HIV, I found the extra 1 U/µL of RNase inhibitor in the RT-RPA mastermix to be optional and chose to only add it to the sample

treatment portion of the assay to reduce overall cost. For HCV, it was necessary to add 1 U/µL of RNase inhibitor to the sample treatment and 0.5 U/µL to the RT-RPA mastermix.

Overall, in response to these changes, the optimized formulation for the extraction-free method for HIV is 1 U/µL RNase inhibitor, 10 mM DTT, plasma or serum sample, and nuclease-free water for the sample treatment. The sample to dilutant ratio maintains a 1:3 ratio and the sample is incubated at 70 °C for 5 minutes. 16 - 20 µL of the diluted sample is then added to RT-RPA to result in a 8 - 10% plasma concentration. The RT-RPA mastermix consists of the custom concentrated buffer with a final concentration of 4% w/v 35,000 MW PEG, 1% w/v Triton-X 100 or EcoSurf EH-9 solution , and 0.5 U/µL Affinity Script Reverse Transcriptase.

For HCV, the sample treatment consists of 1 U/µL RNase inhibitor, 10 mM DTT, plasma or serum sample, and nuclease-free water for the sample treatment. The sample is diluted to a 1:3 sample to dilutant ratio and incubated at 70 °C for 5 minutes. 16 µL of the diluted sample is added to RT-RPA to result in an 8% sample concentration. The RT-RPA mastermix consists of the custom concentrated buffer with a final concentration of 3% w/v 35,000 MW PEG, 0.5 U/µL RNase inhibitor, 125 ng/µL gp32 SSB protein, and 2 U/µL SuperScript IV Reverse Transcriptase. For both HIV and HCV, the sample treatment can tolerate higher DTT concentrations if needed.

3.3.7 Validation of Extraction-free Sample Prep and RT-RPA with HCV Clinical Samples

To validate the extraction-free method, I looked at 15 positive clinical samples and 5 negative samples to observe the assay performance across multiple genotypes and serum matrices. The samples were sourced from SeraCare, UW Hepatitis Clinic, and NIBSC. Many patients who are symptomatic often have high viral loads for hepatitis C. As a result, majority of these samples were

at very high viral loads. The worldwide distribution of HCV is mainly in genotypes 1 and 2 with less than 5% being composed of genotypes 5 and 6.[53,152] As a result, I tested six genotype 1, five genotype 2 samples, and three genotype 3 samples. Due to availability, I could only test one genotype 5 sample. In total, 15 samples were tested and I found a 100% specificity and 100% sensitivity for this limited sample group.

CS ID	Genotype	Viral Load (either in cps/µL or IU/µL)	HCV detected?
9348	1a	3,182 IU/µL	Yes
8843	1a	17,460 cps/µL	Yes
1345	1a	94,000 cps/µL	Yes
2676	1a	150,000 cps/µL	Yes
6412	1	16,500 cps/µL	Yes
1528	1b	6,220 cps/µL	Yes
SeraCare 2	2	6,260 cps/µL	Yes
1636	2b	30,373 IU/µL	Yes
2967	2	93,350 cps/µL	Yes
2154	2	28,700 cps/µL	Yes
2853	2b	10,011 cps/µL	Yes
593	3	1,283 IU/µL	Yes
SeraCare 3	3	24,430 cps/µL	Yes
6818	3	830 cps/µL	Yes
SeraCare 5	5	49.7 IU/µL	Yes
1517704	n/a	0 cps/µL	No
1517702	n/a	0 cps/µL	No
1517712	n/a	0 cps/µL	No
1517715	n/a	0 cps/µL	No
750953	n/a	0 cps/µL	No

Table 1. HCV Clinical samples tested with the custom buffer extraction-free method.

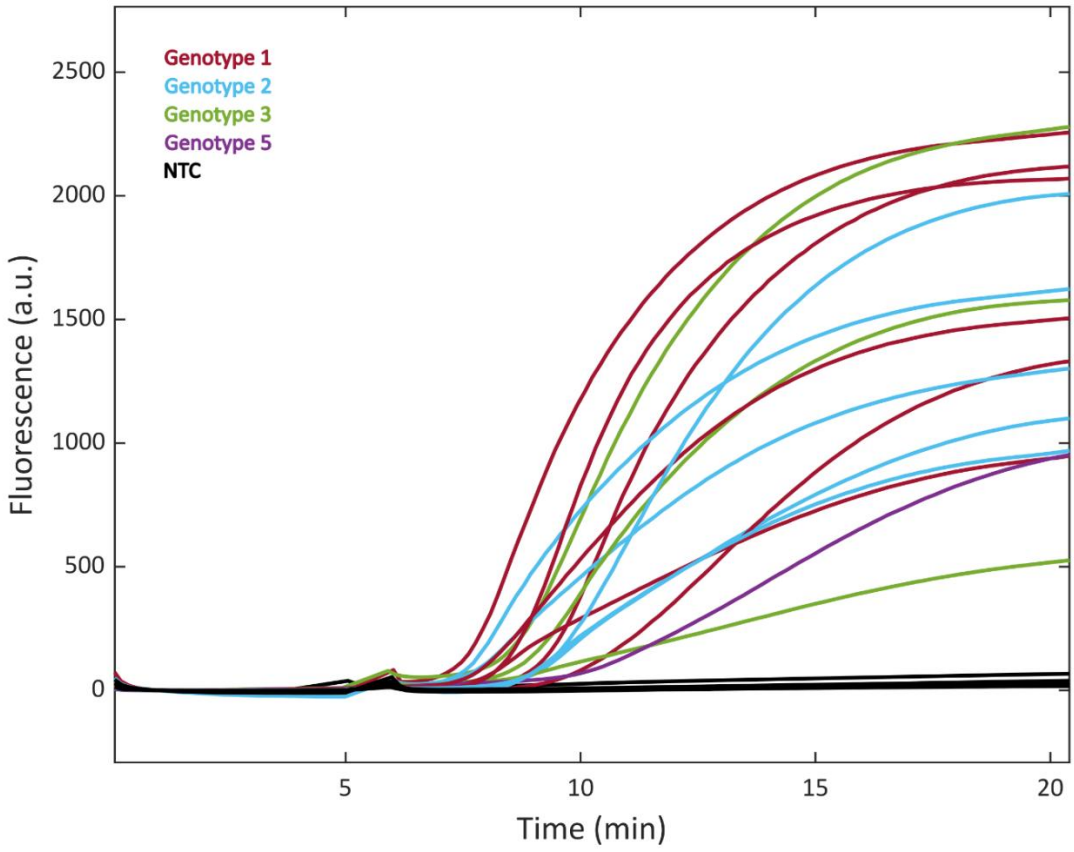

Figure 36. Amplification curves for clinical samples using the extraction-free method. Tested sample ranged from genotype 1-5. NTCs were negative human serum samples.

Table 1 shows the viral loads, genotypes for each positive clinical sample, and whether HCV was successfully detected or not. Clinical samples quantified via qPCR are labeled as copies/µL and were tested in 2018 while samples quantified via UW testing services are labeled in IU/µL and were tested in 2026. In the future, majority or all the tested clinical samples will be sent to UW testing services to provide a consistent and more recent form of quantification. We found that extraction-free sample preparation paired with RT-RPA was able to detect 100% of the HCV samples that we tested. The clinical samples included genotypes 1, 2, 3, and 5. Genotypes 1 - 3

are the most common genotypes found worldwide.[43,152] The viral loads tested ranged from 49.7 - 30,373 IU/µL or from 830 - 150,000 copies/µL depending on the quantification method and had a median of 2232.5 IU/µL and 17,460 copies/µL. The viral loads are high, but this is typical because chronic, untreated HCV often presents high VLs. In an assessment of HCV clinical samples, researchers found 98% of positive samples were above 10,000 IU/mL.[153]

In Figure 36, I show the amplification curves for the tested samples. Most of the amplification curves did not follow a specific trend in terms of time-to-threshold or overall amplification that correlated well with the sample's quantified viral load. The observed variability may arise from multiple sources, including variations in inhibitor concentrations in patient samples, sequence variation or target compatibility to the assay primers and probe, the inherent variability of RPA amplification curves, and the day-to-day variation in the extraction-free protocol. While most amplified well, a couple tests had overall low amplification curves. The two lowest amplification experiments were CS 6818 genotype 3 (green line) and SeraCare genotype 5 (purple line). The SeraCare genotype 5 was at a low quantification of 47.7 IU/µL. Interestingly, CS 6818 was partially hemolyzed, with clear evidence of hemoglobin contamination. Hemoglobin is a well-known inhibitor to amplification methods and can significantly impair amplification efficiency.[39,154,155] The observed of a low overall fluorescence output is consistent with the expected amplification behavior of a hemolyzed sample. These results highlight how the variability in clinical sample matrices can significantly impact overall amplification performance. It also suggests that reliable quantification using this method may be challenging, as substantial matrix-to-matrix variation exists between patient samples.

3.4 Conclusions

I present extraction-free sample preparation for in-tube and paper-based RT-RPA detection of HIV-positive plasma. I demonstrate a low-complexity workflow for HIV detection from human plasma that incorporates viral lysis, RNase inactivation, and direct addition of crude lysate into a rapid RT-RPA assay, achieving a total runtime of 25 minutes (5 minutes for sample treatment and 15 - 20 minutes for amplification). I demonstrate scalable RT-RPA reactions, from 50 - 300 µL. Larger reaction volumes enable larger plasma samples volumes to be added and results in lower LODs. As a result, I achieved an LOD of 800 copies/mL (16 copies/reaction) of HIV positive plasma for both tube-based and paper-based RT-RPA reactions. Previous examples for the detection of HIV via extraction-free NAAT approaches have used LAMP for amplification, which requires a runtime of 45 - 60 minutes.[71,75,156] To my knowledge, this is the first example of extraction-free HIV detection from plasma using RT-RPA, leveraging its rapid runtime (15 minutes) and low incubation temperature (40 °C). I then improved the robustness and repeatability of the extraction-free method by transitioning to a custom buffer and optimizing the assays additives for both HIV and HCV targets. Using the optimized extraction-free method for hepatitis C, I validated the assay with 20 patient samples, 15 clinical positive HCV samples and 5 negatives patient samples. This method demonstrates that laborious nucleic acid extraction of HIV and HCV RNA from blood plasma samples can be avoided by adding minimally processed lysate to RT-RPA reactions for rapid detection. This approach may assist in simplifying NAAT detection platforms and, with further development, could improve accessibility to rapid and affordable detection of blood-borne viruses.

While 300 µL large volume reactions achieve a lower LOD, this increases the reagents costs 6-fold compared to typical 50 µL reactions RT-RPA reactions. Bulk manufacturing and lyophilization will reduce costs, but for assays with higher acceptable LODs, small reaction volumes are possible.

For 50 µL reactions, I achieve an LOD of 1E4 copies/mL. For hepatitis C, the acceptable LOD is significantly higher than HIV at 3,000 IU/mL with studies finding that 98% of positive patient samples were over 10,000 IU/mL.[52,58,153] For this reason, I tested HCV samples using 50 µL reactions.

Microfluidic paper-based analytical devices (µPADs) are popular due to their application in POC NAATs. Paper is low-cost and conducive to manufacturing, storage, transportation, stacking, and deposition and lyophilization of reagents.[86,87] Paper-based devices are an exciting approach for low-cost, fully integrated, self-contained, and minimally instrumented diagnostics that are required for POC NAAT deployment.[115,157–160] Previous research has shown worse RPA performance on membranes which has limited its deployment in paper-based NAATs.[79] I found that with continuous mixing, paper-based and in-tube RT-RPA reactions had the same LOD for the extraction-free sample addition method in large 300 µL volume reactions. Although the current method does not encompass a fully paper-based workflow, the reported results demonstrate that extraction-free sample preparation and RT-RPA on membranes can achieve sensitive detection for bloodborne viruses. This demonstrates feasibility for adapting this method into a fully paper-based, low-cost POC HIV diagnostic.

While extraction-free amplification is compatible with plasma and serum samples, using the commercial buffer provides variable amplification results and significantly restricts the assays flexibility, particularly in adjusting additives, sample dilution ratios, and plasma input. Although the buffer volume is typically not a constraint in RT-RPA, situations requiring substantial sample dilution can restrict overall assay performance and adaptability. To improve assay flexibility and repeatability, I developed a custom, concentrated rehydration buffer to improve assay consistency while enabling higher sample input. This optimized extraction-free formulation allowed higher

plasma input and enabled easy adoption of the method to both HIV and HCV assays. I validated the assay using 50 µL reaction volumes for HCV clinical samples and observed its performance with a variety of patient serum and plasma matrices. I ran 15 clinical samples ranging from genotype 1-3 and 5 and 5 HCV-negative serum samples. I found 100% sensitivity and 100% specificity for this limited sample set. These extraction-free results highlight the potential for scalable, user-friendly, and sensitive molecular diagnostics for blood-borne diseases in resource-limited settings.

For future work, sample treatment will be developed to additionally work on paper. The current method excludes the plasma extraction step as the HIV and HCV samples were received stored in plasma. Future work will investigate plasma separation from whole blood using low-cost plasma separation membranes or other alternative methods. Additional efforts to improve the assay will focus on improving sensitivity and addressing variations in patient samples.

Chapter 4 Low Complexity Diagnostic Device for the Detection of Bloodborne Viruses

4.1 Motivation

The NAAT workflow for whole blood samples remains complex, often requiring multiple user steps, several separate pieces of equipment, and extended processing time of several hours. Commercialized POC platforms such as the Abbott *m-PIMA,* Diagnostics for the Real World *SAMBA II,* and the *Enigma* ML were designed to simplify user steps and minimize the requirement for specialized training. While they are accurate and easy to use, their long runtimes and high upfront costs remain a significant barrier to their adoption at community and primary healthcare levels. Home-base POC respiratory tests such as Cue and Lucira, seen in Figure 6, integrates a simplified sample preparation for saliva and nasal swab samples with isothermal NAATs for SARS-CoV-2 and Flu. One of the key factors enabling their viability is that saliva or nasal swab samples are easier to collect, require only simple sample treatment, and often contain high target concentrations. In contrast, blood and plasma samples can be particularly challenging due to the presence of amplification inhibitors and the need for more complex sample preparation and extraction workflows. Blood-based testing therefore remains a significant challenge for POC NAAT development.[37,38] Significant efforts toward reducing device complexity and the associated costs are still needed for blood-based POC NAAT platforms targeting these sample types.

As detailed in Chapter 3, I developed a POC friendly sample preparation workflow to minimize complexity, reduce user steps, and shorten total assay time for bloodborne pathogen detection. While this extraction-free method demonstrates a strong proof-of-concept, its usability for POC use in low-resource settings remains limited. The current workflow still requires multiple user

steps, including pipetting and mixing, relies on reagents and buffers that are freshly prepared and stored across a wide temperature range (-20 to 4 °C), and depends on complex instrumentation for thermal incubation and real-time fluorescence detection.

To address some of these limitations, I developed a cartridge-based system that integrates extraction-free sample preparation and RT-RPA in fewer than 5 user steps and delivers results in under 30 minutes with only the addition of plasma sample. This single-use device comes preloaded with all necessary reagents, consolidating the workflow into an easy-to-use, self-contained format. A low-cost reusable heating platform interfaces with the cartridge to provide two-zone thermal incubation and facilitate mixing during the reaction. I then validated this device using HCV DNA spiked in plasma as well as an HCV genotype 1 clinical sample. Together, this system represents a practical and scalable approach for real-world deployment particularly in resource-limited settings, highlighting the potential for user-friendly and accessible molecular testing for bloodborne diseases.

4.2 Experimental Section

4.2.1 HCV Samples

For HCV validation, I use synthetic DNA (gBlocks Gene Fragments, Integrated DNA Technologies, USA) that contain 978 base pairs from the 5' UTR region of the HCV genome (genotype 1). The HCV RNA clinical sample was obtained by the Gastrointestinal Center for Analytical Research and Exploratory Science (GiCasRes) at the University of Washington. The patient sample was originally collected from the Hepatitis & Liver Clinic at Harborview Medical

Center (Seattle, USA) under ethical approval by the UW review board. For the extraction-free protocol, the HCV serum sample was aliquoted and stored at -80 °C.

4.2.2 RPA Reactions

To enable extraction-free detection with the custom buffer formulation in the cartridge, I separate sample treatment, mastermix, enzymes and additives, and a TwistAmp exo kit lyophilized pellet into individual storage chambers.

The mastermix chamber consists of 18.75 µL custom concentrated buffer, 3.75 µL of 280 mM magnesium acetate, 1.05 µL of 30 µM forward and reverse primers, 0.9 µL of 10 µM exo-probe, and water to reach a total volume of 51 µL. This is to make a 1.5X mastermix recipe to account for any losses during the chamber integration phase. The custom concentrated buffer is a 4X solution consisting of 140 mM Tris Acetate pH 8, 400 mM Potassium Acetate, and 12% w/v 35,000 MW PEG.

The additive chamber consists of 0.94 µL T4 gene 32 protein (NEB, Massachusetts, USA), 0.94 U/µL RNasin Plus, and 0.75 U/µL of SuperScript IV reverse transcriptase (Thermo Fisher Scientific, USA) since these are typically stored in glycerol and cannot be frozen. Again, this is increased to make a 1.5X recipe when compared to a traditional 50 µL in-tube reaction. This is to account for any losses during chamber integration. For DNA-based experiments, these proteins and enzymes are unnecessary and can therefore be omitted from the assay.

For the sample treatment chamber, I use dithiothreitol (DTT), RNase inhibitor, and thermal treatment to inactivate ribonucleases. Samples are diluted 1:3 in nuclease-free water containing 30 mM dithiothreitol (DTT, Sigma-Aldrich, MA, USA) and 1U/µL RNasin Plus Ribonuclease

Inhibitor (N2611, Promega, Wisconsin, USA) to a 16 μL total volume of diluted sample. This chamber is not a 1.5X recipe as it is the closest chamber to the lyophilized pellet and does not see as much liquid loss as the previous chambers. From food dye and fluorescein experiments, I found that increasing the volume for the previous two chambers by 1.5X was necessary as there was significant liquid loss but increasing the volume for the sample treatment chamber was not needed. The RNase inhibitor is stable against oxidation and heat, with activity up to 15 minutes at 70 °C.

The lyophilized pellet chamber contains one TwistAmp exo kit pellet. Ideally, if most components could by lyophilized, this chamber could also contain lyophilized buffer, magnesium acetate, primers, probe, SSB protein, RNasin Plus, and SuperScript IV reverse transcriptase.

4.2.3 Data Collection and Analysis

I image paper-based reactions using an epifluorescence microscope (AZ100, Nikon, JPN) and illumination system (X-Cite exacte, Excelitas Technologies, USA) with a 0.5X objective lens. I use an epifluorescence filter cube set (Semrock, USA) and CMOS camera (Prime BSI Express, Teledyne, Photometric, USA) to capture grayscale images every 5 seconds for 20 minutes. I use an image analysis algorithm (MATLAB, MathWorks, USA) to calculate the fluorescence intensity over the full 20 minutes. For analysis of membrane reactions, I imaged the entire pad area. I set a region of interest as the active membrane. The ROI was a 7.82 mm x 8.4 mm rectangle. I perform a background subtraction to eliminate auto-fluorescence from the reaction pad, LDPE cartridge film, and initial nonspecific assay interactions. For each specific timepoint, I calculated the total fluorescence by summing the intensities over the ROI. The intensity over the entire pad is averaged and plotted against time. To define the threshold between positive and negative reactions across

all experiments, the cutoff was set as the mean fluorescence intensity of the no-template control (NTC) over the full 20-minute incubation period plus three standard deviations.

4.3 Results and Discussion

4.3.1 Overview of Integrated Cartridge Design

The disposable cartridge consists of a flexible multi-chambered frangible-seal pouch that stores various components in the extraction-free protocol. The pouch is separated into four distinct chambers with four frangible seal mechanisms to integrate the individually stored components into a GF/DVA membrane for paper-based RPA, as seen in Figure 37. The liquid components are integrated from right to left and hydrate a lyophilized RPA kit before being imbibed into a GF/DVA membrane. From right to left, the 4 compartments contain: RPA mastermix, additives and enzymes that are typically stored in glycerol, sample treatment buffer, and a lyophilized RPA kit. The enzymes and protein additives that are typically stored in glycerol are temperature sensitive and cannot be fully frozen. As a result, they require their own separate compartment for now, until they can be lyophilized into the RPA pellet. The sample incubation chamber contains the sample treatment buffer and is placed in the middle of the pouch to ensure that the entire sample makes it into the last chamber to rehydrate the RPA pellet.

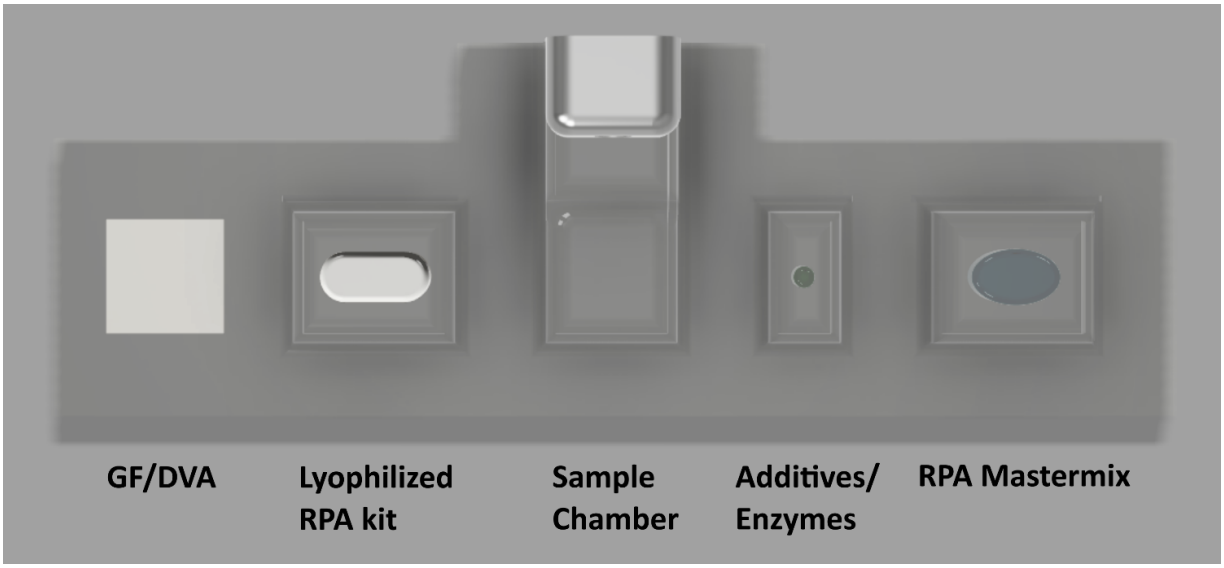

Figure 37. Rendered schematic of the disposable frangible-seal pouch. The pouch consists of four chambers; from far right to left, these chambers store: (i) RPA mastermix, (ii) additives and enzymes in glycerol, (iii) sample incubation buffer, and (iv) a lyophilized RPA pellet. A GF/DVA membrane is positioned on the left side of the pouch to imbibe the RPA reaction and limit liquid redistribution toward the pouch edges via capillary forces.

The frangible-seal pouch was fabricated by heat-sealing two low-density polyethylene (LDPE) film sheets (8593K71, Mc-Master-carr, USA). The top sheet was thermoformed using an FDM printed ABS mold to create four distinct chambers. The top and bottom sheets are then cleaned using isopropyl alcohol (Sigma Aldrich, Massachusetts, USA), RNase away (Sigma Aldrich, Massachusetts, USA), and two washes of nuclease free water (VWR, Pennsylvania, USA), followed by overnight drying in a desiccator at room temperature.

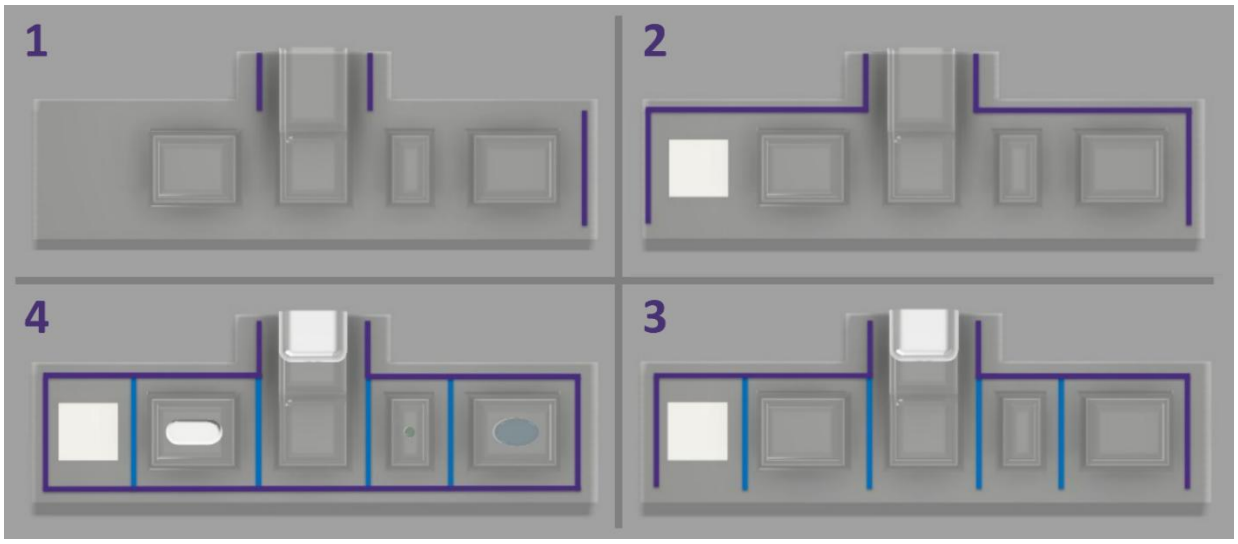

Figure 38. Rendered schematic of the heat sealing operations used to fabricate the frangible-seal pouch. Purple lines represent fully sealed sheets, and blue lines represent frangible seals that will break when pressure is applied to a nearby chamber. Clockwise from top left: (1) The outer right edge of the pouch and edges of the port seal is fully sealed, (2) the top long edge and left edge of the pouch is fully sealed, (3) four frangible seals are placed, and (4) the chambers are filled with their respective buffers and reagents and the bottom long edge of the pouch is placed to fully seal the pouch.

Pouch assembly was performed using an impact heat sealer (AIE, CA, USA). For permanent seals, the sealing level was set to 3 out of 7. The full sealing operations can be seen in Figure 38. The outer edge of the pouch is fully sealed as well as the edges where the port is located (purple lines). A thin Teflon sheet is placed between the LDPE sheets and on the heat strip to prevent the interior of the pouch from permanently sealing. The long edge of the pouch and the far left edge of the pouch are fully sealed using the same operations. To form the frangible seals (blue lines), the heat sealer is then set to a sealing level of ~1 out of 7. Between step 3 and 4 in Figure 38, a 3D FDM port is printed (Bambu Labs, CN) out of PETG (Bambu Labs, CN) and a 3mm threaded insert (Ktehloy, CN) is pressed into the port using a portable soldering iron (Weller, USA). The port is

sealed with two coats of clear acrylic spray to prevent water from getting trapped in the 3D print. The port is glued into the top edge of the pouch in between the LDPE sheets using a 2-part acrylic adhesive (TA4610, Permabond, Hampshire, UK) and left to cure at room temperature overnight. The pouch is then filled with the buffers and reagents before being fully sealed. To seal the 3D printed port, two fluorine rubber O-rings (Uxcell, CN) were placed on a threaded M3 screw (Helifouner, CN) to ensure a watertight seal. If used on the same day, the pouch can be stored at 4 °C. However, for long term storage, the flexible pouch will need to be stored in -20 °C.

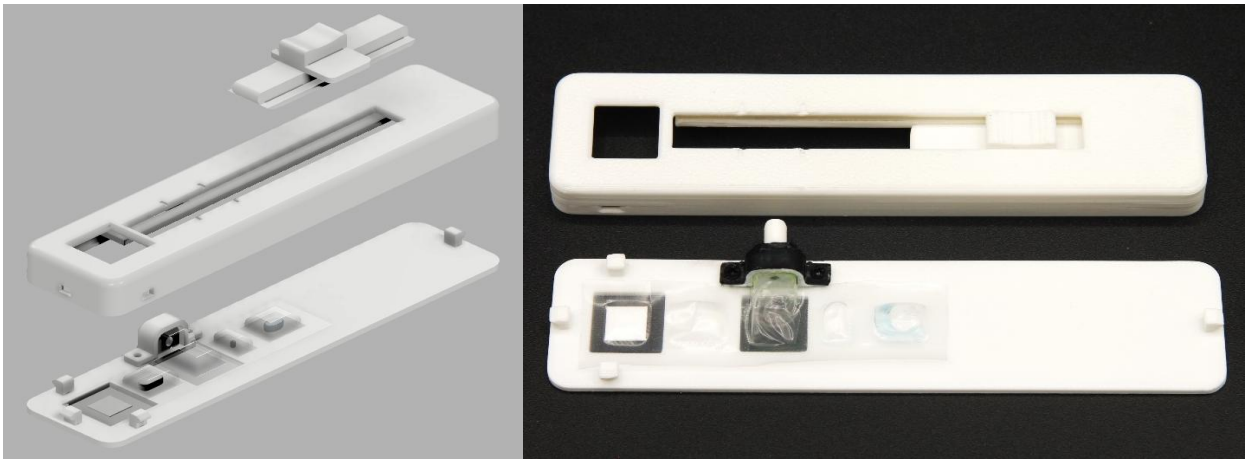

Figure 39. Images of the cartridge housing. Left: CAD render of the cartridge with the slider, top housing, and bottom housing separate. Right: Top view of the fully assembled cartridge. Here, the top housing is separated from the bottom plate to see the frangible-seal pouch.

The outer housing used to contain the frangible-seal pouch was fabricated via 3D FDM printing on the Bambu Lab X1C printer (Figure 39) in PETG. 3M double sided adhesive was laser cut to the pouch dimensions and used to secure the pouch to the housing. A small vent hole was punctured on the top left corner of the membrane compartment to allow air to escape during operation, preventing air entrapment that would otherwise impede proper imbibition of the RPA reaction into the membrane. PCR film is additionally laser cut and placed over the GF/DVA membrane portion

of the sealed pouch to further seal the vent hole after the RPA reaction is imbibed into the membrane and ensure proper alignment of the membrane over the heater. A sliding mechanism is 3D printed and snapped into place in the top cartridge housing. Silicone nano tape is added to the bottom of the slide mechanism to allow even pressure when bursting the chambers. The nano tape is covered with a Polypropylene-based PCR film (Sigma Aldrich, MO, USA) to prevent adhesion to the frangible-seal pouch and to reduce the friction coefficient between the interfacing surfaces, enabling smooth sliding operation during seal rupture. The top cartridge housing is secured to the bottom plate using four snap-fit joints.

For future work, critical reagents could be lyophilized or dried onto or near the amplification membrane to improve assay stability and storage capabilities. Lyophilized and dried reagents exhibit greater stability at room temperature and can reduce or eliminate the need for cold-chain shipping and refrigerated storage. Enzymes and proteins such as T4 gp32 SSB protein, Rnase inhibitor, and reverse transcriptase are typically stored in glycerol to protect against freeze-thaw degradation. Lyophilizing these reagents together with the primers, probe, and RPA mastermix, could simplify cartridge design by reducing the required storage to one or two chambers while also minimizing liquid loss when integrating the chambers together.

4.3.2 Design of Heating Platform

The heating platform is a reusable system that provides two incubation temperatures: 70 °C for sample treatment and 40 °C for amplification. Additionally, an ERM coin cell vibration motor is positioned beneath the 40 ºC heater to facilitate continuous membrane mixing during RPA and improve paper-based reactions. This is the same motor used in Chapters 2 and 3 to enhance paper-based RPA performance.

Two metal ceramic heater (MCH) elements were used for the incubation steps because they are lightweight, compact heaters with a rapid thermal ramp-up time, enabling fast and efficient temperature control. MCH elements also provide uniform heat distribution, low thermal mass, high thermal efficiency, and stable performance over repeated heating cycles, making them well suited for portable POC diagnostic devices.[161]

To control the heaters a proportional-integral-derivative (PID) feedback control loop was implemented using an Arduino Nano microcontroller (Arduino, ITA). The heating elements and coin vibration motor were independently actuated through three MOSFET switching circuits, enabling precise temperature regulation, rapid heater response, and low-power control of the integrated mixing system. Temperature monitoring was achieved using two thermistors attached to the heating elements and aluminum interface plates that directly contact the flexible frangible-seal pouch. The complete circuit diagram is shown in Figure 40.

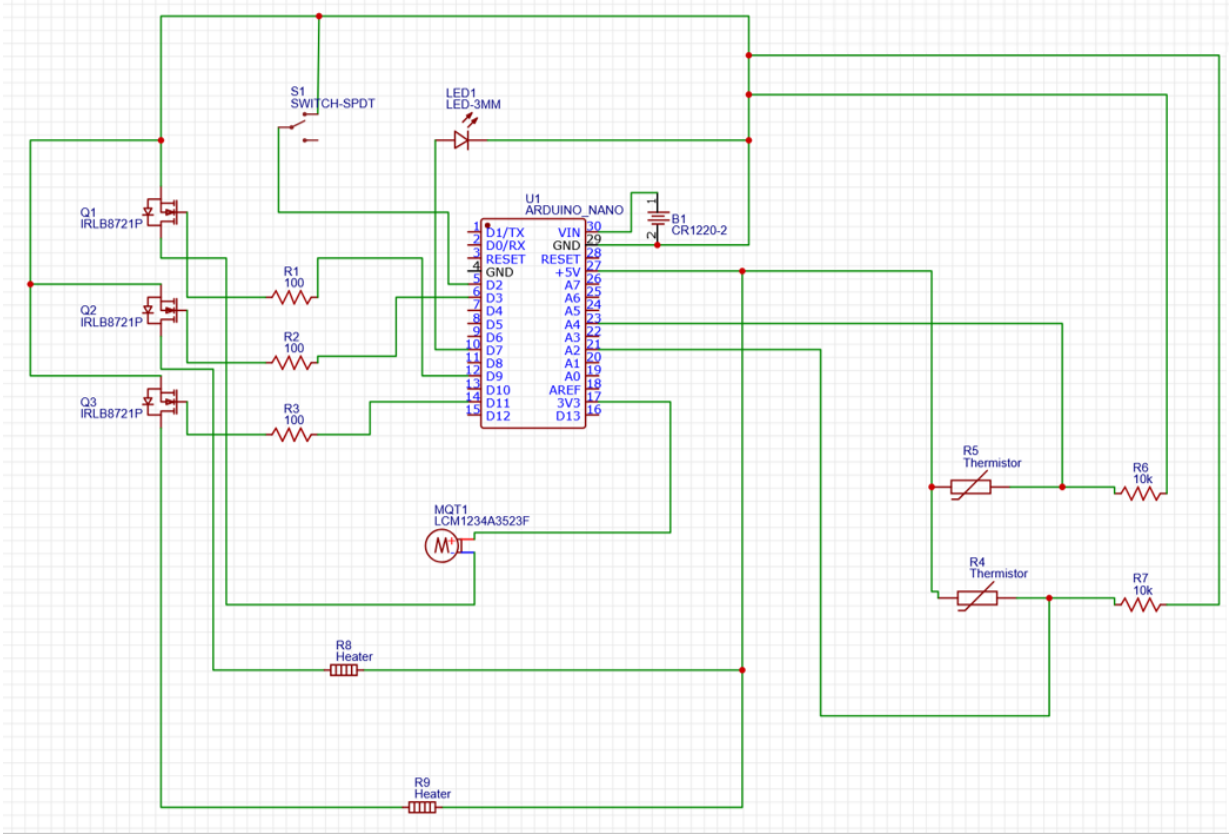

Figure 40. Circuit diagram of the heating platform. A 5V microcontroller (Arduino Nano) is used to control the heaters and motor. Two MCH elements are used to heat the cartridge at 70 and 40 ºC. Thermistors are additionally attached to the heating elements to monitor and control the temperature via PID control. MOSFETs are used to switch the current flow to selectively turn on the heaters and ERM motor based on test initiation.

A 1000 mAh 3.7V lithium-polymer (LiPo) battery was incorporated along with a boost charge module, allowing the system to operate either through USB-C 5V power or from the onboard battery. Based on measured power consumption, the 1000 mAh battery can support approximately four complete heating cycles per charge. Due to the USB-C input being an easy and consistent power source, this input was used for all validation experiments. A two-position sliding switch was additionally incorporated to power the system on and off. A red LED provides the user with a

visual notification when the 5-minute incubation step is complete, and the sliding mechanism needs to be actuated to burst the frangible seals to start the amplification reaction.

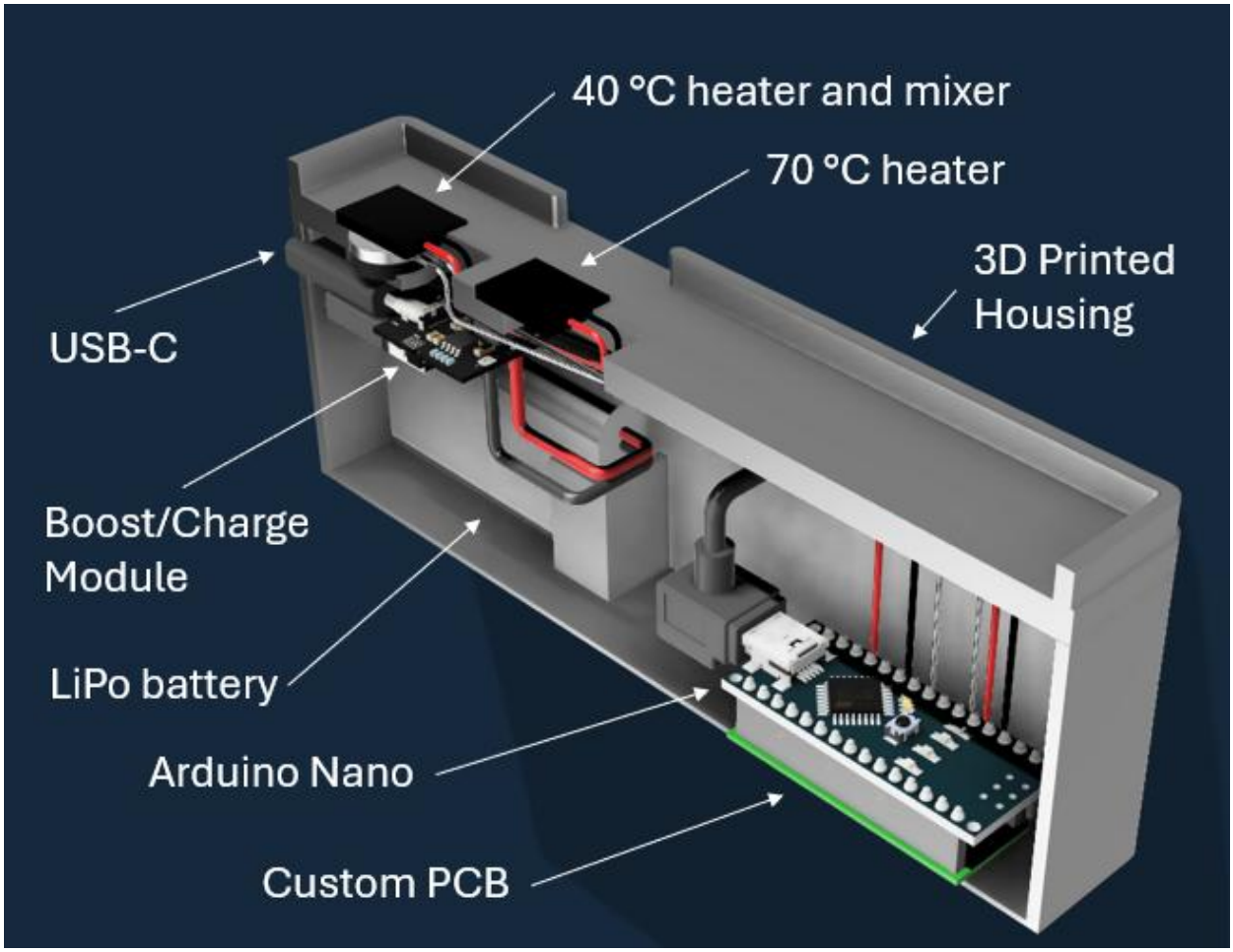

Figure 41. Image of heating platform with internal cut view. An Arduino controls two MCH heaters, an ERM coin cell motor, and an LED. Device is turned off and on using a slide switch and can be powered via USB-C or LiPo battery.

A general cut view section of the reusable platform is seen in Figure 41. The main circuit and its elements, excluding the two position slider and LED light, are shown. The MOSFETS, main connection points, and resistors are soldered onto a protoboard that is fitted underneath the Arduino

Nano. Additional space was allocated to accommodate excess wire length required to connect the various components to the protoboard, ensuring ease of assembly, strain relief, and reliable electrical connections. The system is contained in a PETG housing that was 3D printed on a BambuLabs X1C printer.

PID coefficients were experimentally determined. In the future, improving PID coefficients and temperature control will allow quicker ramp up time and more stable heating. A proportional-integral-derivative (PID) is a feedback control loop used to automatically regulate systems through precise corrective adjustments. The controller compares a desired target value, or setpoint, to the system's measured value and applies a correction based on the resulting error. The proportional term applies to a proportional correction to the error between the measured value and setpoint. The integral term reduces steady-state error by accumulating past errors over time, while the derivative term improves transient response by predicting future error trends and reducing overshoot. The control function is defined as:

$$u(t) = K_p e(t) + K_i \int_0^t e\,(\tau) d\tau + K_d \frac{de(t)}{dt}$$

Where K_p, K_i, and K_d are non-negative coefficients corresponding to the proportional, integral, and derivative terms respectively.[162]

Since the MCH heaters possess a low thermal mass and respond quickly to initial power input, a high proportional gain range of (K_p= 20 - 25) was selected to decrease heater rise time and allow the system to rapidly approach the target temperatures without significant delay. Lower K_i values were selected since steady-state temperature error caused by environmental heat loss and cartridge loading was minimal. With higher integral values, overshoot and stabilization time was

significantly higher. Lastly, a low K_d value of 0.5 - 1 was selected for the heaters as there was a delayed thermal response due to thermal inertia from the ceramic substrate once at an elevated temperature. Higher K_d values introduced unnecessary sensitivity to the sensor noise and did not significantly improve the system performance. While there is some overshoot, the smaller derivative gain is sufficient in damping the overshoot while maintaining a stable temperature. These values were additionally adjusted and refined through experimentation. The specific values used for each heater can be seen in the Arduino code below in the Appendix. In future work, systematic optimization using heater step response characterization and analyzing overshoot, settling time, and oscillatory behavior could further optimize controller performance and identify ideal PID coefficients.

4.3.3 Platform Operation

The disposable cartridge friction fits onto the heating platform and can be placed either before or after the user adds their sample to the sample treatment chamber. The user is required to perform two timed steps, to add the sample to the cartridge and to push the sliding mechanism to incorporate the separate components together. After the test is completed, the user can dispose of the cartridge in biohazard trash and perform another experiment.

Figure 42. Images of disposable cartridge placed on heating platform. Left: CAD render of cartridge and heating platform. Right: Photo of fabricated cartridge and platform.

Figure 42 depicts the rendered assembly and image of the fully fabricated cartridge and heater platform. Although the cartridge is just friction-fitted onto the platform, it remains securely in place under mechanical disturbance and when oriented in different directions. Since the cartridge is fabricated from PETG, it retains sufficient flexibility to allow easy removal upon completion of the experiment. To operate the platform, the user switches on the perform, opens the sample port and adds their plasma or serum sample to the bottom of the chamber, and after five minutes of incubation the red LED will turn on and the user will then push the slide mechanism to burst the frangible seals to integrate the individually stored reagents to initiate the paper-based RPA reaction. After 20 minutes, the reaction amplifies and produces a fluorescent output when positive or remains non-fluorescent when negative.

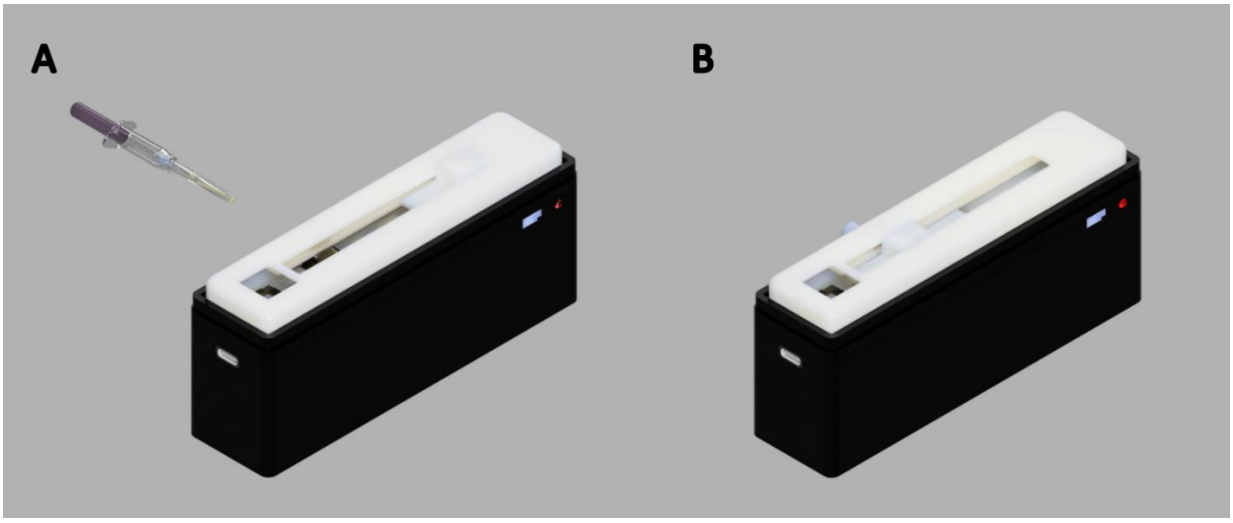

Figure 43. Overview of main user steps. After switching the platform on, (A) The user opens the sample port, adds the plasma or serum sample to the bottom of the chamber, and then shuts the port. (B) After five minutes of incubation, the LED light turns on to indicate for the user to push the slide mechanism and burst the frangible seals. The reaction is imbibed into the membrane and paper-based RPA is incubated for 20 minutes with continuous mixing.

While the overall workflow is reduced to only two timed user interactions, maintaining precise timing may still be difficult and variable between users, which is not ideal for a POC system. To automate the slide mechanism, DC motors or linear actuators could be integrated to actuate the timed compression sequence, either by directly compressing each chamber or by driving a rotational wheel that sequentially compresses them. This would further simplify the workflow to a simple sample addition step while reducing potential user error associated with intermediate time-sensitive operations.

4.3.4 Synthetic DNA Testing

I performed initial testing on the device using synthetic HCV DNA spiked in pooled plasma. This served as a proof of concept to evaluate overall device functionality while reducing experimental

variables, such as precise thermal incubation requirements associated with sample treatment and the additional complexities of RT-RPA that can complicate successful target detection. Compared to RNA targets, DNA targets are more stable and less susceptible to degradation during sample handling and processing. In contrast, successful RNA detection would depend on maintaining proper sample treatment conditions, including accurate incubation temperatures and effective reagent performance, as factors such as oxidized DTT or incomplete RNase inactivation could negatively impact assay performance. Furthermore, RT-RPA introduces additional complexity through the incorporation of sensitive enzymatic components, including reverse transcriptase, single-stranded binding proteins, and RNase inhibitors, all of which must be stored separately and function effectively to enable successful amplification. Using HCV DNA spiked into pooled plasma, successful amplification was achieved for both 200 and 2000 copies per reaction, demonstrating the feasibility of the integrated platform under simplified proof-of-concept conditions.

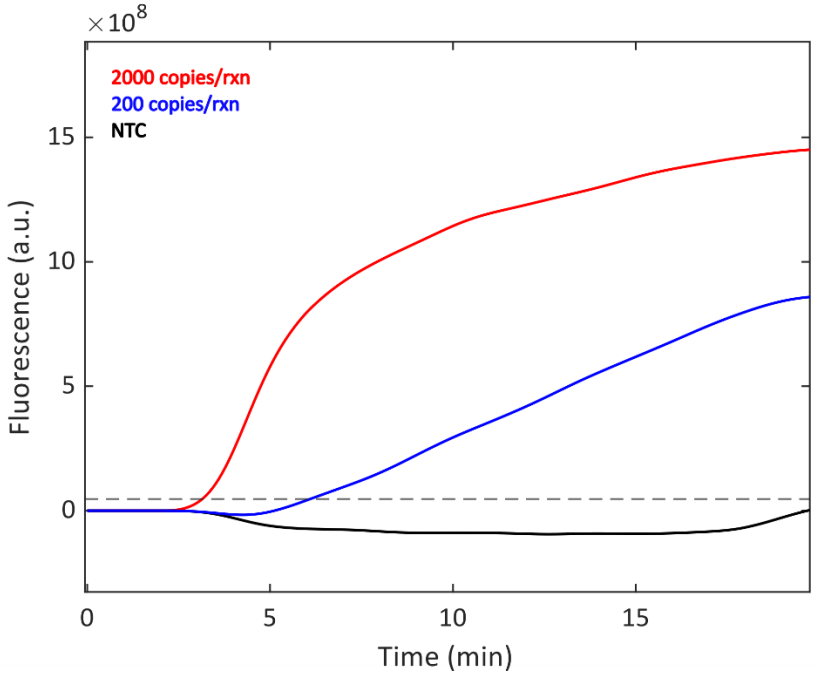

Figure 44. Total fluorescence curves for the amplification of HCV DNA spiked in pooled plasma. Concentrations ranged from 0 to 2000 copies/reaction for RPA reactions with the extraction-free sample preparation method.

In Figure 44, the fluorescence curves were plotted to show real-time amplification during the 20-minute RPA incubation period. While the non-template control (NTC) did not amplify, as seen in the black line, there was amplification for both 200 and 2000 copies per reaction. As expected, the higher concentration sample had a quicker time-to-threshold and an overall higher fluorescence output when compared to the lower concentration sample.

These results provided a positive initial indication that the integrated cartridge and heating platform were functioning as intended. Successful amplification suggested that the device is maintaining the thermal conditions necessary for RPA while also supporting some reagent mixing, fluid handling, and membrane-based amplification within the cartridge format. Furthermore, the ability to detect amplification at both tested concentrations demonstrated preliminary analytical sensitivity under proof-of-concept conditions using plasma samples. These findings support the feasibility of the overall platform design and demonstrated that the integrated system could successfully perform nucleic acid amplification within the intended workflow. Additionally, these results provided confidence to proceed with testing using RNA targets.

4.3.5 HCV Sample Testing

Following the positive performance observed with spiked DNA samples, I then performed an initial validation of the device and complete workflow using an RNA clinical serum sample (HCV genotype 1a). Unlike the previous proof-of-concept experiments with DNA, this experiment

evaluated the full extraction-free workflow, including effective viral lysis, RNA preservation, reverse transcription, and amplification within the integrated platform. This represented a more rigorous assessment of the device functionality as successful detection depended not only on amplification performance, but also on effective viral lysis and RNA handling throughout the process.

Successful amplification was observed for HCV clinical sample 9348, which had a viral load of 3,182 IU/µL. The corresponding in-tube amplification curve is shown in Figure 36. Figure 45 shows the amplification results for the clinical sample compared to a no template control (negative pooled plasma). The clinical sample exhibited strong amplification, while the NTC remained flat throughout the 20-minute incubation period, indicating minimal nonspecific amplification or contamination under tested conditions. The observed amplification signal from the clinical sample further supported successful viral RNA detection using the integrated extraction-free workflow. Additional clinical samples were not tested due to limited time and resources, but future work in the lab is focused on an expanded validation of the test cartridge using clinical samples.

Amplification for the clinical sample remains primarily localized to the top half of the membrane, suggesting inadequate mixing with the main RPA reagents. This uneven amplification distribution was caused by incomplete reagent diffusion, with a greater concentration of active RPA components collecting near the side of the membrane closest to the lyophilized pellet chamber. These findings indicate that while amplification was successful, reagent distribution across the membrane was not fully uniform during the reaction. For future work, additional optimization is required to better integrate more effective continuous mixing within the heating platform to improve reaction uniformity and overall assay consistency.

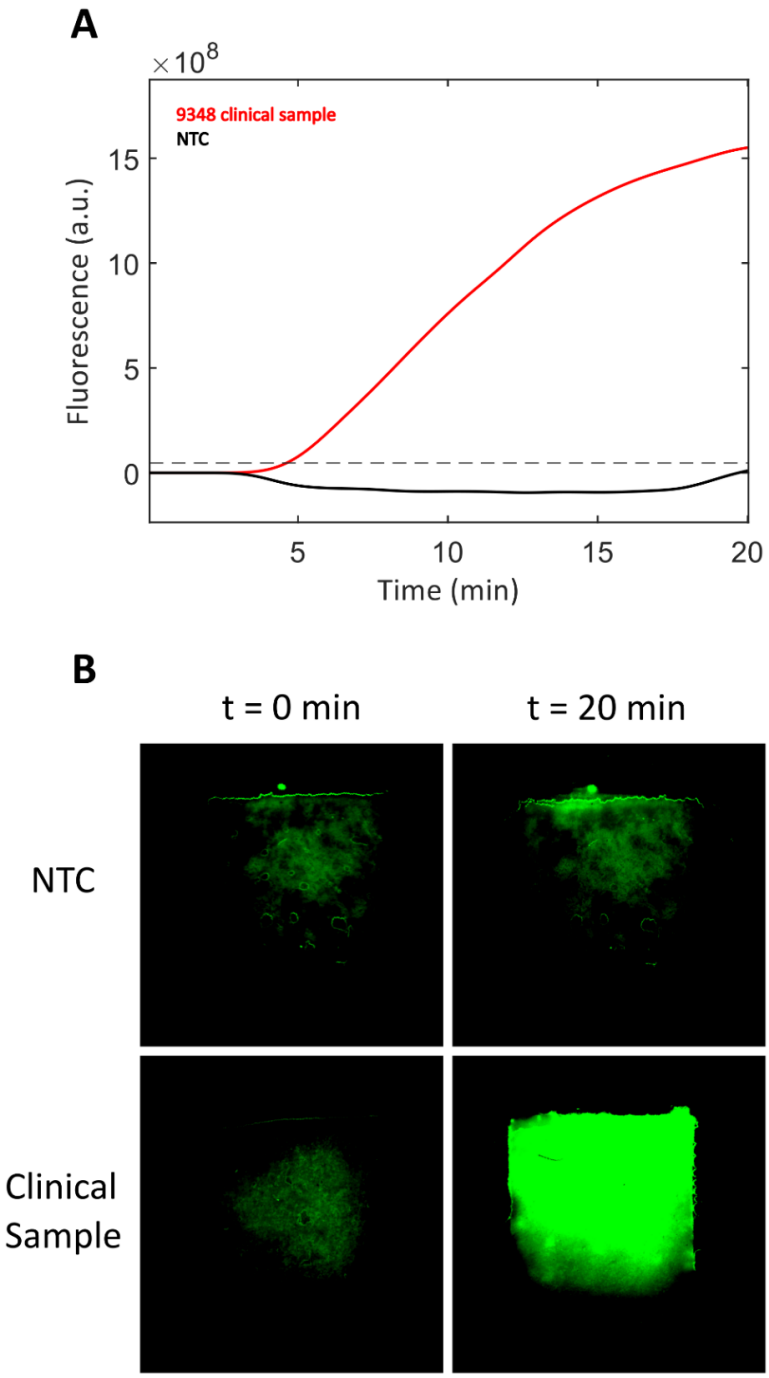

Figure 45. Results for amplification of a genotype 1a HCV RNA sample, CS 9843. (A) shows that total fluorescence curves for the clinical sample against a negative pooled plasma sample, labeled no template control (NTC). This sample concentration was tested by UW testing services to be 3,182 IU/µL. (B) Fluorescence images of the NTC (top row) and the clinical sample (bottom row) at t = 0 minutes (left column) and t = 20 minutes (right column).

Nevertheless, as a preliminary validation study, these results provided encouraging evidence that the cartridge, heating platform, and complete extraction-free workflow were functioning as intended. Detection of amplification from this RNA clinical sample indicated that the sample treatment conditions were sufficient to support viral lysis and RNA preservation. Furthermore, the results suggested that the integrated heating system could adequately support both the sample preparation incubation and the subsequent RT-RPA reaction conditions required for successful target amplification. Overall, this experiment served as an important early demonstration that the integrated platform could process and detect clinically relevant RNA targets using the intended extraction-free workflow.

4.4 Conclusions

In conclusion, the cartridge-based system can perform a complete extraction-free workflow for HCV detection. The integrated system requires only two user steps: adding plasma or serum sample and pushing a slide mechanism after five minutes of incubation. The platform delivers results in under 30 minutes and works toward a practical point-of-care diagnostic format. The workflow is consolidated into a simple, self-contained cartridge that is easy to use and reduces contamination risk. A low-cost reusable heating platform facilitates the required two-step thermal incubation and mixing for the reaction. The system successfully detected HCV DNA for 200 and 2,000 copies per reaction and demonstrated successful detection of a genotype 1 clinical sample, which validated the that full workflow, cartridge, and platform were working as intended. These results further support the feasibility of the approach toward a POC diagnostic device.

Future work will focus on aspects such as reducing user steps by automating the sliding mechanism, lyophilizing critical reagents to improve assay stability and storage, optimizing PID coefficients to improve temperature control, and improving mixing efficiency. Lastly, additional validation studies comparing cartridge performance with conventional in-tube will also be important in establishing the system's clinical utility and scalability for decentralized testing applications.

Chapter 5 Summary and Recommendations

5.1 Summary

This work sets out to address key bottlenecks in the NAAT workflow, specifically in paper-based amplification and sample preparation for bloodborne pathogen detection. I sought to overcome challenges in (i) improving paper-based RPA reactions through continuous mixing, (ii) reducing complexity of sample preparation for blood-based matrices, and (iii) developing a user-friendly POC test device. Collectively, these advances demonstrate pathways toward more robust, sensitive, and deployable NAAT systems.

To improve paper-based RPA reactions, I incorporated continuous vibration-based mixing to enhance reaction kinetics and mass transport within the paper matrix. This approach improved the limit of detection, reduced the time-to-threshold, and increased the overall fluorescence signal intensity. With continuous mixing, I found a 6.4x improvement in LOD with a sensitivity of 12 copies per reaction for HIV DNA, up to a 5-minute reduction in time-to-threshold, and an overall fluorescence output up to 16 times brighter when compared to unmixed experiments. I additionally show successful amplification for various scenarios such as uneven distributions of magnesium cofactor and target and without any heating module, indicating that active mixing can partially overcome diffusion limitations inherent to porous substrates.

I next focused on reducing the complexity of sample preparation for blood-based samples by developing an extraction-free method compatible with both plasma and serum. By optimizing the extraction-free chemistry and scaling the reaction volume, I achieved a limit of detection of 800 copies/mL across both tube-based and paper-based amplification formats. I further refined the

method to improve its repeatability and adaptability and extended its application to HCV detection. The assay was validated using HCV clinical samples ranging from genotypes 1-3 and 5, yielding a sensitivity of 100% and a specificity of 100%. Together, these results suggest that simplified, extraction-free sample preparation workflows can enable more accessible and practical home-based diagnostics for bloodborne pathogens.

Lastly, I sought to reduce instruments required and user steps for the extraction-free workflow by developing an integrated sample treatment and nucleic acid amplification device for bloodborne diagnostics. This cartridge-based system can execute a complete extraction-free workflow in 2 timed user steps, delivering results in under 30 minutes. The single-use cartridge is preloaded with all the necessary reagents and consolidates the workflow into a simple, self-contained format. It interfaces with a low-cost, reusable platform that provides two-stage thermal incubation and enables continuous mixing during amplification. I validated this device by successfully amplifying synthetic DNA spiked into plasma as well as an HCV genotype 1 clinical sample. This system represents a meaningful step toward a POC diagnostic format.

This dissertation demonstrates that improving paper-based amplification, simplifying sample preparation, integrating workflows into disposable cartridge-based systems, and minimizing user-dependent steps can improve the accessibility and reproducibility of nucleic acid amplification tests. Continued efforts to mitigate sample-derived inhibitors, further refine cartridge manufacturability, and reduce operational complexity will be critical for closing remaining gaps and enabling widespread adoption of bloodborne NAAT diagnostics in POC and home-based settings.

5.2 Reflections and Future Work

5.2.1 Analysis of Optimal Mixing Conditions

Future work can focus on further optimizing the mixing conditions for paper-based amplification reactions to improve reaction repeatability and sensitivity. Additional studies could evaluate alternative motors with different vibration frequencies, amplitudes, and power requirements to determine their effects on reagent distribution and amplification efficiency within porous membranes. Actuators that operate along a single axis directed toward the membrane, such as linear resonant actuator (LRA) motors, tweeters, and piezo stacks may additionally provide more empirical insight into how actuation input, displacement, and vibration frequency influence mixing behavior and amplification efficiency within paper matrices. Evaluating these controlled actuation methods could help establish more quantitative relationships between mechanical stimulation, fluid transport, and assay performance in porous membrane systems. Other mixing strategies, including purely rotational mixing, surface acoustic waves, or passive capillary-driven approaches, may also be explored to identify methods that provide more uniform fluid transport while maintaining low-cost and portable device operation for POC applications.

5.2.2 Sample Preparation Optimization

Sample preparation is an incredibly important aspect in the NAAT workflow. Future work should further optimize the extraction-free sample preparation method to improve compatibility with complex clinical specimens and reduce amplification inhibition. Additional improvements to the sample treatment include higher dilution ratios and buffering agents such as MOPS or HEPES, to reduce likelihood of temperature or pH-based coagulation in samples and improve sample treatment tolerance across sample types. Alternative reducing agents, including tris(2-

carboxyethyl)phosphine (TCEP), and β-meracaptoethanol, may also be investigated to determine their effectiveness in RNase inactivation and compatibility with downstream amplification reactions.

Patient samples can contain highly variable concentrations of amplification inhibitors, proteins, and cellular debris. Future studies should also investigate sample cleanup and preprocessing strategies to improve assay robustness and consistency. Methods such as membrane-based filtration, magnetic bead purification, or a simplified liquid-phase extraction approach could help reduce inhibitory components while maintaining rapid and low-complexity workflows suitable for POC diagnostics. Evaluating these approaches may also help establish an optimal balance between sample preparation simplicity, inhibitor removal, nucleic acid recovery, and overall assay sensitivity.

5.2.3 Analysis of Various Sample Types

Alternative matrices such as saliva, urine, nasal swabs, sputum, and stool-derived extracts present distinct biochemical environments with varying levels of nucleases, inhibitors, and other debris that may impact amplification performance. Systematic comparison across these sample types would help identify matrix-specific challenges and guide tailored modifications for pre-processing requirements and assay chemistry. In addition, evaluating alternative sampling formats for blood, such as dried blood spots, could further extend the utility of the system for decentralized testing.

5.2.4 Multiplex Assay

Future work should further motivate the development of multiplexed point-of-care assays targeting clinically relevant co-circulating bloodborne pathogens, particularly HIV, HBV, HCV, given their

high global burden and direct impact on treatment selection and long-term disease management. Co-infections among these viruses are well documented in high-risk populations; for example, HIV-HBV co-infection affects an estimated ~10% of people living with HIV globally and is associated with accelerated liver disease progression and increased clinical complexity.[163] HIV requires lifelong antiretroviral therapy (ART) with routine viral load monitoring being essential in confirming treatment efficacy.[50,51] HBV also requires long-term suppression therapy, often using nucleoside reverse transcriptase inhibitors (NRTIs). Several FDA-approved agents, including tenofovir alafenamide, tenofovir disoproxil fumarate, lamivudine, and emtricitabine, are active against both HIV and HBV, further emphasizing the importance of accurate co-detection in determining optimal therapeutic selection and long-term management strategies.[164]

The clinical management of HCV adds complexity, as direct-acting antivirals (DAAs) achieve a cure rate of approximately 90 - 95% over short treatment courses lasting 8 - 12 weeks.[165] In co-infection scenarios such as HCV-HBV, HCV can suppress HBV replication, potentially masking active HBV infection until HCV is cleared. Following HCV eradication, HBV reactivation can occur, making pre-treatment HBV screening and concurrent antiviral management critical to prevent severe outcomes.[43]

Given these clinical interdependencies, a multiplex diagnostic assay capable of simultaneously identifying HIV, HBV, and HCV from a single blood sample would provide significant clinical value by enabling more informed treatment selection, reducing risk of adverse drug interactions, and helping prevent complications such as HBV reactivation.

Beyond viral targets, two opportunistic infections strongly associated with HIV that can significantly impact treatment outcomes include syphilis and tuberculosis (TB). Co-infections of these pathogens with HIV carry meaningful clinical consequences but are mismatched in terms of

a single molecular bloodborne platform due to differences in pathogen biology, specimen requirements, and diagnostic modality. For example, TB detection typically relies on respiratory specimens, and syphilis is primarily diagnosed via serological methods. These pathogens are therefore better addressed through complementary diagnostic platforms rather than a single consolidated assay format.

Several commercial assays already demonstrate the feasibility of multiplex pathogen detection. The Cobas MPX, for instance, is a multiplex PCR test that is used to detect HIV, HCV, and HBV using plasma or serum samples. In 2025, the WHO prequalified the *Determine™ Antenatal Care Panel*, a triple antibody test for the detection of HIV, HBV, and syphilis from human capillary whole blood.[166] Another example is the INSTI Multiple HIV-1/HIV-2/Syphilis Antibody Test. Together, these platforms highlight the clinical value and the practical boundaries of multiple target detection. They point toward a future where expanded multiplex assays can more meaningfully improve diagnostic coverage, guide treatment selection, and reduce preventable morbidity in the populations that need it most.

5.2.5 Towards a Fully Integrated Device and Cartridge

Lastly, more work can focus on progressing toward a fully integrated sample-to-answer device that consolidates all steps of sample processing, amplification, and detection into a single streamlined workflow. A key component for this effort will be the direct integration of whole blood input, eliminating the need for centrifuging. Existing blood fractionation devices, such as MDI's PlasmaDrop kits or CanaryQ, leverage stack filters or asymmetric membranes and can extract plasma from whole blood samples. Spending more time and research to implement these devices can bring the work closer to a fully sample-to-answer assay.

Additionally, small improvements such as improving mixing and further reducing user steps by automating the required sliding mechanism would improve the repeatability and ease of use of the cartridge. Storage chambers can also be consolidated with lyophilization or paper-based drying methods to further reduce cartridge size, improve repeatability, and enable storage without any refrigeration or freezer requirements.

Lastly, the system can be further developed to incorporate an integrated fluorescence-based detection for real-time readout. Embedding optical detection elements within the reusable platform would enable sensitive signal measurement while preserving portability and ease of use. Together, these advancements would move the platform close to a fully self-contained POC diagnostic system capable of handling raw clinical samples and delivering a rapid time to results without external instrumentation or manual handling steps.

Appendix

6.1 Details on Whole Blood Fractionation Devices

6.1.1 Preliminary Assessment of Blood Fractionation Devices and Prototypes

I ran initial validations for whole blood fractionation with a commercial device, CanaryQ, that can extract plasma from 100 µL of blood. This device uses a pressure based system with an asymmetric membrane to fractionate blood. When tested, this device had a 45.5% extraction efficiency to produce 25 µL of plasma. Since the main driving force is applied pressure from a pipette, syringe, or similar system, there was evidence of slight hemolysis. While easy to use, the presence of some hemoglobin may affect the RPA assay when paired with the extraction-free sample treatment. While the company's main devices do not handle a broad range of input volumes, they are able to make a custom device with a specific plasma output for your needs.

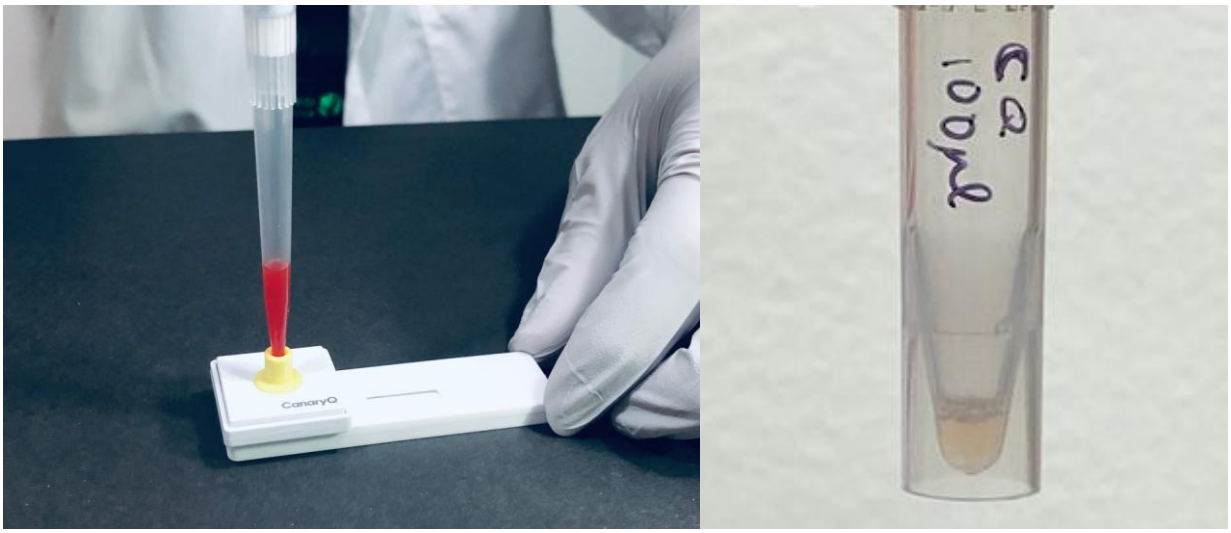

Figure 46. Left image: Image from CanaryQ depicting the use of the device.[167] Right image: Extracted plasma obtained from adding 100 µL of whole blood into the CanaryQ device.

I additionally fabricated custom devices designed to process a 50 µL whole blood input and evaluated their performance for plasma extraction. These devices used an asymmetric Vivid plasma separation membrane in an SLA printed housing. These were similar to the blood fractionation devices developed by Deiana and Smith*, 2024*. I compared a non-pressurized pipette extraction approach where after pipetting whole blood onto the membrane, I flipped the device and pipette extracted the plasma out of the opposite end. In the non-pressurized system, plasma was extracted and achieved a 40% extraction efficiency, yielding approximately 11 µL of plasma. I additionally made pressurized devices with a smaller input port to generate the required pressure to push whole blood through the device using a pipette and generate a plasma droplet out through the device without requiring pipette extraction from the opposite end. The pressurized device performed significantly worse with a 25.5% extraction efficiency to produce 7 µL of extracted plasma and had evidence of slight hemolysis. To improve the flow through the devices, Triton X-100 was applied to the interior of the SLA housing and dried at room temperature; however, this modification may also impact downstream sample preparation as the detergent will likely lyse HCV virus before any Rnase inhibition is performed.

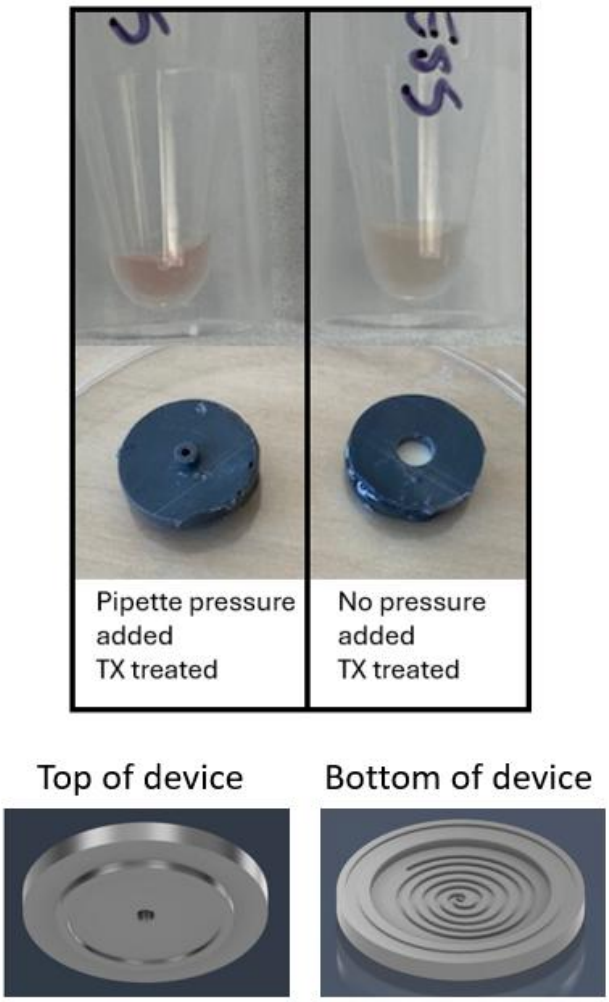

Figure 47. Custom SLA printed devices that housed a vivid plasma separation membrane. Design was inspired by research from Deiana and Smith (2024) and the existing commercial CanaryQ device.[146,168]

The custom printed devices using the Vivid plasma separation membrane can be seen in Figure 47. For higher extraction efficiency and cleaner samples, the non-pressurized device performed significantly better than the pressurized device. For the pressurized device, the overall extraction efficiency was poor and did not match the performance of the commercial CanaryQ device. The benefit of the pressurized device is that plasma does not need to be pipette extracted out of the

opposite end of the device and the overall cost is quite low when considering just the material required to fabricate the device. In comparison, while the non-pressurized device worked much better, there are more user steps required to extract the plasma. For the CanaryQ device, while it works well, the overall cost can be a bit high at ~$20 per device.

While these blood fractionation devices can extract plasma from a whole blood sample, they were still far from being easy to implement into the diagnostic device or cartridge. With the extraction-free method, only 4 - 5 µL of plasma or serum can be added to a 50 µL reaction. These devices generated significantly more plasma and would need modifications to adjust the output to match the requirements for the sample treatment. Additionally, the current HCV clinical samples we had were already extracted serum and stored at -80 ºC. Logistically, it would be difficult to procure fresh positive HCV clinical samples and involved to add red blood cells to the existing clinical samples just to "re-extract" the sample. As a result, this work did not progress further and was left out in the device integration. In future work, revisiting these devices would be beneficial when incorporating a full workflow with whole blood samples into the cartridge and heater system.

6.2 Details on Paper-based RPA

6.2.1 Amplification on Fusion 5 Membranes

RPA amplification performance is highly dependent on membrane type, GF/DVA membranes consistently produced the strongest RPA signals with other membrane types exhibiting varying degrees of success.[79] Fusion 5, a proprietary glass fiber and synthetic polymer membrane, supported only weak amplification under standard conditions. However, membrane pretreatment improved amplification performance. I evaluated two pretreatment methods: (1) a 10-minute wash

in nuclease-free water followed by overnight drying at room temperature, and (2) a 10-minute wash in 10% acetic acid followed by two 5-minute rinses in nuclease-free water and overnight drying at room temperature. Both pretreatments improved amplification relative to the untreated membrane, with the acetic acid wash producing the greatest improvement, as seen in Figure 48.

These findings suggest that residual contaminants, manufacturing additives, surface treatments, or other membrane-associated compounds may inhibit paper-based RPA on Fusion 5 membranes. Removal of these inhibitory substances through washing appears to improve amplification efficiency, particularly when an acid wash is included. While the exact mechanism remains unclear, the results indicate that membrane compatibility with paper-based RPA may depend not only on the intrinsic properties of the membrane but also on removable surface contaminants introduced during manufacturing. Membranes previously considered unsuitable for RPA may become compatible following simple pretreatment procedures, expanding the range of materials available for assay design. Membrane pretreatment may also represent a strategy to further improve amplification performance on GF/DVA membranes, which are typically employed without prior washing.

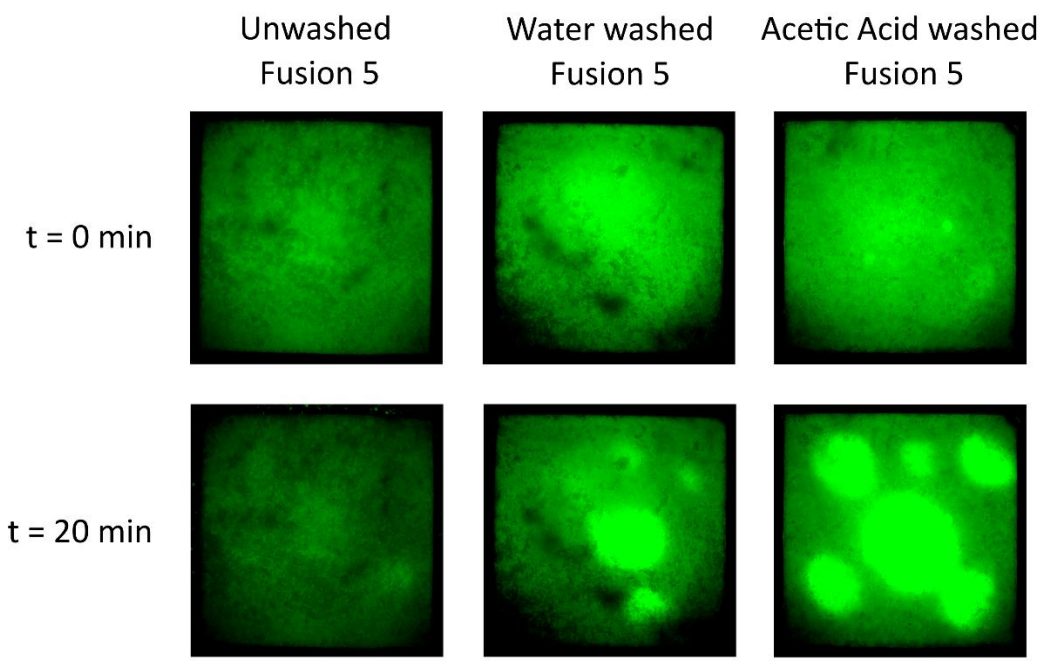

Figure 48. Unmixed Fusion 5 membrane experiments for 1000 copies of HCV DNA with varying levels of washing or preprocessing. Top row represents membrane images at t = 0 minutes. Bottom row represents images at t = 20 minutes. Left column to right represents an unwashed membrane, membrane washed with nuclease-free water for 10 minutes and dried at room temperature before amplification, membrane washed with 10% acetic acid followed by two 5-minute nuclease-free water rinses and dried at room temperature before amplification.

6.2.2 Analysis Code for Square Membranes

```
clear; close all; clc;

% Set defaults
set(0,...
   'DefaultAxesFontSize',16,...
   'DefaultTextFontSize',16,...
   'DefaultLineMarkerSize',12,...
   'DefaultLineLineWidth', 1);
```

```
%% User inputs
namefile = '2000_closed'; %be careful of which file is being used. Numbers could either mean copies/reaction, copies/mL, or something else
bg = 50; % background
multiplier = 1.02; % can be changed. Higher than 1 does a more aggressive background subtraction.

%% Crop image
% figure(1)
preview=mimread('',namefile,24,1);
imshow(preview,[0 102000])
h = drawline('SelectedColor','blue');
points = h.Position;
slope = (points(1,2)-points(2,2))/(points(1,1)-points(2,1));
angle = tanh(slope);
degangle = rad2deg(angle);
I2 = imrotate(preview,degangle);
namefile
imshow(I2,[0 102000])
rect = getrect();
xmin = double(rect(1));
ymin = double(rect(2));
height = double(rect(4));
L = double(rect(3));

%% Compile image data

% Establish background using the same circular region
crop = imcrop(I2,[xmin ymin L height]);
background_stack = zeros(size(crop)); % background matrix
```

```
for i = 1: bg
    frame = double(mimread('', namefile, i, 1));
    rotframe = imrotate(frame,degangle);
    cropframe = imcrop(rotframe,[xmin ymin L height]);
    background_stack = background_stack + cropframe;
end

background = background_stack / bg; %average background for frame 1 to frame bg
background = background * multiplier;

k = length(imfinfo([namefile '.tif'])); % Number of frames in data stack
bulkfluor = zeros(1, k-bg); % Preallocate fluorescence array

m = 1;
for j = bg+1:k
    Image = double(mimread('', namefile, j, 1));  % Read frame
    I2 = imrotate(Image,degangle);
    X = imcrop(I2,[xmin ymin L height])-background; % Apply mask and subtract background
    bulkfluor(m) = sum(X(:)); % Sum only within ROI

    % Display processed image
%     figure(1)
    set(gcf, 'Position', [700, 540, 230, 180]);
%     imshow(X, [])
    F(m) = getframe(gcf); % Store frames for video

    m = m + 1;
end
%% Generate video of background-subtracted images
```

```
% v = VideoWriter(namefile,'MPEG-4');
% v.FrameRate = 5;  % Adjust frames per second as needed
% open(v);
% writeVideo(v, F);
% close(v)

%% Plot bulk fluorescence over time
bulkfluor = [zeros(1,bg),bulkfluor];

% bulkfluor(bulkfluor < 0) = 0; %set negative values to zero. Use if only looking at positive amplification values. Otherwise keep commented out.

t = linspace(0, 20, length(bulkfluor)); % Create time series over 20-25 mins

plotscale = movmean(bulkfluor, [1 1]); % Scale & smooth
plotscale = smoothdata(plotscale, "gaussian",45);

figure
plot(t, plotscale, 'linewidth', 1.5)
set(gca, 'linewidth', 1)
ylabel('Fluorescence (a.u.)')
xlabel('Time (min)')
```

6.3 Details on Extraction-free Sample Preparation

6.3.1 RNase Activity within the First Minute of Incubation

While the RNase alert assay can detect RNase activity after treatment incubation, it is not as useful when looking at active RNase reduction during the treatment incubation. This is important as RNases can easily degrade exogeneous RNA within 15 seconds of contact.[117] To learn more about

active RNase inactivation during treatment incubation, I performed short, timed incubations at 70 °C with and without DTT to look at how the reducing agent inactivates RNases within the first minute of incubation. These preliminary results suggest that DTT quickly inactivated RNases within the first minute of incubation, thus protecting RNA during concurrent viral lysis. Having early and effective RNase inhibition is important in retaining as much of the RNA for downstream amplification. The ability to detect RNA and RNase activity during the incubation or treatment process is especially important in finding the optimal chemicals, conditions, and methods required to protect the RNA.

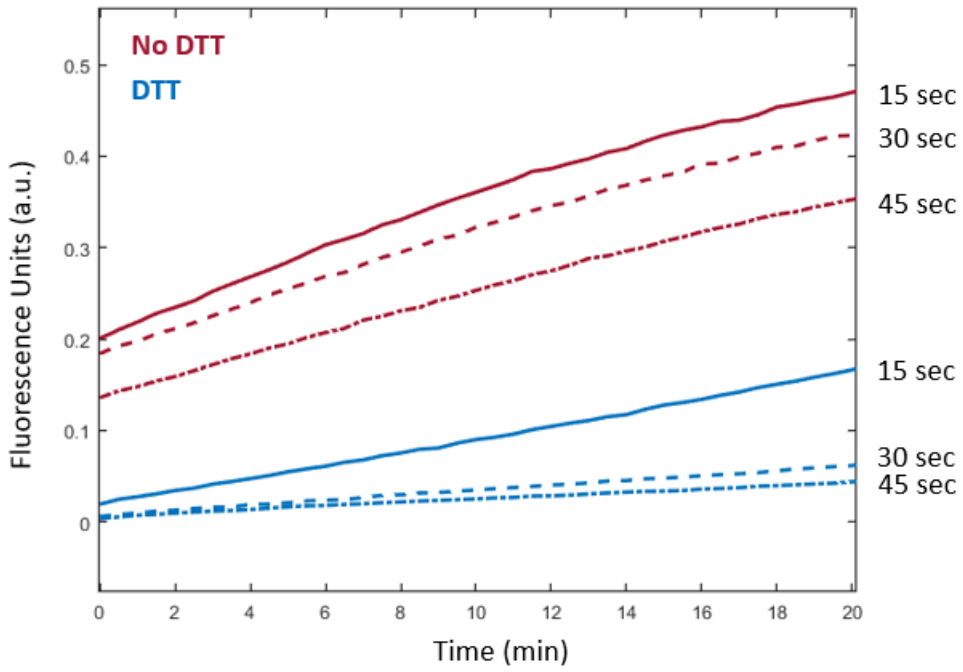

Figure 49. Timed incubation experiments to look at initial RNase inactivation during the first minute of 70 °C thermal treatment.

6.4 Details on POC Device

6.4.1 Heating Platform Code

```
// ---------------- PINS ----------------
int Thermistor1Pin = A4; // 40Â°C heater
int Thermistor2Pin = A2; // 70Â°C heater

int Heater40Pin = 7;
int Heater70Pin = 6;
int LEDPin = 2;
int MotorPin = 5;
int SwitchPin = 10;

// ---------------- THERMISTOR ----------------
int Vo;
float R1 = 10000;
float logR2, R2, T;

float c1 = 1.009249522e-03;
float c2 = 2.378405444e-04;
float c3 = 2.019202697e-07;

// ---------------- PID ----------------
float Kp1 = 20.0, Ki1 = 0.5, Kd1 = 0.5;   // 40Â°C
float Kp2 = 12.0, Ki2 = 0.15, Kd2 = 0.8;  // 70Â°C

float integral1 = 0, lastError1 = 0;
float integral2 = 0, lastError2 = 0;

unsigned long lastTime = 0;

// ---------------- STAGES ----------------
int stage = 0;
unsigned long stageStartTime = 0;

// Durations
unsigned long stage1Duration = 5UL * 60UL * 1000UL;
unsigned long stage2Duration = 30UL * 1000UL;
unsigned long stage3Duration = 20UL * 60UL * 1000UL;

// Motor
int motorPWM = 180;

// Safety
float maxTemp = 80.0;

// ---------- Time Remaining ----------
float getTimeRemainingMinutes(unsigned long start, unsigned long duration,
unsigned long now) {
  unsigned long elapsed = now - start;
  if (elapsed >= duration) return 0.0;
```

```
  return (duration - elapsed) / 60000.0;
}

// ---------------- SETUP ----------------
void setup() {
  Serial.begin(9600);
  pinMode(Heater40Pin, OUTPUT);
  pinMode(Heater70Pin, OUTPUT);
  pinMode(LEDPin, OUTPUT);
  pinMode(MotorPin, OUTPUT);
  pinMode(SwitchPin, INPUT_PULLUP);
}

// ---------------- THERMISTOR ----------------
float readTemp(int pin) {
  Vo = analogRead(pin);
  R2 = R1 * (1023.0 / (float)Vo - 1.0);
  logR2 = log(R2);
  T = (1.0 / (c1 + c2 * logR2 + c3 * pow(logR2, 3)));
  T = T - 273.15;
  return T;
}

// ---------------- LOOP ----------------
void loop() {
  bool systemOn = (digitalRead(SwitchPin) == LOW);

  if (!systemOn) {
    analogWrite(Heater40Pin, 0);
    analogWrite(Heater70Pin, 0);
    analogWrite(MotorPin, 0);
    digitalWrite(LEDPin, LOW);

    stage = 0;
    integral1 = integral2 = 0;
    lastError1 = lastError2 = 0;

    Serial.println("SYSTEM OFF");
    delay(500);
    return;
  }

  unsigned long now = millis();

  // -------- Stage change cleanup --------
  static int lastStage = -1;
  if (stage != lastStage) {
    analogWrite(Heater40Pin, 0);
    analogWrite(Heater70Pin, 0);
    analogWrite(MotorPin, 0);
    digitalWrite(LEDPin, LOW);

    integral1 = 0;
    integral2 = 0;
```

```
  lastError1 = 0;
  lastError2 = 0;

  lastStage = stage;

  Serial.print("Switched to stage ");
  Serial.println(stage);
}

// -------- Start process --------
if (stage == 0) {
  stage = 1;
  stageStartTime = now;
  Serial.println("Stage 1 START");
}

// -------- Stage transitions --------
if (stage == 1 && (now - stageStartTime >= stage1Duration)) {
  stage = 2;
  stageStartTime = now;
  Serial.println("Stage 2 START");
}
else if (stage == 2 && (now - stageStartTime >= stage2Duration)) {
  stage = 3;
  stageStartTime = now;  // FIXED
  Serial.println("Stage 3 START");
}

// -------- Stage 1: 70Â°C --------
if (stage == 1) {
  float temp = 0;
  for (int i = 0; i < 5; i++) {
    temp += readTemp(Thermistor2Pin);
    delay(5);
  }
  temp /= 5;

  if (temp > maxTemp) {
    analogWrite(Heater70Pin, 0);
    Serial.println("OVER TEMP");
    return;
  }

  float error = 70.0 - temp;
  integral2 += error * dt;
  float derivative = (error - lastError2) / dt;

  float output = Kp2 * error + Ki2 * integral2 + Kd2 * derivative;
  output = constrain(output, 0, 255);

  int pwmValue = (int)output;
  analogWrite(Heater70Pin, pwmValue);

  lastError2 = error;
```

```
    Serial.print("70C Temp: ");
    Serial.println(temp);
  }

  // -------- Stage 2: LED --------
  else if (stage == 2) {
    digitalWrite(LEDPin, HIGH);

    float timeLeft = (stage2Duration - (now - stageStartTime)) / 1000.0;

    Serial.print("LED ON | Time Left: ");
    Serial.print(timeLeft, 1);
    Serial.println(" sec");
  }

  // -------- Stage 3: 40Â°C + MOTOR --------
  else if (stage == 3) {
    analogWrite(MotorPin, motorPWM);

    float temp = 0;
    for (int i = 0; i < 5; i++) {
      temp += readTemp(Thermistor1Pin);
      delay(5);
    }
    temp /= 5;

    if (temp > maxTemp) {
      analogWrite(Heater40Pin, 0);
      Serial.println("OVER TEMP");
      return;
    }

    float error = 40.0 - temp;
    integral1 += error * dt;
    float derivative = (error - lastError1) / dt;

    float output = Kp1 * error + Ki1 * integral1 + Kd1 * derivative;
    output = constrain(output, 0, 255);

    int pwmValue = (int)output;
    analogWrite(Heater40Pin, pwmValue);

    lastError1 = error;

    Serial.print("40C Temp: ");
    Serial.print(temp);
    Serial.print(" | Motor PWM: ");
    Serial.println(motorPWM);
  }

  delay(200);
}
```

References

(1) WHO. *The top 10 causes of death*. https://www.who.int/news-room/fact-sheets/detail/the-top-10-causes-of-death.

(2) Niemz, A.; Ferguson, T. M.; Boyle, D. S. Point-of-Care Nucleic Acid Testing for Infectious Diseases. *Trends Biotechnol.* **2011**, *29* (5), 240–250. https://doi.org/10.1016/j.tibtech.2011.01.007.

(3) Abel, G. Current Status and Future Prospects of Point-of-Care Testing around the Globe. *Expert Rev. Mol. Diagn.* **2015**, *15* (7), 853–855. https://doi.org/10.1586/14737159.2015.1060126.

(4) Peeling, R. W.; Holmes, K. K.; Mabey, D. Rapid Tests for Sexually Transmitted Infections (STIs): The Way Forward. *Sex. Transm. Infect.* **2006**, *82* (Suppl 5), v1–v6. https://doi.org/10/d23mr8.

(5) Land, K. J.; Boeras, D. I.; Chen, X.-S.; Ramsay, A. R.; Peeling, R. W. REASSURED Diagnostics to Inform Disease Control Strategies, Strengthen Health Systems and Improve Patient Outcomes. *Nat. Microbiol.* **2019**, *4* (1), 46–54. https://doi.org/10.1038/s41564-018-0295-3.

(6) Emaus, M. N.; Varona, M.; Eitzmann, D. R.; Hsieh, S.-A.; Zeger, V. R.; Anderson, J. L. Nucleic Acid Extraction: Fundamentals of Sample Preparation Methodologies, Current Advancements, and Future Endeavors. *TrAC Trends Anal. Chem.* **2020**, *130*, 115985. https://doi.org/10.1016/j.trac.2020.115985.

(7) Lee, S. M.; Balakrishnan, H. K.; Doeven, E. H.; Yuan, D.; Guijt, R. M. Chemical Trends in Sample Preparation for Nucleic Acid Amplification Testing (NAAT): A Review. *Biosensors* **2023**, *13* (11), 980. https://doi.org/10.3390/bios13110980.

(8) Wilkinson, A. F.; Barra, M. J.; Novak, E. N.; Bond, M.; Richards-Kortum, R. Point-of-Care Isothermal Nucleic Acid Amplification Tests: Progress and Bottlenecks for Extraction-Free Sample Collection and Preparation. *Expert Rev. Mol. Diagn.* **2024**, *24* (6), 509–524. https://doi.org/10.1080/14737159.2024.2375233.

(9) Katevatis, C.; Fan, A.; Klapperich, C. M. Low Concentration DNA Extraction and Recovery Using a Silica Solid Phase. *PLOS ONE* **2017**, *12* (5), e0176848. https://doi.org/10.1371/journal.pone.0176848.

(10) McPherson, M. J.; Møller, S. G. *PCR*; BIOS ; Springer: Oxford, New York, NY, 2000.

(11) Innis, M. A.; Gelfand, D. H.; Sninsky, J. J.; White, T. J. *PCR Protocols: A Guide to Methods and Applications*; Academic Press, 2012.

(12) Heid, C. A.; Stevens, J.; Livak, K. J.; Williams, P. M. Real Time Quantitative PCR. *Genome Res.* **1996**, *6* (10), 986–994. https://doi.org/10/cnzzwv.

(13) Gudnason, H.; Dufva, M.; Bang, D. D.; Wolff, A. Comparison of Multiple DNA Dyes for Real-Time PCR: Effects of Dye Concentration and Sequence Composition on DNA Amplification and Melting Temperature. *Nucleic Acids Res.* **2007**, *35* (19), e127. https://doi.org/10.1093/nar/gkm671.

(14) *A quantitative PCR (TaqMan) assay for pathogenic Leptospira spp | BMC Infectious Diseases | Full Text*. https://bmcinfectdis.biomedcentral.com/articles/10.1186/1471-2334-2-13 (accessed 2021-11-16).

(15) Drummond, T. G.; Hill, M. G.; Barton, J. K. Electrochemical DNA Sensors. *Nat. Biotechnol.* **2003**, *21* (10), 1192–1199. https://doi.org/10.1038/nbt873.

(16) Tomita, N.; Mori, Y.; Kanda, H.; Notomi, T. Loop-Mediated Isothermal Amplification (LAMP) of Gene Sequences and Simple Visual Detection of Products. *Nat. Protoc.* **2008**, *3* (5), 877–882. https://doi.org/10.1038/nprot.2008.57.

(17) Enzo. *What are the differences between PCR, RT-PCR, qPCR, and RT-qPCR?* https://www.enzo.com/note/what-are-the-differences-between-pcr-rt-pcr-qpcr-and-rt-qpcr/ (accessed 2026-03-31).

(18) Drain, P. K.; Hyle, E. P.; Noubary, F.; Freedberg, K. A.; Wilson, D.; Bishai, W. R.; Rodriguez, W.; Bassett, I. V. Diagnostic Point-of-Care Tests in Resource-Limited Settings. *Lancet Infect. Dis.* **2014**, *14* (3), 239–249.

(19) Becherer, L.; Borst, N.; Bakheit, M.; Frischmann, S.; Zengerle, R.; Stetten, F. von. Loop-Mediated Isothermal Amplification (LAMP) – Review and Classification of Methods for Sequence-Specific Detection. *Anal. Methods* **2020**, *12* (6), 717–746. https://doi.org/10.1039/C9AY02246E.

(20) Notomi, T.; Mori, Y.; Tomita, N.; Kanda, H. Loop-Mediated Isothermal Amplification (LAMP): Principle, Features, and Future Prospects. *J. Microbiol.* **2015**, *53* (1), 1–5. https://doi.org/10.1007/s12275-015-4656-9.

(21) Curtis, K. A.; Morrison, D.; Rudolph, D. L.; Shankar, A.; Bloomfield, L. S. P.; Switzer, W. M.; Owen, S. M. A Multiplexed RT-LAMP Assay for Detection of Group M HIV-1 in Plasma or Whole Blood. *J. Virol. Methods* **2018**, *255*, 91–97. https://doi.org/10.1016/j.jviromet.2018.02.012.

(22) Witkowska McConnell, W.; Davis, C.; Sabir, S. R.; Garrett, A.; Bradley-Stewart, A.; Jajesniak, P.; Reboud, J.; Xu, G.; Yang, Z.; Gunson, R.; Thomson, E. C.; Cooper, J. M. Paper Microfluidic Implementation of Loop Mediated Isothermal Amplification for Early Diagnosis of Hepatitis C Virus. *Nat. Commun.* **2021**, *12* (1), 6994. https://doi.org/10/gnz7ds.

(23) Rabe, B. A.; Cepko, C. SARS-CoV-2 Detection Using Isothermal Amplification and a Rapid, Inexpensive Protocol for Sample Inactivation and Purification. *Proc. Natl. Acad. Sci.* **2020**, *117* (39), 24450–24458. https://doi.org/10.1073/pnas.2011221117.

(24) NEB. *Loop-Mediated Isothermal Amplification*. Loop-Mediated Isothermal Amplification. https://www.neb.com/en-us/applications/dna-amplification-pcr-and-qpcr/isothermal-amplification/loop-mediated-isothermal-amplification-lamp.

(25) TwistAmp DNA Amplification Kits Assay Design Manual, 2018. https://www.twistdx.co.uk/docs/default-source/RPA-assay-design/twistamp-assay-design-manual-v2-5.pdf (accessed 2021-09-27).

(26) Lillis, L.; Siverson, J.; Lee, A.; Cantera, J.; Parker, M.; Piepenburg, O.; Lehman, D. A.; Boyle, D. S. Factors Influencing Recombinase Polymerase Amplification (RPA) Assay Outcomes at Point of Care. *Mol. Cell. Probes* **2016**, *30* (2), 74–78. https://doi.org/10.1016/j.mcp.2016.01.009.

(27) Lobato, I. M.; O'Sullivan, C. K. Recombinase Polymerase Amplification: Basics, Applications and Recent Advances. *TrAC Trends Anal. Chem.* **2018**, *98*, 19–35. https://doi.org/10.1016/j.trac.2017.10.015.

(28) Zhang, J. Y.; Bender, A. T.; Boyle, D. S.; Drain, P. K.; Posner, J. D. Current State of Commercial Point-of-Care Nucleic Acid Tests for Infectious Diseases. *Analyst* **2021**, *146* (8), 2449–2462. https://doi.org/10.1039/D0AN01988G.

(29) Drain, P. K.; Dorward, J.; Bender, A.; Lillis, L.; Marinucci, F.; Sacks, J.; Bershteyn, A.; Boyle, D. S.; Posner, J. D.; Garrett, N. Point-of-Care HIV Viral Load Testing: An Essential Tool for a Sustainable Global HIV/AIDS Response. *Clin. Microbiol. Rev.* **2019**, *32* (3), e00097-18. https://doi.org/10.1128/CMR.00097-18.

(30) Mukherjee, S.; Cohn, J.; Ciaranello, A. L.; Sacks, E.; Adetunji, O.; Chadambuka, A.; Mafaune, H.; Makayi, M.; McCann, N.; Turunga, E. Estimating the Cost of Point-of-Care Early Infant Diagnosis in a Program Setting: A Case Study Using Abbott m-PIMA and Cepheid GeneXpert IV in Zimbabwe. *JAIDS J. Acquir. Immune Defic. Syndr.* **2020**, *84*, S63. https://doi.org/10.1097/QAI.0000000000002371.

(31) Rebbapragada, A.; Cariazo, L.; Elchuk, D.; Abdelrahman, H.; Pham, D.; Raveendraraj, J.; Chokshi, K.; Joseph, N.; Gouzenkova, E.; Gill, H.; Blecher, P. Performance of the Cue COVID-19 Point-of-Care Molecular Test: Insights from a Multi-Site Clinic Service Model. *Microbiol. Spectr.* **2023**, *11* (5), e04064-22. https://doi.org/10.1128/spectrum.04064-22.

(32) Lucira Health. *Lucira™ COVID-19 All-In-One Test Kit Instructions for Use*; INST011 Rev 1. https://www.fda.gov/media/143808/download (accessed 2022-10-24).

(33) Donato, L. J.; Trivedi, V. A.; Stransky, A. M.; Misra, A.; Pritt, B. S.; Binnicker, M. J.; Karon, B. S. Evaluation of the Cue Health Point-of-Care COVID-19 (SARS-CoV-2 Nucleic Acid Amplification) Test at a Community Drive through Collection Center. *Diagn. Microbiol. Infect. Dis.* **2021**, *100* (1), 115307. https://doi.org/10.1016/j.diagmicrobio.2020.115307.

(34) Vetri, V.; Librizzi, F.; Leone, M.; Militello, V. Thermal Aggregation of Bovine Serum Albumin at Different pH: Comparison with Human Serum Albumin. *Eur. Biophys. J.* **2007**, *36* (7), 717–725. https://doi.org/10.1007/s00249-007-0196-5.

(35) Dyer, K. D.; Rosenberg, H. F. The RNase a Superfamily: Generation of Diversity and Innate Host Defense. *Mol. Divers.* **2006**, *10* (4), 585–597. https://doi.org/10.1007/s11030-006-9028-2.

(36) Y. Zhang, J.; T. Bender, A.; S. Boyle, D.; K. Drain, P.; D. Posner, J. Current State of Commercial Point-of-Care Nucleic Acid Tests for Infectious Diseases. *Analyst* **2021**, *146* (8), 2449–2462. https://doi.org/10.1039/D0AN01988G.

(37) Chin, C. D.; Linder, V.; Sia, S. K. Lab-on-a-Chip Devices for Global Health: Past Studies and Future Opportunities. *Lab. Chip* **2006**, *7* (1), 41–57. https://doi.org/10.1039/B611455E.

(38) Mariella, R. Sample Preparation: The Weak Link in Microfluidics-Based Biodetection. *Biomed. Microdevices* **2008**, *10* (6), 777–784. https://doi.org/10.1007/s10544-008-9190-7.

(39) Zhang, J.; Bender, A.; Boyle, D.; Drain, P.; Posner, J. Current State of Commercial Point-of-Care Nucleic Acid Tests for Infectious Diseases. *The Analyst* **2021**, *146* (8), 2449–2462. https://doi.org/10.1039/d0an01988g.

(40) *Information on Collection of Respiratory Specimens for Influenza Virus Testing | CDC*. https://www.cdc.gov/flu/professionals/diagnosis/info-collection.htm (accessed 2020-08-24).

(41) Sidstedt, M.; Hedman, J.; Romsos, E. L.; Waitara, L.; Wadsö, L.; Steffen, C. R.; Vallone, P. M.; Rådström, P. Inhibition Mechanisms of Hemoglobin, Immunoglobulin G, and Whole Blood in Digital and Real-Time PCR. *Anal. Bioanal. Chem.* **2018**, *410* (10), 2569–2583. https://doi.org/10.1007/s00216-018-0931-z.

(42) Schrader, C.; Schielke, A.; Ellerbroek, L.; Johne, R. PCR Inhibitors – Occurrence, Properties and Removal. *J. Appl. Microbiol.* **2012**, *113* (5), 1014–1026. https://doi.org/10.1111/j.1365-2672.2012.05384.x.

(43) World Health Organization. *WHO Guidelines on Hepatitis B and C Testing*; World Health Organization: Geneva, 2017.

(44) WHO. *HIV statistics, globally and by WHO region, 2023*. Epidemiological Fact Sheet. https://cdn.who.int/media/docs/default-source/hq-hiv-hepatitis-and-stis-library/j0294-who-hiv-epi-factsheet-v7.pdf.

(45) Cooper, C. Rapid HCV RNA Testing: Removing the Final Obstacle to Elimination. *Lancet Gastroenterol. Hepatol.* **2017**, *2* (7), 468–469. https://doi.org/10.1016/S2468-1253(17)30086-9.

(46) Balasubramaniam, M.; Pandhare, J.; Dash, C. Immune Control of HIV. *JoLS J. Life Sci.* **2019**, *1* (1). https://doi.org/10.36069/JoLS/20190603.

(47) Bbosa, N.; Kaleebu, P.; Ssemwanga, D. HIV Subtype Diversity Worldwide. *Curr. Opin. HIV AIDS* **2019**, *14* (3), 153–160. https://doi.org/10.1097/COH.0000000000000534.

(48) HIV Prevention, A. V. A. C. G. A. PrEP Works If You Take It. In *Effectiveness and adherence in trials of oral and topical tenofovir-based prevention*; 2016.

(49) *HIV Diagnostic Tests in Low- and Middle-Income Countries: Forecasts of Global and Regional Demand For 2021-2025*, 1st ed.; World Health Organization: Geneva, 2022.

(50) World Health Organization (WHO). *Guideline on when to start antiretroviral therapy and on pre-exposure prophylaxis for HIV*. http://apps.who.int/iris/bitstream/10665/186275/1/9789241509565_eng.pdf.

(51) World Health Organization (WHO). *The Use of Antiretroviral Drugs for Treating and Preventing HIV Infection: Recommendations for a Publich Health Approach*. http://www.who.int/hiv/pub/arv/arv-2016/en/ (accessed 2017-06-20).

(52) World Health Organization. *WHO Guidelines on Hepatitis B and C Testing*; World Health Organization: Geneva, 2017.

(53) World Health Organization; Global Hepatitis Programme. *WHO Guidelines on Hepatitis B and C Testing.*; 2017.

(54) Chigbu, D.; Loonawat, R.; Sehgal, M.; Patel, D.; Jain, P. Hepatitis C Virus Infection: Host–Virus Interaction and Mechanisms of Viral Persistence. *Cells* **2019**, *8* (4), 376. https://doi.org/10.3390/cells8040376.

(55) Lindenbach, B. D.; Rice, C. M. Unravelling Hepatitis C Virus Replication from Genome to Function. *Nature* **2005**, *436* (7053), 933–938. https://doi.org/10.1038/nature04077.

(56) Budd, J.; Robertson, R. Hepatitis C and General Practice: The Cruicial Role of Primary Care in Stemming the Epidemic. *Br. J. Gen. Pract. J. R. Coll. Gen. Pract.* **2005**, No. 55, 259–260.

(57) World Health Organization; World Health Organization; Global Hepatitis Programme. *Global Hepatitis Report, 2017*; 2017.

(58) Ivanova Reipold, E.; Easterbrook, P.; Trianni, A.; Panneer, N.; Krakower, D.; Ongarello, S.; Roberts, T.; Miller, V.; Denkinger, C. Optimising Diagnosis of Viraemic Hepatitis C

Infection: The Development of a Target Product Profile. *BMC Infect. Dis.* **2017**, *17* (S1), 707. https://doi.org/10.1186/s12879-017-2770-5.

(59) Adedokun, G.; Sidhu, G.; Alipanah, M.; Wang, G. P.; Fan, Z. H. A Handheld HIV Detection Platform Using Paper-Based Sample Preparation and Real-Time Isothermal Amplification. *Microsyst. Nanoeng.* **2024**, *10* (1), 181. https://doi.org/10.1038/s41378-024-00822-1.

(60) Shi, X.; Chen, C.-H.; Gao, W.; Chao, S.; Meldrum, D. R. Parallel RNA Extraction Using Magnetic Beads and a Droplet Array. *Lab. Chip* **2015**, *15* (4), 1059–1065. https://doi.org/10.1039/C4LC01111B.

(61) Ngo, H. T.; Jin, M.; Trick, A. Y.; Chen, F.-E.; Chen, L.; Hsieh, K.; Wang, T.-H. Sensitive and Quantitative Point-of-Care HIV Viral Load Quantification from Blood Using a Power-Free Plasma Separation and Portable Magnetofluidic Polymerase Chain Reaction Instrument. *Anal. Chem.* **2022**, acs.analchem.2c03897. https://doi.org/10.1021/acs.analchem.2c03897.

(62) Wheeler, E. K.; Hara, C. A.; Frank, J.; Deotte, J.; Hall, S. B.; Benett, W.; Spadaccini, C.; Beer, N. R. Under-Three Minute PCR: Probing the Limits of Fast Amplification. *The Analyst* **2011**, *136* (18), 3707. https://doi.org/10.1039/c1an15365j.

(63) Park, S.; Zhang, Y.; Lin, S.; Wang, T.-H.; Yang, S. Advances in Microfluidic PCR for Point-of-Care Infectious Disease Diagnostics. *Biotechnol. Adv.* **2011**, *29* (6), 830–839. https://doi.org/10.1016/j.biotechadv.2011.06.017.

(64) Chen, S.; Sun, Y.; Fan, F.; Chen, S.; Zhang, Y.; Zhang, Y.; Meng, X.; Lin, J.-M. Present Status of Microfluidic PCR Chip in Nucleic Acid Detection and Future Perspective. *TrAC Trends Anal. Chem.* **2022**, *157*, 116737. https://doi.org/10.1016/j.trac.2022.116737.

(65) Chen, D.; Mauk, M.; Qiu, X.; Liu, C.; Kim, J.; Ramprasad, S.; Ongagna, S.; Abrams, W. R.; Malamud, D.; Corstjens, P. L. A. M.; Bau, H. H. An Integrated, Self-Contained Microfluidic Cassette for Isolation, Amplification, and Detection of Nucleic Acids. *Biomed. Microdevices* **2010**, *12* (4), 705–719. https://doi.org/10.1007/s10544-010-9423-4.

(66) Baier, T.; Hansen-Hagge, T. E.; Gransee, R.; Crombé, A.; Schmahl, S.; Paulus, C.; Drese, K. S.; Keegan, H.; Martin, C.; O'Leary, J. J.; Furuberg, L.; Solli, L.; Grønn, P.; Falang, I. M.; Karlgård, A.; Gulliksen, A.; Karlsen, F. Hands-Free Sample Preparation Platform for Nucleic Acid Analysis. *Lab. Chip* **2009**, *9* (23), 3399. https://doi.org/10.1039/b910421f.

(67) Chan, K.; Weaver, S. C.; Wong, P.-Y.; Lie, S.; Wang, E.; Guerbois, M.; Vayugundla, S. P.; Wong, S. Rapid, Affordable and Portable Medium-Throughput Molecular Device for Zika Virus. *Sci. Rep.* **2016**, *6*, 38223. https://doi.org/10.1038/srep38223.

(68) Yang, H.; Chen, Z.; Cao, X.; Li, Z.; Stavrakis, S.; Choo, J.; deMello, A. J.; Howes, P. D.; He, N. A Sample-in-Digital-Answer-out System for Rapid Detection and Quantitation of

Infectious Pathogens in Bodily Fluids. *Anal. Bioanal. Chem.* **2018**, *410* (27), 7019–7030. https://doi.org/10.1007/s00216-018-1335-9.

(69) Sullivan, B. P.; Bender, A. T.; Ngyuen, D. N.; Zhang, J. Y.; Posner, J. D. Nucleic Acid Sample Preparation from Whole Blood in a Paper Microfluidic Device Using Isotachophoresis. *J. Chromatogr. B* **2021**, *1163*, 122494. https://doi.org/10.1016/j.jchromb.2020.122494.

(70) Bender, A. T.; Sullivan, B. P.; Zhang, J. Y.; Juergens, D. C.; Lillis, L.; Boyle, D. S.; Posner, J. D. HIV Detection from Human Serum with Paper-Based Isotachophoretic RNA Extraction and Reverse Transcription Recombinase Polymerase Amplification. *The Analyst* **2021**, *146* (9), 2851–2861. https://doi.org/10.1039/D0AN02483J.

(71) Curtis, K. A.; Rudolph, D. L.; Owen, S. M. Sequence-specific Detection Method for Reverse Transcription, Loop-mediated Isothermal Amplification of HIV-1. *J. Med. Virol.* **2009**, *81* (6), 966–972. https://doi.org/10.1002/jmv.21490.

(72) Myhrvold, C.; Freije, C. A.; Gootenberg, J. S.; Abudayyeh, O. O.; Metsky, H. C.; Durbin, A. F.; Kellner, M. J.; Tan, A. L.; Paul, L. M.; Parham, L. A.; Garcia, K. F.; Barnes, K. G.; Chak, B.; Mondini, A.; Nogueira, M. L.; Isern, S.; Michael, S. F.; Lorenzana, I.; Yozwiak, N. L.; MacInnis, B. L.; Bosch, I.; Gehrke, L.; Zhang, F.; Sabeti, P. C. Field-Deployable Viral Diagnostics Using CRISPR-Cas13. *Science* **2018**, *360* (6387), 444–448. https://doi.org/10.1126/science.aas8836.

(73) Novak, E. N.; Ma, A.; Kundrod, K. A.; Chang, M. M.; Hansen, C. J.; Montealegre, J. R.; Scheurer, M. E.; Castle, P. E.; Guo, M.; Salcedo, M. P.; Schmeler, K.; Richards-Kortum, R. Extraction-Free RT-RPA Assay for Detection of HPV16, HPV18, and HPV45 mRNA Expression. *Sci. Rep.* **2025**, *15* (1), 30450. https://doi.org/10.1038/s41598-025-13583-2.

(74) Mora, A. C.; Tierney, A. J.; Sogn, A. K.; Lawrence, P. T.; Tzavaras, E.; Singh, M. L.; Mahn Arteaga, G.; Omenetto, F. G.; Papas, A.; Mace, C. R. A One-Pot RT-LAMP Diagnostic Assay for SARS-CoV-2 from Saliva Samples. Chemistry March 11, 2025. https://doi.org/10.26434/chemrxiv-2025-b40mr.

(75) Wang, Q.; Gilligan-Steinberg, S. D.; Kim, W.; Kline, E. C.; Hull, I. T.; Lai, J. J.; Lutz, B. R. Large-Volume RT-LAMP Enables Extraction-Free Amplification of HIV RNA from Fingerstick Plasma. *Anal. Chim. Acta* **2024**, *1307*, 342560. https://doi.org/10.1016/j.aca.2024.342560.

(76) *WHO | HIV/AIDS*. WHO. http://www.who.int/gho/hiv/en/ (accessed 2019-10-09).

(77) Kubo, S.; Niimi, H.; Kitajima, I. Improved Reverse Transcription-Recombinase Polymerase Amplification Assay for Blood mRNA Screening: Comparison with One-Step RT-qPCR Assay. *Forensic Sci. Int. Genet.* **2023**, *63*, 102808. https://doi.org/10.1016/j.fsigen.2022.102808.

(78) Ahn, H.; Batule, B. S.; Seok, Y.; Kim, M.-G. Single-Step Recombinase Polymerase Amplification Assay Based on a Paper Chip for Simultaneous Detection of Multiple Foodborne Pathogens. *Anal. Chem.* **2018**, *90* (17), 10211–10216. https://doi.org/10/gd38fq.

(79) Sullivan, B. P.; Chou, Y.-S.; Bender, A. T.; Martin, C. D.; Kaputa, Z. G.; March, H.; Song, M.; Posner, J. D. Quantitative Isothermal Amplification on Paper Membranes Using Amplification Nucleation Site Analysis. *Lab. Chip* **2022**, *22* (12), 2352–2363. https://doi.org/10/gqmxgs.

(80) Batule, B. S.; Seok, Y.; Kim, M.-G. Paper-Based Nucleic Acid Testing System for Simple and Early Diagnosis of Mosquito-Borne RNA Viruses from Human Serum. *Biosens. Bioelectron.* **2020**, *151*, 111998. https://doi.org/10.1016/j.bios.2019.111998.

(81) Seok, Y.; Joung, H.-A.; Byun, J.-Y.; Jeon, H.-S.; Shin, S. J.; Kim, S.; Shin, Y.-B.; Han, H. S.; Kim, M.-G. A Paper-Based Device for Performing Loop-Mediated Isothermal Amplification with Real-Time Simultaneous Detection of Multiple DNA Targets. *Theranostics* **2017**, *7* (8), 2220–2230. https://doi.org/10.7150/thno.18675.

(82) Rodriguez, N. M.; Wong, W. S.; Liu, L.; Dewar, R.; Klapperich, C. M. A Fully Integrated Paperfluidic Molecular Diagnostic Chip for the Extraction, Amplification, and Detection of Nucleic Acids from Clinical Samples. *Lab Chip* **2016**, *16* (4), 753–763. https://doi.org/10.1039/C5LC01392E.

(83) Kim, J.-H.; Yoo, I. S.; An, J. H.; Kim, S. A Novel Paper-Plastic Hybrid Device for the Simultaneous Loop-Mediated Isothermal Amplification and Detection of DNA. *Mater. Lett.* **2018**, *214*, 243–246. https://doi.org/10/gct3w7.

(84) Kaur, N.; Michael, J. S.; Toley, B. J. A Modular Paper-and-Plastic Device for Tuberculosis Nucleic Acid Amplification Testing in Limited-Resource Settings. *Sci. Rep.* **2019**, *9* (1), 15367. https://doi.org/10/gmfjb7.

(85) Rohrman, B. A.; Richards-Kortum, R. R. A Paper and Plastic Device for Performing Recombinase Polymerase Amplification of HIV DNA. *Lab. Chip* **2012**, *12* (17), 3082–3088. https://doi.org/10.1039/C2LC40423K.

(86) Martinez, A. W.; Phillips, S. T.; Whitesides, G. M.; Carrilho, E. Diagnostics for the Developing World: Microfluidic Paper-Based Analytical Devices. *Anal Chem* **2010**, *82* (1), 3–10. https://doi.org/10.1021/ac9013989.

(87) Magro, L.; Escadafal, C.; Garneret, P.; Jacquelin, B.; Kwasiborski, A.; Manuguerra, J.-C.; Monti, F.; Sakuntabhai, A.; Vanhomwegen, J.; Lafaye, P.; Tabeling, P. Paper Microfluidics for Nucleic Acid Amplification Testing (NAAT) of Infectious Diseases. *Lab. Chip* **2017**, *17* (14), 2347–2371. https://doi.org/10.1039/C7LC00013H.

(88) Chin, C. D.; Linder, V.; Sia, S. K. Commercialization of Microfluidic Point-of-Care Diagnostic Devices. *Lab. Chip* **2012**, *12* (12), 2118–2134. https://doi.org/10.1039/C2LC21204H.

(89) Weigl, B.; Domingo, G.; LaBarre, P.; Gerlach, J. Towards Non- and Minimally Instrumented, Microfluidics-Based Diagnostic Devices. *Lab. Chip* **2008**, *8* (12), 1999. https://doi.org/10.1039/b811314a.

(90) Connelly, J. T.; Rolland, J. P.; Whitesides, G. M. "Paper Machine" for Molecular Diagnostics. *Anal. Chem.* **2015**, *87* (15), 7595–7601. https://doi.org/10.1021/acs.analchem.5b00411.

(91) Govindarajan, A. V.; Ramachandran, S.; Vigil, G. D.; Yager, P.; Böhringer, K. F. A Low Cost Point-of-Care Viscous Sample Preparation Device for Molecular Diagnosis in the Developing World; an Example of Microfluidic Origami. *Lab. Chip* **2011**, *12* (1), 174–181. https://doi.org/10.1039/C1LC20622B.

(92) Trinh, T. N. D.; Lee, N. Y. A Foldable Isothermal Amplification Microdevice for Fuchsin-Based Colorimetric Detection of Multiple Foodborne Pathogens. *Lab. Chip* **2019**, *19* (8), 1397–1405. https://doi.org/10.1039/C8LC01389F.

(93) Kaur, N.; Toley, B. J. Paper-Based Nucleic Acid Amplification Tests for Point-of-Care Diagnostics. *The Analyst* **2018**, *143* (10), 2213–2234. https://doi.org/10.1039/C7AN01943B.

(94) Gubala, V.; Harris, L. F.; Ricco, A. J.; Tan, M. X.; Williams, D. E. Point of Care Diagnostics: Status and Future. *Anal. Chem.* **2012**, *84* (2), 487–515. https://doi.org/10.1021/ac2030199.

(95) Nguyen, H. V.; Nguyen, V. D.; Nguyen, H. Q.; Chau, T. H. T.; Lee, E. Y.; Seo, T. S. Nucleic Acid Diagnostics on the Total Integrated Lab-on-a-Disc for Point-of-Care Testing. *Biosens. Bioelectron.* **2019**, *141*, 111466. https://doi.org/10.1016/j.bios.2019.111466.

(96) Linnes, J. C.; Rodriguez, N. M.; Liu, L.; Klapperich, C. M. Polyethersulfone Improves Isothermal Nucleic Acid Amplification Compared to Current Paper-Based Diagnostics. *Biomed. Microdevices* **2016**, *18* (2). https://doi.org/10.1007/s10544-016-0057-z.

(97) Villermaux, E. Mixing Versus Stirring. *Annu. Rev. Fluid Mech.* **2019**, *51* (1), 245–273. https://doi.org/10.1146/annurev-fluid-010518-040306.

(98) Osborn, J. L.; Lutz, B.; Fu, E.; Kauffman, P.; Stevens, D. Y.; Yager, P. Microfluidics without Pumps: Reinventing the T-Sensor and H-Filter in Paper Networks. *Lab. Chip* **2010**, *10*, 2659. https://doi.org/10.1039/c004821f.

(99) Jang, I.; Song, S. Facile and Precise Flow Control for a Paper-Based Microfluidic Device through Varying Paper Permeability. *Lab. Chip* **2015**, *15* (16), 3405–3412. https://doi.org/10.1039/C5LC00465A.

(100) Lim, Y. C.; Kouzani, A. Z.; Duan, W. Lab-on-a-Chip: A Component View. *Microsyst. Technol.* **2010**, *16* (12), 1995–2015. https://doi.org/10.1007/s00542-010-1141-6.

(101) Gervais, L.; De Rooij, N.; Delamarche, E. Microfluidic Chips for Point-of-Care Immunodiagnostics. *Adv. Mater.* **2011**, *23* (24), H151–H176. https://doi.org/10.1002/adma.201100464.

(102) Lee, C.-Y.; Chang, C.-L.; Wang, Y.-N.; Fu, L.-M. Microfluidic Mixing: A Review. *Int. J. Mol. Sci.* **2011**, *12* (5), 3263–3287. https://doi.org/10.3390/ijms12053263.

(103) Guan, Y.; Xu, F.; Sun, B.; Meng, X.; Liu, Y.; Bai, M. A Hybrid Electrically-and-Piezoelectrically Driven Micromixer Built on Paper for Microfluids Mixing. *Biomed. Microdevices* **2020**, *22* (3), 47. https://doi.org/10.1007/s10544-020-00502-7.

(104) Rezk, A. R.; Qi, A.; Friend, J. R.; Li, W. H.; Yeo, L. Y. Uniform Mixing in Paper-Based Microfluidic Systems Using Surface Acoustic Waves. *Lab Chip* **2012**, *12* (4), 773–779. https://doi.org/10.1039/C2LC21065G.

(105) Ito, Y.; Komori, S. A Vibration Technique for Promoting Liquid Mixing and Reaction in a Microchannel. *AIChE J.* **2006**, *52* (9), 3011–3017. https://doi.org/10.1002/aic.10919.

(106) Liu, W.-S.; Wolf, M. F.; Elwell, D.; Feigelson, R. S. Low Frequency Vibrational Stirring: A New Method for Rapidly Mixing Solutions and Melts during Growth. *J. Cryst. Growth* **1987**, *82* (4), 589–597. https://doi.org/10.1016/S0022-0248(87)80003-9.

(107) Oberti, S.; Neild, A.; Wah Ng, T. Microfluidic Mixing under Low Frequency Vibration. *Lab. Chip* **2009**, *9* (10), 1435. https://doi.org/10.1039/b819739c.

(108) Zhan, X.; He, Y.; Sun, Z.; Shen, B.; Li, X. Mixing Characteristics of High-Viscosity Fluids under Forced Vertical Vibration. *Chem. Eng. Technol.* **2020**, *43* (7), 1327–1335. https://doi.org/10.1002/ceat.201800546.

(109) Zhang, D.; Gao, R.; Huang, S.; Huang, Y.; Zhang, J.; Su, X.; Zhang, S.; Ge, S.; Zhang, J.; Xia, N. All-in-One Microfluidic Chip for 30-Min Quantitative Point-of-Care-Testing of Nucleic Acids. *Sens. Actuators B Chem.* **2023**, *390*, 133939. https://doi.org/10.1016/j.snb.2023.133939.

(110) Chen, Y. Quantitative and Ultrasensitive in Situ Immunoassay Technology for SARS-CoV-2 Detection in Saliva. *Sci. Adv.* **2022**.

(111) Lim, S. Y.; Lee, T. J.; Shin, S. Y.; Bae, N. H.; Lee, S. J.; Park, Y. M. Development of a Bacterial DNA Extraction Modular Chip Using a Magnetic Particle and Portable Vibration Motor. *Anal. Methods* **2020**, *12* (9), 1197–1202. https://doi.org/10.1039/C9AY02690H.

(112) Nguyen, H. Q.; Bui, H. K.; Phan, V. M.; Seo, T. S. An Internet of Things-Based Point-of-Care Device for Direct Reverse-Transcription-Loop Mediated Isothermal Amplification to

Identify SARS-CoV-2. *Biosens. Bioelectron.* **2022**, *195*, 113655. https://doi.org/10.1016/j.bios.2021.113655.

(113) Qiu, X.; Chen, D.; Liu, C.; Mauk, M. G.; Kientz, T.; Bau, H. H. A Portable, Integrated Analyzer for Microfluidic – Based Molecular Analysis. *Biomed. Microdevices* **2011**, *13* (5), 809–817. https://doi.org/10.1007/s10544-011-9551-5.

(114) Choi, J. R.; Hu, J.; Tang, R.; Gong, Y.; Feng, S.; Ren, H.; Wen, T.; Li, X.; Wan Abas, W. A. B.; Pingguan-Murphy, B.; Xu, F. An Integrated Paper-Based Sample-to-Answer Biosensor for Nucleic Acid Testing at the Point of Care. *Lab. Chip* **2016**, *16* (3), 611–621. https://doi.org/10.1039/C5LC01388G.

(115) Phillips, E. A.; Moehling, T. J.; Ejendal, K. F. K.; Hoilett, O. S.; Byers, K. M.; Basing, L. A.; Jankowski, L. A.; Bennett, J. B.; Lin, L.-K.; Stanciu, L. A.; Linnes, J. C. Microfluidic Rapid and Autonomous Analytical Device (microRAAD) to Detect HIV from Whole Blood Samples. *Lab. Chip* **2019**. https://doi.org/10.1039/C9LC00506D.

(116) Jiang, K. P.; Bennett, S.; Heiniger, E. K.; Kumar, S.; Yager, P. UbiNAAT: A Multiplexed Point-of-Care Nucleic Acid Diagnostic Platform for Rapid at-Home Pathogen Detection. *Lab. Chip* **2024**, *24* (3), 492–504. https://doi.org/10.1039/D3LC00753G.

(117) Tsui, N. B. Y.; Ng, E. K. O.; Lo, Y. M. D. Stability of Endogenous and Added RNA in Blood Specimens, Serum, and Plasma. *Clin. Chem.* **2002**, *48* (10), 1647–1653.

(118) Moody, C.; Newell, H.; Viljoen, H. A Mathematical Model of Recombinase Polymerase Amplification under Continuously Stirred Conditions. *Biochem. Eng. J.* **2016**, *112*, 193–201. https://doi.org/10.1016/j.bej.2016.04.017.

(119) Lillis, L.; Lehman, D. A.; Siverson, J. B.; Weis, J.; Cantera, J.; Parker, M.; Piepenburg, O.; Overbaugh, J.; Boyle, D. S. Cross-Subtype Detection of HIV-1 Using Reverse Transcription and Recombinase Polymerase Amplification. *J. Virol. Methods* **2016**, *230*, 28–35. https://doi.org/10.1016/j.jviromet.2016.01.010.

(120) Özay, B.; McCalla, S. E. A Review of Reaction Enhancement Strategies for Isothermal Nucleic Acid Amplification Reactions. *Sens. Actuators Rep.* **2021**, *3*, 100033. https://doi.org/10.1016/j.snr.2021.100033.

(121) Attia, S.; Egger, M.; Müller, M.; Zwahlen, M.; Low, N. Sexual Transmission of HIV According to Viral Load and Antiretroviral Therapy: Systematic Review and Meta-Analysis: *AIDS* **2009**, *23* (11), 1397–1404. https://doi.org/10.1097/QAD.0b013e32832b7dca.

(122) LeMessurier, J.; Traversy, G.; Varsaneux, O.; Weekes, M.; Avey, M. T.; Niragira, O.; Gervais, R.; Guyatt, G.; Rodin, R. Risk of Sexual Transmission of Human Immunodeficiency Virus with Antiretroviral Therapy, Suppressed Viral Load and Condom Use: A Systematic

Review. *CMAJ Can. Med. Assoc. J. J. Assoc. Medicale Can.* **2018**, *190* (46), E1350–E1360. https://doi.org/10/gfrpmv.

(123) Sanchez, A. M.; DeMarco, C. T.; Hora, B.; Keinonen, S.; Chen, Y.; Brinkley, C.; Stone, M.; Tobler, L.; Keating, S.; Schito, M.; Busch, M. P.; Gao, F.; Denny, T. N. Development of a Contemporary Globally Diverse HIV Viral Panel by the EQAPOL Program. *J. Immunol. Methods* **2014**, *409*, 117–130. https://doi.org/10/f6rhcm.

(124) Stroock, A. D.; Dertinger, S. K. W.; Ajdari, A.; Mezić, I.; Stone, H. A.; Whitesides, G. M. Chaotic Mixer for Microchannels. *Science* **2002**, *295* (5555), 647–651. https://doi.org/10.1126/science.1066238.

(125) Wheat, P. M.; Posner, J. D. Quantifying Mixing Using Equilibrium Reactions. *Phys. Fluids* **2009**, *21* (3), 037101. https://doi.org/10.1063/1.3078247.

(126) Panić, S.; Loebbecke, S.; Tuercke, T.; Antes, J.; Bošković, D. Experimental Approaches to a Better Understanding of Mixing Performance of Microfluidic Devices. *Chem. Eng. J.* **2004**, *101* (1–3), 409–419. https://doi.org/10.1016/j.cej.2003.10.026.

(127) Song, H.; Tice, J. D.; Ismagilov, R. F. A Microfluidic System for Controlling Reaction Networks in Time. *Angew. Chem. Int. Ed.* **2003**, *42* (7), 768–772. https://doi.org/10.1002/anie.200390203.

(128) Park, H. Y.; Kim, S. A.; Korlach, J.; Rhoades, E.; Kwok, L. W.; Zipfel, W. R.; Waxham, M. N.; Webb, W. W.; Pollack, L. Conformational Changes of Calmodulin upon Ca $^{2+}$ Binding Studied with a Microfluidic Mixer. *Proc. Natl. Acad. Sci.* **2008**, *105* (2), 542–547. https://doi.org/10.1073/pnas.0710810105.

(129) Daher, R. K.; Stewart, G.; Boissinot, M.; Bergeron, M. G. Recombinase Polymerase Amplification for Diagnostic Applications. *Clin. Chem.* **2016**, *62* (7), 947–958. https://doi.org/10.1373/clinchem.2015.245829.

(130) Tartakovsky, D. M.; Dentz, M. Diffusion in Porous Media: Phenomena and Mechanisms. *Transp. Porous Media* **2019**, *130* (1), 105–127. https://doi.org/10.1007/s11242-019-01262-6.

(131) Medveď, I.; Černý, R. Surface Diffusion in Porous Media: A Critical Review. *Microporous Mesoporous Mater.* **2011**, *142* (2–3), 405–422. https://doi.org/10.1016/j.micromeso.2011.01.015.

(132) Weissberg, H. Effective Diffusion Coefficient in Porous Media. *J Appl Phys* **1963**, No. 34, 2636–2639. https://doi.org/https://doi.org/10.1063/1.1729783.

(133) Dineva, M. A.; Mahilum-Tapay, L.; Lee, H. Sample Preparation: A Challenge in the Development of Point-of-Care Nucleic Acid-Based Assays for Resource-Limited Settings. *The Analyst* **2007**, *132* (12), 1193. https://doi.org/10.1039/b705672a.

(134) Sun, D.; Han, C.; Sheng, J. The Role of Human Ribonuclease A Family in Health and Diseases: A Systematic Review. *iScience* **2022**, *25* (11), 105284. https://doi.org/10.1016/j.isci.2022.105284.

(135) Bender, A. T.; Sullivan, B. P.; Lillis, L.; Posner, J. D. Enzymatic and Chemical-Based Methods to Inactivate Endogenous Blood Ribonucleases for Nucleic Acid Diagnostics. *J. Mol. Diagn.* **2020**, *22* (8), 1030–1040. https://doi.org/10/gg892k.

(136) *TwistAmp manuals | Downloads | Support | TwistDx*. https://www.twistdx.co.uk/en/support/manuals/twistamp-manuals (accessed 2019-10-11).

(137) Lillis, L.; Lehman, D. A.; Siverson, J. B.; Weis, J.; Cantera, J.; Parker, M.; Piepenburg, O.; Overbaugh, J.; Boyle, D. S. Cross-Subtype Detection of HIV-1 Using Reverse Transcription and Recombinase Polymerase Amplification. *J. Virol. Methods* **2016**, *230*, 28–35. https://doi.org/10.1016/j.jviromet.2016.01.010.

(138) Bartlett, J. M. S.; Stirling, D. *PCR Protocols*, Second Edition.; Methods in Molecular Biology™; Humana Press: Totowa, NJ, 2003. https://doi.org/10.1385/1592593844.

(139) Kojima, K.; Juma, K. M.; Akagi, S.; Hayashi, K.; Takita, T.; O'Sullivan, C. K.; Fujiwara, S.; Nakura, Y.; Yanagihara, I.; Yasukawa, K. Solvent Engineering Studies on Recombinase Polymerase Amplification. *J. Biosci. Bioeng.* **2021**, *131* (2), 219–224. https://doi.org/10.1016/j.jbiosc.2020.10.001.

(140) Recombinase Polymerase Amplification (RPA) an Isothermal Technique Suitable for a Range of Applications- Evaluation of RPA Volume Tolerance. *BioTechniques* **2017**, *62* (6), 295–295. https://doi.org/10.2144/000114561.

(141) N. Shimazu, K.; T. Bender, A.; G. Reinhall, P.; D. Posner, J. Vibration Mixing for Enhanced Paper-Based Recombinase Polymerase Amplification. *Lab. Chip* **2024**, *24* (20), 4879–4891. https://doi.org/10.1039/D4LC00592A.

(142) Becskei, A.; Rahaman, S. The Life and Death of RNA across Temperatures. *Comput. Struct. Biotechnol. J.* **2022**, *20*, 4325–4336. https://doi.org/10.1016/j.csbj.2022.08.008.

(143) PALL Life Sciences. Vivid Plasma Separation Membrane. https://www.pall.com/pdfs/OEM-Materials-and-Devices/09.2730_VividPlasma_DS_6pg.pdf (accessed 2017-06-20).

(144) Cytiva. *Whatman blood separators for lateral-flow immunoassays*. https://www.cytivalifesciences.com/en/us/insights/blood-separators (accessed 2025-11-11).

(145) MDI Membrane Technologies. *PlasmaDrop Kits for Free Liquid Plasma*. https://mdimembrane.com/product/products/membrane-for-immunodiagnostics/blood-separation/plasmadrop-kits-for-free-liquid-plasma/ (accessed 2025-11-11).

(146) CanaryQ. *Rapid Plasma Separation Device*. https://canaryq.com/product/ (accessed 2025-11-11).

(147) Tang, R.; Yang, H.; Choi, J. R.; Gong, Y.; You, M.; Wen, T.; Li, A.; Li, X.; Xu, B.; Zhang, S.; Mei, Q.; Xu, F. Capillary Blood for Point-of-Care Testing. *Crit. Rev. Clin. Lab. Sci.* **2017**, *54* (5), 294–308. https://doi.org/10.1080/10408363.2017.1343796.

(148) A. Rohrman, B.; R. Richards-Kortum, R. A Paper and Plastic Device for Performing Recombinase Polymerase Amplification of HIV DNA. *Lab. Chip* **2012**, *12* (17), 3082–3088. https://doi.org/10.1039/C2LC40423K.

(149) Ahn, H.; Batule, B. S.; Seok, Y.; Kim, M.-G. Single-Step Recombinase Polymerase Amplification Assay Based on a Paper Chip for Simultaneous Detection of Multiple Foodborne Pathogens. *Anal. Chem.* **2018**, *90* (17), 10211–10216. https://doi.org/10.1021/acs.analchem.8b01309.

(150) Wetzel, R.; Becker, M.; Behlke, J.; Billwitz, H.; BoHM, S.; Ebert, B.; Hamann, H.; Krumbiegel, J.; Lassmann, G. Temperature Behaviour of Human Serum Albumin. *Eur. J. Biochem.* **1980**, *104* (2), 469–478. https://doi.org/10.1111/j.1432-1033.1980.tb04449.x.

(151) ECHA. Inclusion of Substances of Very High Concern in the Candidate List, 2012.

(152) Petruzziello, A.; Marigliano, S.; Loquercio, G.; Cozzolino, A.; Cacciapuoti, C. Global Epidemiology of Hepatitis C Virus Infection: An Up-Date of the Distribution and Circulation of Hepatitis C Virus Genotypes. *World J. Gastroenterol.* **2016**, *22* (34), 7824. https://doi.org/10.3748/wjg.v22.i34.7824.

(153) Helm, E. W.; Kim, H. N.; Greninger, A. L. Optimizing Hepatitis C Virus Testing in the Era of Point-of-Care RNA Diagnostics. *J. Clin. Microbiol.* **2026**, *64* (1), e01259-25. https://doi.org/10.1128/jcm.01259-25.

(154) Al-Soud, W. A.; Rådström, P. Purification and Characterization of PCR-Inhibitory Components in Blood Cells. *J. Clin. Microbiol.* **2001**, *39* (2), 485–493. https://doi.org/10.1128/JCM.39.2.485-493.2001.

(155) Wang, Q.; Gilligan-Steinberg, S. D.; Kim, W.; Kline, E. C.; Hull, I. T.; Lai, J. J.; Lutz, B. R. Large-Volume RT-LAMP Enables Extraction-Free Amplification of HIV RNA from Fingerstick Plasma. *Anal. Chim. Acta* **2024**, 342560. https://doi.org/10.1016/j.aca.2024.342560.

(156) Khan, M. J. R.; Bhuiyan, M. A.; Tabassum, S.; Munshi, S. U. Use of Whole Blood and Dried Blood Spot for Detection of HIV-1 Nucleic Acids Using Reverse Transcription Loop-Mediated Isothermal Amplification. *J. Virol. Methods* **2023**, *312*, 114642. https://doi.org/10.1016/j.jviromet.2022.114642.

(157) Connelly, J. T.; Rolland, J. P.; Whitesides, G. M. “Paper Machine” for Molecular Diagnostics. *Anal. Chem.* **2015**, *87* (15), 7595–7601. https://doi.org/10.1021/acs.analchem.5b00411.

(158) Lafleur, L. K.; Bishop, J. D.; Heiniger, E. K.; Gallagher, R. P.; Wheeler, M. D.; Kauffman, P.; Zhang, X.; Kline, E. C.; Buser, J. R.; Kumar, S.; Byrnes, S. A.; Vermeulen, N. M. J.; Scarr, N. K.; Belousov, Y.; Mahoney, W.; Toley, B. J.; Ladd, P. D.; Lutz, B. R.; Yager, P. A Rapid, Instrument-Free, Sample-to-Result Nucleic Acid Amplification Test. *Lab Chip* **2016**, *16* (19), 3777–3787. https://doi.org/10.1039/C6LC00677A.

(159) Trinh, K. T. L.; Trinh, T. N. D.; Lee, N. Y. Fully Integrated and Slidable Paper-Embedded Plastic Microdevice for Point-of-Care Testing of Multiple Foodborne Pathogens. *Biosens. Bioelectron.* **2019**, *135*, 120–128. https://doi.org/10.1016/j.bios.2019.04.011.

(160) Seok, Y.; Joung, H.-A.; Byun, J.-Y.; Jeon, H.-S.; Shin, S. J.; Kim, S.; Shin, Y.-B.; Han, H. S.; Kim, M.-G. A Paper-Based Device for Performing Loop-Mediated Isothermal Amplification with Real-Time Simultaneous Detection of Multiple DNA Targets. *Theranostics* **2017**, *7* (8), 2220–2230. https://doi.org/10.7150/thno.18675.

(161) Analog Technologies. *MCH*. https://www.analogtechnologies.com/document/MCH.pdf (accessed 2026-05-15).

(162) PID Control System Analysis and Design. *IEEE Control Syst.* **2006**, *26* (1), 32–41. https://doi.org/10.1109/MCS.2006.1580152.

(163) Peng, A.; Wang, L.; Waleed, K.; Qiu, L.; Tong, X.; Tu, Z.; ShuYang; Cui, Y.; Hu, F.; Lu, L.; Huang, P. The Prognosis Characteristics of HIV/HBV Co-Infection after Antiviral Therapy: A Comprehensive Review. *Infect. Agent. Cancer* **2026**, *21* (1), 15. https://doi.org/10.1186/s13027-025-00724-5.

(164) Guidelines for the Use of Antiretroviral Agents in Adults and Adolescents With HIV.

(165) Baumert, T. F.; Berg, T.; Lim, J. K.; Nelson, D. R. Status of Direct-Acting Antiviral Therapy for Hepatitis C Virus Infection and Remaining Challenges. *Gastroenterology* **2019**, *156* (2), 431–445. https://doi.org/10.1053/j.gastro.2018.10.024.

(166) WHO. WHO Prequalifies the First Triple Diagnostic Test. July 11, 2025. https://extranet.who.int/prequal/news/who-prequalifies-first-triple-diagnostic-test (accessed 2026-05-21).

(167) CanaryQ. *The solution to the hematocrit effect*. https://canaryq.com/product/ (accessed 2026-05-17).

(168) Deiana, G.; Smith, S. 3D Printed Devices for the Separation of Blood Plasma from Capillary Samples. *Micromachines* **2024**, *15* (3), 359. https://doi.org/10.3390/mi15030359.